

8-2013

ADVANCED BIOMATERIALS FROM RENEWABLE RESOURCES: AN INVESTIGATION ON CELLULOSE NANOCRYSTAL COMPOSITES AND CO₂ EXTRACTION OF RENDERED MATERIALS

Jose Orellana

Clemson University, jloh222@hotmail.com

Follow this and additional works at: https://tigerprints.clemson.edu/all_dissertations



Part of the [Chemical Engineering Commons](#)

Recommended Citation

Orellana, Jose, "ADVANCED BIOMATERIALS FROM RENEWABLE RESOURCES: AN INVESTIGATION ON CELLULOSE NANOCRYSTAL COMPOSITES AND CO₂ EXTRACTION OF RENDERED MATERIALS" (2013). *All Dissertations*. 1183.
https://tigerprints.clemson.edu/all_dissertations/1183

This Dissertation is brought to you for free and open access by the Dissertations at TigerPrints. It has been accepted for inclusion in All Dissertations by an authorized administrator of TigerPrints. For more information, please contact kokeefe@clemson.edu.

ADVANCED BIOMATERIALS FROM RENEWABLE RESOURCES:
AN INVESTIGATION ON CELLULOSE NANOCRYSTAL
COMPOSITES AND CO₂ EXTRACTION OF
RENDERED MATERIALS

A Dissertation
Presented to
the Graduate School of
Clemson University

In Partial Fulfillment
of the Requirements for the Degree
Doctor of Philosophy
Chemical Engineering

by
José Luis Orellana
August 2013

Accepted by:
Dr. Christopher L. Kitchens, Committee Chair
Dr. Douglas E. Hirt
Dr. Mark C. Thies
Dr. O. Thompson Mefford

ABSTRACT

The annual global consumption of petroleum-based plastics is approximately 280 million tons and is impacting the sustainability of our planet and prosperity of future generations. One solution is the development of bio-based polymer materials with advanced properties for commercial applications. Therefore, the ultimate goal of this dissertation is to investigate the properties of new bio-based materials for broader applications. This dissertation includes two research areas: cellulose nanocomposites, and CO₂ extractions of rendered fat. In the first half, cellulose nanocrystals (CNCs), which exhibit excellent mechanical and optical properties, were investigated for the reinforcement of a biodegradable polymer. The properties of these nanocomposites were studied to intellectually contribute to the understanding of the reinforcement mechanisms of CNC nanocomposites. In the second half, a more efficient and greener extraction of fat from rendered materials (RMs) was explored to broaden their potential applications, which include protein-based polymers and biofuels.

Since CNCs are hydrophilic, surface modification with various surfactants was first accomplished in this research, increasing the dispersion stability in non-polar solvents by at least a month. Only 1 wt.% of surfactant with respect to CNCs was needed to afford a significant increase in the CNC stability, representing a much lower percentage than the values reported in the literature. Moreover, these CNCs showed the ability to self-assemble into local liquid crystal structures, a potential advantage for polymer reinforcement. CNCs were subsequently investigated as an additive for polylactic acid (PLA), which is the most widely used synthetic biopolymer in the market. CNC addition

yielded a 61% increase in toughness at 1 wt.% CNC load. The tensile strength and modulus were not affected by the CNC addition, addressing one of the most frequent issues in the toughening of polymers. In addition, polarized microscopy revealed self-assembly formation of the enhanced composites indicating that the reinforcement was influenced by the CNC nanoscale structure on the matrix. These structures were found to be distributed in different directions along the extrusion line, suggesting that an angled CNC orientation favored a higher toughness as observed in natural cellulose fibers. PLA was also modified by grafting polyacrylic acid (PAA), which provided a stiffer and more hydrophilic surface for the addition of unmodified CNCs. In this case, the toughness of the PLA copolymer decreased with CNC concentration, while the tensile modulus increased. This effect was attributed to an increase of polymer crystallinity upon addition of CNCs, probably due to an enhanced compatibility provided by the PAA chains.

For the purpose of obtaining a more efficient separation of proteins and fats from RMs, liquid and supercritical CO₂ (LCO₂ and SCCO₂) were explored as solvents for the extraction, demonstrating the ability to extract up to 97% of the fat in the RMs. Higher fat solubilities in LCO₂ were obtained compared to SCCO₂, a result attributed to a retrograde phenomenon. These results are advantageous for the separation of rendered fats at relatively low temperatures and pressures, obtaining higher yields than screw pressing currently used in the industry. However, this extraction requires high amounts of CO₂ due to low fat solubilities. This issue was addressed using CO₂-assisted mechanical extraction, resulting in yields up to 81%, representing a 98% increase compared to conventional extraction, and significantly reducing the amount of CO₂ for the extraction.

DEDICATION

A Dios y a mis padres, Delmi Estela Hernandez y Jose Luis Orellana Tobar.

To God and to my parents, Delmi Estela Hernandez and Jose Luis Orellana Tobar.

ACKNOWLEDGMENTS

First of all, I thank God for all the blessings and challenges that He has given me, for my loving family, and for all the people that He has placed in my life. I thank Him for guiding me and for giving me the wisdom, knowledge, and strength to finish my PhD.

I would like to thank my mother for her patience and encouragement to become a more studious and responsible person. To my dad for teaching me to never give up and for getting me excited about engineering. To my siblings: Estelita, Lucia, and Elias, for believing on me and for motivating me to be a good example to them. To my grandparents who are always caring for me, and to my Tia Olga who is always praying for everyone in our family.

I would like to thank my advisor Dr. Christopher Kitchens for his guidance, support and trust throughout these years.

To my research committee: Dr. Douglas Hirt, Dr. Mark Thies, and Dr. Thompson Mefford, for their time and guidance in my dissertation.

To my research group: Greg White, Esteban Ureña, Fiaz Mohammed, Ashley Hart, Ming, and Brandon. To Greg and Esteban especially for not only becoming my mentors, but also for making me part of their families.

To all undergraduate students with whom I worked closely: Michael Mauhar, Tyler Smith, Kyle Johnson, Anne Kelly, Katie McGreevey, Fritz Wewers, Nikki Demass, Matt McMillan, and Derek Wichhart.

To my Salvadorean family here at Clemson: Alexandra, Alexito, Milagro, Iris, Julian, Julio, Kryssia, Lizzie, Ruben, Andrea, Ivan, Marlon, Byron and Aaron. Thanks for all of the good moments, the company, and the support, especially in those more needed moments. To Sarah Mena who helped me to apply and come to Clemson. To Linda and Esteban and to Greg and Marta for giving me a special place in their families. To Bob Lippert for recruiting me to Clemson and for being a mentor to me.

Lastly, I would like to thank my Saint Andrew Parish family for welcoming me and receiving me as part of their family here in Clemson and for helping me to discern the next steps in my life. I also want to thank the youth of the parish with whom I had the opportunity to work and to share my experiences, and more importantly, to become a friend and, for many, a brother.

TABLE OF CONTENTS

	Page
TITLE PAGE	i
ABSTRACT.....	ii
DEDICATION.....	iv
ACKNOWLEDGMENTS	v
LIST OF TABLES.....	x
LIST OF FIGURES	xi
CHAPTER	
I. INTRODUCTION AND BACKGROUND	1
Cellulose Nanocrystals.....	2
Biodegradable Polymers	21
CO ₂ Extraction of Rendered Materials	26
Dissertation Outline	33
References.....	36
II. PHASE BEHAVIOR AND DISPERSIBILITY OF SURFACE MODIFIED CELLULOSE NANOCRYSTALS IN ORGANIC SOLVENTS BY MEANS OF SURFACTANTS	48
Introduction.....	48
Materials and Methods.....	52
Results and Discussion	55
Conclusions.....	67
References.....	68
III. REINFORCEMENT OF POLYLACTIC ACID FILMS WITH SURFACE MODIFIED CELLULOSE NANOCRYSTALS.....	72

Table of Contents (Continued)

	Page
Introduction.....	72
Materials and Methods.....	75
Results and Discussion	80
Conclusions.....	94
References.....	95
IV. CELLULOSE NANOCRYSTALS VERSUS POLYETHYLENE GLYCOL AS TOUGHENING AGENTS FOR POLY(LACTIC ACID)- POLY(ACRYLIC ACID) GRAFT COPOLYMER	100
Introduction.....	100
Materials and Methods.....	102
Results and Discussion	106
Conclusions.....	119
References.....	121
V. LIQUID AND SUPERCRITICAL CO ₂ EXTRACTION OF FAT FROM RENDERED MATERIALS	126
Introduction.....	126
Materials and Methods.....	130
Results and Discussion	132
Conclusions.....	142
References.....	143
VI. CO ₂ ASSISTED MECHANICAL EXPRESSION OF FAT FROM RENDERED MATERIALS	147
Introduction.....	147
Materials and Methods.....	149
Results and Discussion	153
Conclusions.....	158
References.....	158
VII. FUTURE WORK.....	161
Introduction.....	161
Processing and Properties of Cellulose Nanocrystals for MEMS Applications	161

Table of Contents (Continued)

	Page
Nanocomposites with Optical Properties.....	167
References.....	171
VIII. CONCLUSIONS AND RECOMMENDATIONS.....	173
Conclusions.....	173
Recommendations.....	176
References.....	180
APPENDICES.....	182
A: Additional Polarized Microscopy Images.....	183
B: Experimental Methods.....	186
C: Extraction of Other Rendered Materials and Characterization.....	197
D: Phase Behavior of CNC-HCl and CNC-AA in Water.....	200
E: Permissions.....	206

LIST OF TABLES

Table		Page
1.1	Dimensions of CNC from different sources.	4
1.2	Mechanical properties of several reinforcement materials and crystalline cellulose	5
1.3.	Representative properties of common petroleum-based polymer and PLA.....	24
3.1	Nomenclature and fractions of the PLA-CNC nanocomposites prepared in this work	80
3.2	Approximate percentage of colors of PLA-CNC composites observed under polarized-light microscopy with a first order red plate	92
4.1	Thermal properties of PLA and PLA-PAA loaded with cellulose nanocrystals	112
4.2	Thermal properties of PLA-PAA blends	119
5.1	Solubilities and extraction yield of rendered fat in LCO ₂ and SCCO ₂	137
5.2	Fatty acid mass fraction of extracted fats	142
C.1.	Rendered Materials Composition	199
C.2.	Sludge Composition.....	199
C.3.	Extracted Rendered Materials Composition	199

LIST OF FIGURES

Figure		Page
1.1	Chemical structure of cellulose.....	2
1.2	Schematic representation of the structure of cellulosic materials: from the cellulose sources to the cellulose molecules. Reprinted with permission from ref 11. Copyright 2012 Elsevier	3
1.3	Schematic representation of the isolation of CNCs by acid hydrolysis using sulfuric, hydrochloric, and acetic acid. a) acid hydrolysis mechanism; b) esterification of cellulose surface; and c) macro-scale representation of the CNC isolation from pure cellulose, showing the crystalline and amorphous regions.....	6
1.4	Reaction mechanism of the TEMPO-mediated oxidation of CNCs. Reprinted with permission from ref. 23. Copyright 2008 Springer.....	8
1.5	Schematic of the optical birefringence observation with cross-polarized films.....	9
1.6	Types of liquid crystals: Nematic, smectic and cholesteric.....	10
1.7	Phase behavior of fluid dispersed rods. Reprinted with permission from ref. 32. Copyright 2004 American Chemical Society.	11
1.8	Phase behavior of CNC suspensions. (a) Sulfuric acid-synthesized CNC 9.5 % (w/v) cholesteric LC phase separation and polarized microscopy. Reprinted with permission from ref. 36. Copyright 2012 Taylor and Francis. (b) Acetic acid-synthesized CNC 8.5% (w/v) nematic LC suspended phase and polarized microscopy.....	13

List of Figures (Continued)

Figure	Page
1.9 Schematic representation of the reinforcement mechanisms for CNC composites with low aspect ratios. E = modulus; σ =strength; ϵ =elongation at break. Red color indicates poor adhesion with the matrix. *Network may form at higher concentrations; **Network may phase separate if extremely incompatible, resulting in reduction of properties. Low loads: $<\sim 10\%$; high loads: $10\%-30\%$	15
1.10 Examples of colors observed in nature due in part or completely to ordered structures. (a) Butterfly wings; (b) mantis shrimp eyes and exoskeleton; (c) peacock feathers; (d) moth eyes.....	20
1.11 End-use applications of plastics in Europe in 2011.60	22
1.12 Schematic diagram of the current industrial production of rendered material and fat separation (blue) and the proposed methods investigated in this dissertation (green)	28
1.13 Density of CO_2 as a function of pressure. Critical point: 73.8 bar and 31.1 °C. Data obtained from NIST Chemistry Webbook. 104	30
2.1 TEM micrograph of decylamine stabilized CNC-AA. Scale bar: 500 nm	56
2.2 Thermal gravimetric analysis of unhydrolyzed cellulose (solid line), acetylated CNC (long dash), acetylated CNC modified with surfactant (dash dot) and sulfuric acid synthesized CNC (dots)	57
2.3 Effect of the fraction of surfactant on the stability of CNC-AA suspensions in THF. (a) visual examination after 4 weeks; and (b) concentration of the CNC-AA supernatant (stable suspension) after 90 min of centrifugation at 29 x G where initial total concentration was 0.56% (w/v)	58
2.4 Phase separation of CNC-AA 1 wt/v% suspensions in: a) THF; b) ethyl acetate and c) chloroform.	61

List of Figures (Continued)

Figure	Page
2.5 Birefringence of CNC-AA suspensions in THF (a, b), ethyl acetate (c, d), and chloroform (e, f).....	63
2.6 Polarized microscopy of 4% CNC-AA suspensions in THF (a, b), ethyl acetate (c, d), and chloroform (e, f). Left micrographs are CNC-AA without surfactant (a, c, e) and the right micrographs are CNC-AA with surfactant (b, d, f). Length of the longer side of each image: 1.5 mm.....	64
2.7 Flow birefringence of 0.1% CNC-AA suspensions. Left micrographs: CNC-AA without surfactant (a,c,e); right micrographs: CNC-AA with surfactant (b,d,f). Solvents: (a and b) THF; (c and d) Ethyl acetate; (e and f) chloroform.....	66
3.1 TEM image of cellulose nanocrystals synthesized using acetic acid and stabilized with decylamine surfactant. Bar: 2 μ m.....	81
3.2 TGA weight loss as a function of temperature for the acetylated CNC without surfactant (solid line) and with decylamine surfactant (dashes).....	82
3.3 Mechanical Properties of PLA-CNC composites using different surfactants. \square ,UM; \bullet , -DA; \blacktriangle , -CTAB.....	84
3.4 Polarized-light microscopy images demonstrating the agglomeration level on the 3% CNC nanocomposites. a) UM; b) DA; c) CTAB. Length of the longest side of each image: 1.5mm.....	86
3.5 Polarized-light microscopy images of PLA-CNC-DA composites at different CNC loads: a, 0; b, 1; c, 3; d,5; and e, 10% CNC. At different rotating angles 0°, 45°, 90° and 135°. Images demonstrate the increasing formation of liquid crystals in the composites. Length of the longest side of each image: 1.5mm.....	87

List of Figures (Continued)

Figure	Page
3.6 Schematics of the filter orientations in the polarized-light microscope. A) polarizer (P), analyzer (A) and first order red plate (red slow direction); and B) colors observed when liquid crystals are oriented in the corresponding angles of rotation.....	88
3.7 Polarized-light microscopy images of the 3% CNC loaded nanocomposites using a first order red filter; a, neat PLA; b, UM; c, DA; d, CTAB. At 0°, 45°, 90° and 135° rotation angles. Length of the longest side of each image: 1.5mm	90
3.8 Crystallinity of PLA-CNC composites estimated by DSC. □, -UM; ●, -DA; ▲, -CTAB	93
3.9 Example of the transparency of PLA-CNC-DA composites	94
4.1 Mechanical properties of PLA and PLA-PAA CNC nanocomposites. (a) toughness, (b) tensile strength; and (c) tensile modulus.	108
4.2 Crystallinity of PLA and PLA-PAA loaded with CNCs; Xc obtained from the first run DSC curves.	110
4.3 Second run DSC scan curves of PLA (a) and PLA-PAA (b) loaded with cellulose nanocrystals. The plots are offset for clarity.....	111
4.4 Polarized-light microscopy of PLA (a and b) and PLA-PAA (c and d) loaded with cellulose nanocrystals. (a and c) 1%; and (b and d) 3% CNC loaded nanocomposites. Length of the longer side of each image: 1.5 mm.....	113
4.5 Polarized-light microscopy PLA (a and b) and PLA-PAA (c and d) loaded with cellulose nanocrystals using a first order red filter. (a and c) 1%; and (b and d) 3% CNC loaded nanocomposites. Dotted squared in the picture represents the size of the area used for the color quantification. Length of the longer side of each image: 1.5 mm.....	115

List of Figures (Continued)

Figure	Page
4.6 Mechanical properties of PLA-PAA/PEG blends. (a) toughness, (b) tensile strength; and (c) tensile modulus.....	117
4.7 Second run DSC curves of PLA-PAA/PEG blends.....	118
5.1 Schematic diagram of the semi-batch liquid and supercritical extraction.....	131
5.2 Fat extraction curves. (a-c) Fat content in rendered poultry meal after extraction and (d-f) extraction yields as a function of the amount of CO ₂ . (a and d) Liquid CO ₂ at 25°C; (b and e) supercritical CO ₂ at 40°C; and (c and f) supercritical CO ₂ at 50°C. □, 69 bar; ○, 103 bar; ◆, 138 bar; ●, 207 bar; ■, 276 bar; ▲, 345 bar. 131	131
5.3 Solubility of fat at different liquid CO ₂ flow rates with pressures of □, 69 bar; ○, 103 bar; ◆, 138 bar; and ●, 207 bar; corresponding to CO ₂ / RM ratios of 80, 60, 40 and 20, respectively.	135
5.4 Optical Microscope image of RM. Scale bar: 100 μm. (a) Before the CO ₂ extraction; and (b) After CO ₂ extraction.....	136
5.5 Solubility dependence of (a) pressure and (b) density. ■, 25 °C; ●, 40°C; ▲, 50°C	139
5.6 Plot of $\ln c$ vs $\ln d$ using Chrastil model for the experimental data at pressures between 69 and 345 bar and temperatures: ■, 25 °C; ●, 40°C; ▲, 50°C. Lines represent the results from the Chrastil model: —, 25 °C; -·-·- 40°C; --, 50°C.....	141

List of Figures (Continued)

Figure	Page
6.1 Schematic diagram of the CO ₂ assisted mechanical expression of rendered materials. (1) Hydraulic Ram; (2) Piston assembly; (3) Upper Cylinder; (4) Heating tape; (5) Rendered Material; (6) Sieve Plate and 10 μm frit filter; (7) Lower Cylinder; (8) Collection Chamber; (9) Cylinder Stand; (10) Inlet CO ₂ valve; (11)Outlet CO ₂ /lipid valve; (F) Mechanical Force gauge; (P) Pressure sensor; (T) Thermocouple.	152
6.2 Effects of the equilibrium time (●) and pressing time (○) on the extraction yields of rendered fats.....	154
6.3 Extraction curves at different CO ₂ pressures and 40°C as a function of effective mechanical pressure. (a) Extraction yields and (b) fat contents after extraction. Δ, 0 bar; ◆, 69 bar; □, 103 bar; ▲,172 bar; ○, 241 bar.	156
6.4 Temperature effect on the extraction yield at different pressures.◆, 103 bar; □, 172 bar; ▲, 241 bar.....	157
7.1 Degree of flocculation of CNC suspension at different concentrations. (a) CNC-OH and (b) CNC-AA.....	163
7.2 Birefringence of CNC-HCl (a) and CNC-AA (b) suspensions in 2mm path length cuvettes between cross polarized films indicating the formation of liquid crystals.....	164
7.3 Polarized microscopy of CNC-HCl suspensions, displaying bright phases and agglomerates (white dots). Length of the longest side of each image: 1.5mm	166
7.4 Picture of the CNC films deposited over silicon wafers.....	167
7.5 Overlapping layers of nanocomposites of PLA and 10% DA-modified CNCs showing optical properties (a) normal light, and (b) between crossed polars.....	168
7.6 PLA with 10% CNCs modified with DA rotated between crossed polars at 0°, 45°, and 90°.	168

List of Figures (Continued)

Figure	Page
7.7 Low magnification polarized-light microscopy of the nanocomposites of PLA with 10% CNCs showing colored optical properties.....	169
7.8 PLA composites films with unmodified CNCs (a); DA-modified CNCs (b); and CTAB-modified CNCs (c).	170
A.1. Polarized Microscopy of CNC-AA-DA suspensions in THF at different concentrations: a) 0.5%, b) 1%, c) 2%, d) 3%, e) 4%, f) 5%.	183
A.2. Polarized Microscopy of dried CNC films over glass slides. Top micrographs: Plain CNC-AA; bottom micrographs: CNC-AA using surfactant. Solvents: (a and d) THF; (b and e) Ethyl acetate; (c and f) chloroform.	183
A.3. Polarized microscopy of PLA-CNC-DA films at different CNC loads using a first order red plate (5% and 10% were not presented in Chapter 3)	184
A.4. Polarized microscopy of PLA-CNC films with and without surfactant at 1 and 3% CNC loads using a first order red plate.....	185
B.1. Set-up for the synthesis of CNC-HCl and CNC-AA	186
B.2. Polarized microscope parts	189
B.3. Rotating stage of polarized microscope	190
B.4. Screenshot of selected area for image analysis of films and window to adjust the color levels.....	192
B.5. Selected area with the level adjusted automatically.	193
B.6. Screenshot of the color range selection window.....	194
C.1. Fat content in meat and bone meal after CO ₂ extractions (c=solubility)	197

List of Figures (Continued)

Figure	Page
C.2. Fat content in feather meal after CO ₂ extractions (c=solubility)	197
C.3. Fat content in blood meal after CO ₂ extractions (c=solubility)	198
C.4. Fat content in sludge after CO ₂ extractions at different pressures	198
D.1. Example of the absorbance of CNC-OH suspensions	200
D.2. Calibration curve for CNC-OH suspensions at low concentrations.	201
D.3. Calibration curve for CNC-AA suspensions at low concentrations.	201
D.4. Concentration of the top phase of phase separated CNC-OH suspensions.	202
D.8. Top phase volume of various CNC-OH suspensions.	202
D.5. Concentration of the bottom phase of various CNC-OH suspensions obtained based on the top concentration and the separated bottom phase volume at each concentration.....	203
D.6. Concentration of the top phase of phase separated CNC-AA suspensions.	203
D.9. Top phase volume of various CNC-AA suspensions.	204
D.7. Concentration of the bottom phase of various CNC-AA suspensions obtained based on the top concentration and the separated bottom phase volume at each concentration.	204
D.10. Atomic force microscopy of CNC-SA, CNC-AA and CNC-OH films over silicon wafers.....	205

CHAPTER ONE

INTRODUCTION AND BACKGROUND

The technological and industrial developments of the last half century have led to an increasing consumption of resources and generation of waste, impacting the sustainability for the future generations.¹ This situation has raised awareness among governments, businesses and research institutions, all of which have increasingly invested more resources in sustainable development. In particular, the area of plastics and materials has taken an important role in this philosophy of sustainability and green chemistry by focusing on a wide variety of new bio-based materials for advanced and commercial applications.^{2, 3} These types of materials are derived from or composed totally or partially by biological matter derived from biomass,⁴ meaning they are produced from renewable resources and are generally regarded as biodegradable, biocompatible, and exhibit low toxicity as they degrade.⁵

Bio-based materials are of interest not only because of the interest on sustainable materials, but also because of their potential application in the fabrication of novel advanced functional materials.⁶ Such advanced materials must possess a combination of properties that can outperform conventional materials. These characteristics range from common mechanical and thermal properties (strength, toughness, density, thermal degradation) to novel properties including shape memory, optical properties, stimuli-responsiveness, and others. Among these materials, biopolymers such as cellulose and

polylactic acid, which are widely known for various applications, represent a focus of the current research.

Cellulose Nanocrystals

Cellulose is the most abundant biopolymer on earth and is produced by plants, trees, bacteria, and animals, such as tunicates, via the condensation polymerization of glucose.⁷ It is a polycarbohydrate composed of a series of cellulose units, formed by two anhydroglucose subunits as shown in Figure 1.1, and it has the unique property that it cannot be synthesized from or hydrolyzed into monosaccharides.⁸ This unique property is a result of the structure of the cellulose and its intricate hydrogen bond network, which prevents this biopolymer from melting or dissolving in common solvents.⁹ This network is also responsible for the high mechanical properties of cellulose that are important for its function in nature, as well as making it suitable for composite reinforcement applications.⁸

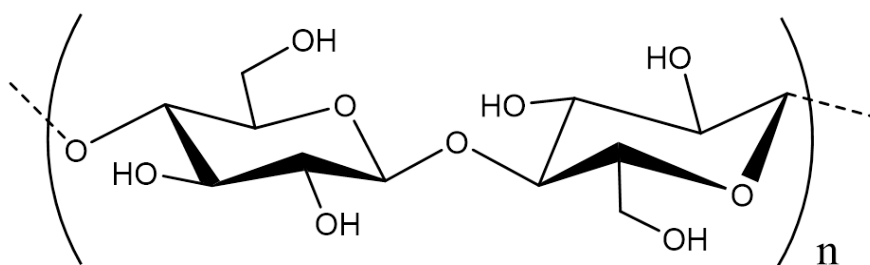


Figure 1.1. Chemical structure of cellulose.

Since its discovery in 1832, the physical and chemical properties of cellulose have been widely studied,¹⁰ leading to a current worldwide production in excess of 10^{10} tons each year, primarily used in paper, textile, materials and chemical industries.¹¹ However,

it was not until approximately 60 years ago that stable colloidal dispersions of crystalline cellulose were first reported and identified as needle-shaped.^{12, 13} The first investigation of this cellulose as a reinforcement material was published in 1995,¹⁴ leading to an area of increasing research interest in the advanced bio-based materials field.⁸

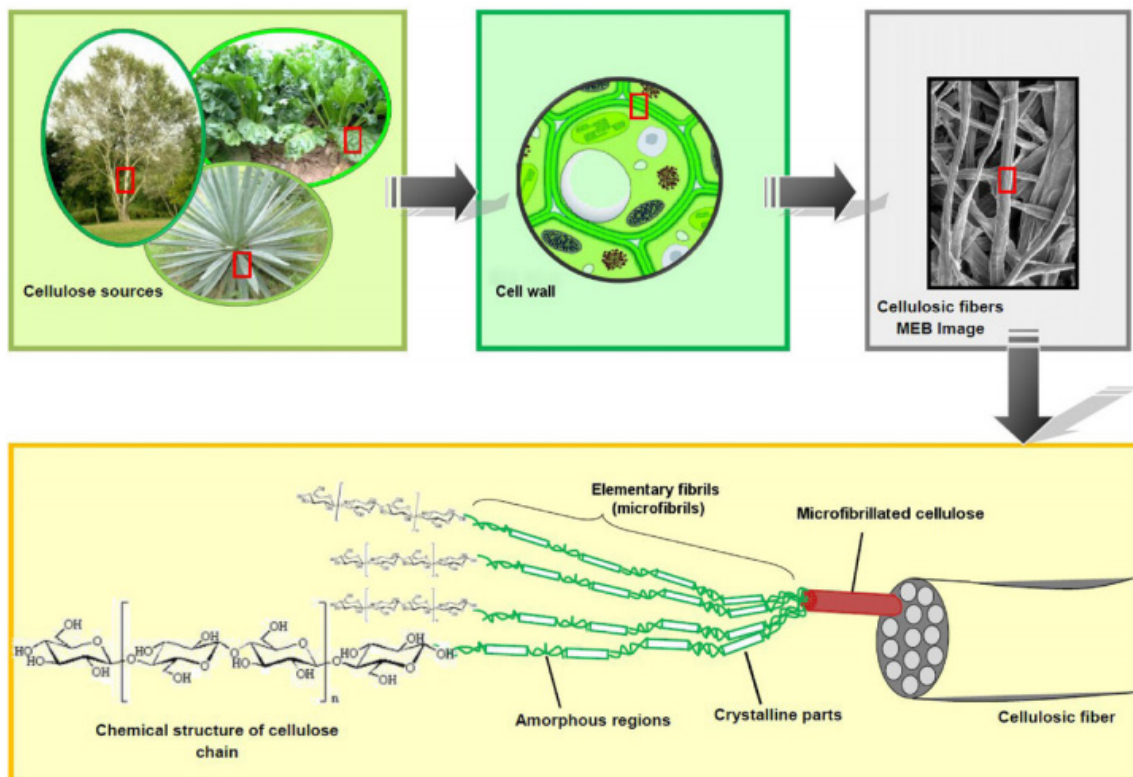


Figure 1.2. Schematic representation of the structure of cellulosic materials: from the cellulose sources to the cellulose molecules. Reprinted with permission from ref 11. Copyright 2012 Elsevier.

These needle-shaped particles, which exhibit high crystallinity, are isolated usually through acid hydrolysis, removing the amorphous cellulose regions from the elementary units, or microfibrils, which form the so-called microfibrillated cellulose as observed schematically in Figure 1.2.¹¹ These microfibrillated fibers form a larger pack called cellulosic fiber, which also forms the cell walls of plant matter. The dimensions of these

units are dependent on the source of cellulose (Table 1.1), ranging in values below 50 nm wide and between 35 and 3000 nm long.¹⁰ These crystalline elementary structures are also referred to as cellulose nanocrystals, nanowhiskers, whiskers, nanofibers or microcrystallites,⁷ and for the purpose of this research they will be referred to as cellulose nanocrystals (CNCs).

Table 1.1. Dimensions of CNC from different sources.¹⁰

Cellulose Source	Length (nm)	Width (nm)
Bacterial	100 – 1000	10 - 50
Cotton	150 – 210	5 - 11
Microcrystalline cellulose	35 – 265	3 - 48
Ramie	150 – 250	6 - 8
Sisal	100- 500	3 - 5
Soft Wood	100 – 150	4 - 5
Hard Wood	140 – 150	4 - 5
Tunicate	1000 – 3000	15 - 30
Tunicate	---	8.8 x 18.2
Valonia	>100	14 - 18

CNCs have received significant research attention due to their low toxicity, abundance, and renewability, but more importantly, due to their high strength (10 GPa),¹⁵ high modulus (143 GPa),¹⁶ and low density (1.6 g/mL). CNCs have a higher elastic modulus than Kevlar and higher tensile strength than steel wire, while having only a fraction of the weight (Table 1.2).¹⁷ As a result of these properties, CNCs have significant potential as reinforcement fillers for nanocomposites; however, the proper surface functionalization has to be conducted to make them compatible with the matrices.

Table 1.2. Mechanical properties of several reinforcement materials and crystalline cellulose.¹⁷

Material	ρ (g/cm³)	σ_f (GPa)	E_A (GPa)
Kevlar-49 Fiber	1.4	3.5	124-130
Carbon Fiber	1.8	1.5-5.5	150-500
Steel Wire	7.8	4.1	210
Clay Nanoparticles	---	---	170
Carbon Nanotubes	---	11-63	270-950
Boron nanowhiskers	---	2-8	250-360
Crystalline Cellulose	1.6	7.5-7.7	110-220

ρ = density, σ_f = tensile strength, E_A = tensile modulus in axial direction.

CNC Preparation and Surface Functionalization

Native cellulose is hydrophilic due to the abundance of hydroxyl groups on its surface and furthermore the intermolecular forces between CNCs are significant. Therefore, the appropriate isolation and surface modification has to be conducted to increase the CNC dispersion forces (steric or electrostatic) in solution or compatibility with other matrices (hydrophilic or hydrophobic). CNCs are primarily isolated through controlled acid hydrolysis from a variety of sources as exemplified in Table 1.1. This reaction involves a rapid protonation of glucosidic oxygen by protons from the acid (Figure 1.3), which will preferentially hydrolyze the amorphous regions of the cellulose fiber due to a better accessibility compared to the crystalline regions.¹⁰

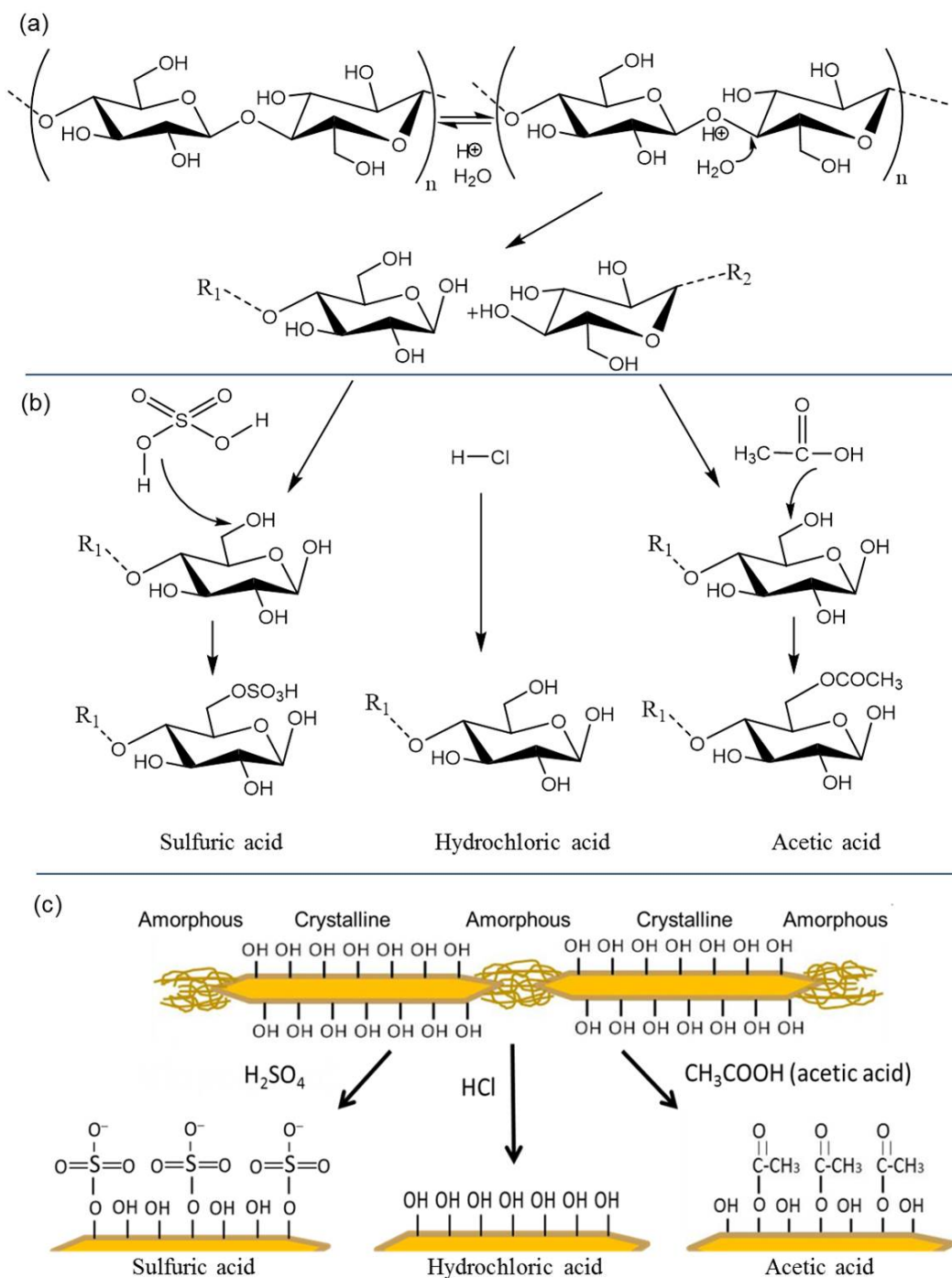


Figure 1.3. Schematic representation of the isolation of CNCs by acid hydrolysis using sulfuric, hydrochloric, and acetic acid. a) Hydrolysis mechanism; b) esterification of cellulose surface; and c) macro-scale representation of the CNC isolation from pure cellulose, showing the crystalline and amorphous regions.

The functionality of the CNCs is initially determined by the nature of the reactant used for this isolation as observed in Figure 1.3. For instance, isolation with sulfuric acid, one of the most common in the literature, introduces charged sulfate groups,¹⁸ while synthesis with hydrochloric acid (HCl) yields hydroxyl groups on the surface.¹⁹ These two modifications do not reduce the hydrophilicity of CNCs; however, other methods such as the reaction with acetic acid will reduce hydrogen bonding and thus also the hydrophilicity. This method proposed by Braun and Dorgan,²⁰ which is based on a Fisher esterification, is a one-step hydrolyzation that combines a carboxylic acid (acetic acid) with a small amount of an acid catalyst such as hydrochloric acid. This reaction produces acetylated CNCs that can be dispersed in water and some organic polymers.

Surface modification of CNCs is challenging to alter only the surface of the crystals, thus preserving their morphology and integrity. Many successful surface modifications have been reported in the literature, such as silylation, polymer grafting, acetylation, oxidation and non-covalent modification including the absorption of surfactants.¹⁰ A widely known modification is the TEMPO (2,2,6,6-tetramethylpiperidine-1-oxyl radical)-mediated oxidation, which is a reaction that introduces negatively charged carboxyl entities ($-O-COO^-$) according to the mechanism shown in Figure 1.4, and induces electrostatic stabilization of CNCs in water.²¹⁻²³ However, CNCs obtained using this method and sulfuric acid synthesis exhibit low thermal stabilities, a disadvantage for the melt processing of polymer nanocomposites.²⁴⁻²⁶ For this reason, there is the need for alternative modifications that do not compromise the morphology and thermal stability of CNCs.

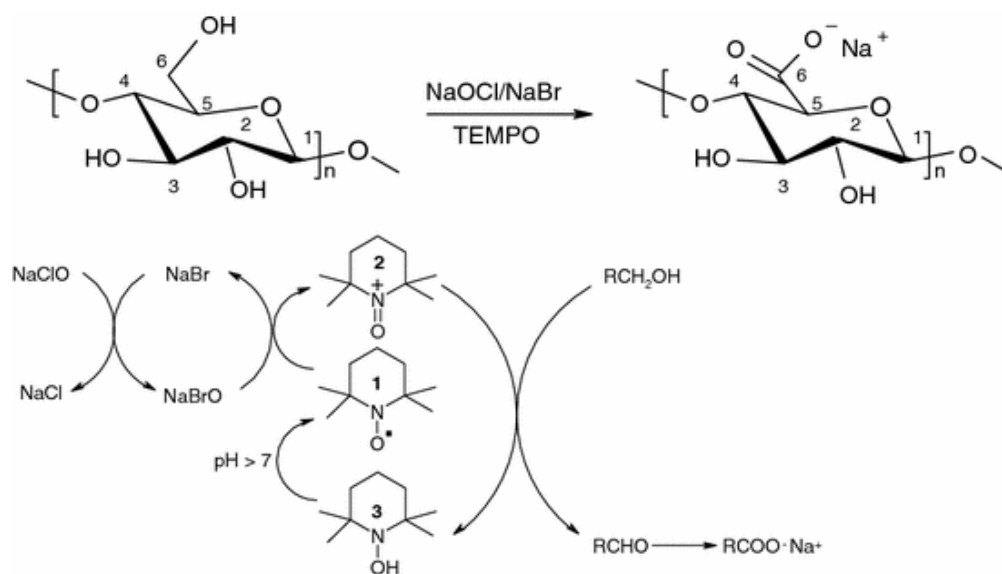


Figure 1.4. Reaction mechanism of the TEMPO-mediated oxidation of CNCs. Reprinted with permission from ref. 23. Copyright 2008 Springer.

The addition of surfactant is another feasible option among these possibilities due to the simplicity of the addition and the inalterability of the CNC structure. The use of surfactants coupled with an alternative isolation method that maintains the CNC thermal properties, such as acetylation using acetic acid,²⁰ are used in this work.

Optical Properties and Self-assembly of Cellulose

It is well-known that rod-shaped particles spontaneously self-assemble to form ordered anisotropic structures or liquid crystals (LC) above a critical concentration.²⁷ In the case of CNC suspensions, display of birefringence was first observed by Marchessault et al. in 1959,²⁸ but it was not until the early 1990s that Revol et al.²⁹ observed the chiral nematic structure of sulfuric acid synthesized CNCs.

A birefringence (“bi” refraction) can be observed when light passing through a LC material is refracted into two rays traveling at different velocities. These rays vibrate parallel to the axes of the LC (n_1 and n_2) and at right angles of each another (Figure 1.5). When a birefringent or anisotropic material is placed between cross-polarized films, the vibrating rays are filtered in the direction of the second polarizer (also called the analyzer), resulting in a retardation effect between the rays displayed as a bright or colored phase. Often, a retardation filter is inserted between the sample and the analyzer to study the specific orientation of the axis of the LC. A first order (full wave) plate introduces a relative retardation of one wavelength, allowing visibility of the colors blue and yellow for LC material oriented at 45° and -45° , and magenta for the $0, 90^\circ$ and disoriented material.

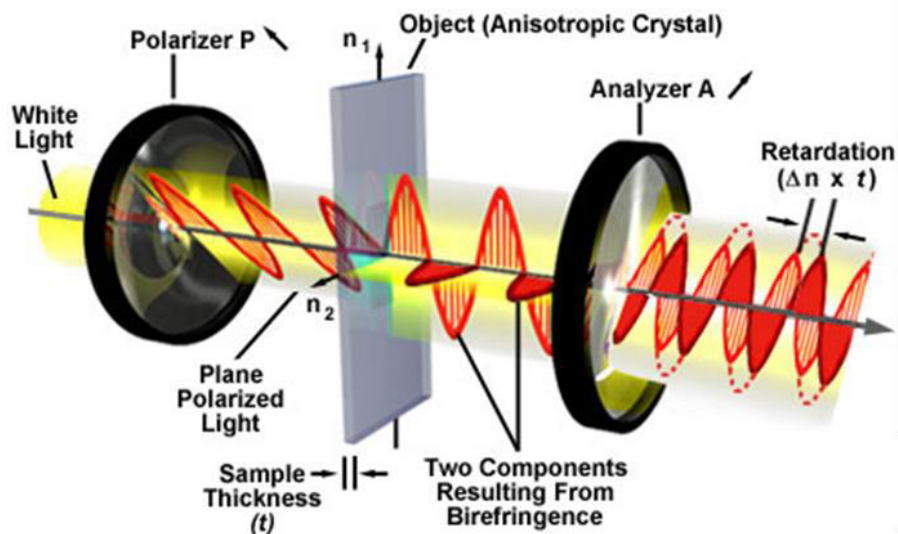


Figure 1.5. Schematic of the optical birefringence observation with cross-polarized films.³⁰

The formation of LCs, among other factors, is an indication of a good CNC dispersion in and compatibility with solvents or polymer matrix, resulting in interesting optical and structural properties.^{31, 32} LCs are structures that can flow as a liquid but have the order of a solid. There are two main types: thermotropic, for which the order is altered by temperature; and lyotropics, which are formed in suspensions and their organization is affected by concentration and temperature.³² LCs are also classified depending on their structure as (i) nematic, (ii) chiral nematic, or cholesteric, and (iii) smectic. The first is characterized by the orientation of the rods along a director; the second is the nematic structure twisted along an axis perpendicular to the director, and the third exhibits both a directional and positional order as seen in Figure 1.6.

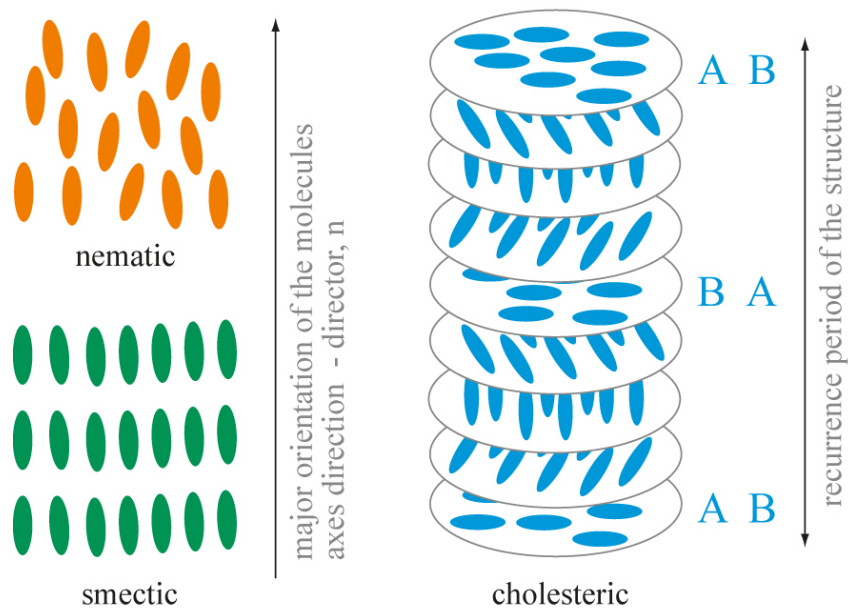


Figure 1.6 Types of liquid crystals: nematic, smectic and cholesteric.³³

The formation of lyotropic LC phases occurs at a certain critical CNC volume concentration (Φ_1), which is dependent of both the nanocrystal aspect ratio (length to diameter) and solvent quality.³² At dilute concentrations, the nanocrystals move freely in the solvent; however, increasing concentration inhibits their movements as depicted in the schematic in Figure 1.7. When a certain critical concentration is reached, some of the CNCs form an anisotropic phase in equilibrium with an isotropic one to form a biphasic system in equilibrium. As the concentration continues to increase, the suspension becomes fully anisotropic at a second critical concentration (Φ_A). However, in some cases, the viscosity of the suspensions increases rapidly with the concentration, reducing phase separation rate and inhibiting the formation of the full anisotropic LC phase.³¹ This effect is commonly observed for the stable suspensions of CNCs lacking electrostatic repulsions, as in the case of acetylated CNCs as shown in Figure 1.8.

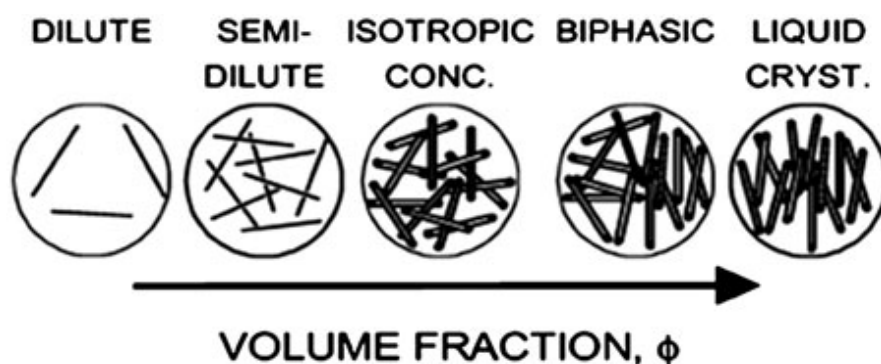


Figure 1.7. Phase behavior of fluid dispersed rods. Reprinted with permission from ref. 32. Copyright 2004 American Chemical Society.

Sulfuric acid synthesized CNCs are known to exhibit excellent colloidal stability and readily organize into chiral nematic phases, which are considered to be the most

organized structure.^{29, 34} This type of assembly is revealed by the appearance of “fingerprint” patterns observed under polarized microscopy, due to optical rotatory power and the helicoidally packing of the CNCs.^{7, 10} It was initially believed this chiral nematic behavior occurred only in the presence of surface charges.²⁹ However, it was later found that this LC phase was achieved in toluene by screening out the surface charge via the addition of surfactants.³⁵ This modification resulted in better packing than for sulfate-charged CNCs in water probably due to the attractive forces between the solvent and the cellulose. It was later confirmed that the origin of this spontaneous self-assembly was due to the helicoidal structures of CNCs, which are also observed in cellulosic materials in nature.¹⁰ On another hand, when the cholesteric phase is not reached, a nematic lyotropic suspension is often observed perhaps due to the reduced interfacial interactions, CNC morphology and the increased viscosity of the suspension. These two scenarios are depicted in Figure 1.8. Further research in this phase behavior in organic solvents is important in order to diversify the use of CNCs, more specifically in the nanocomposites field where many polymers are compatible with organic solvents.

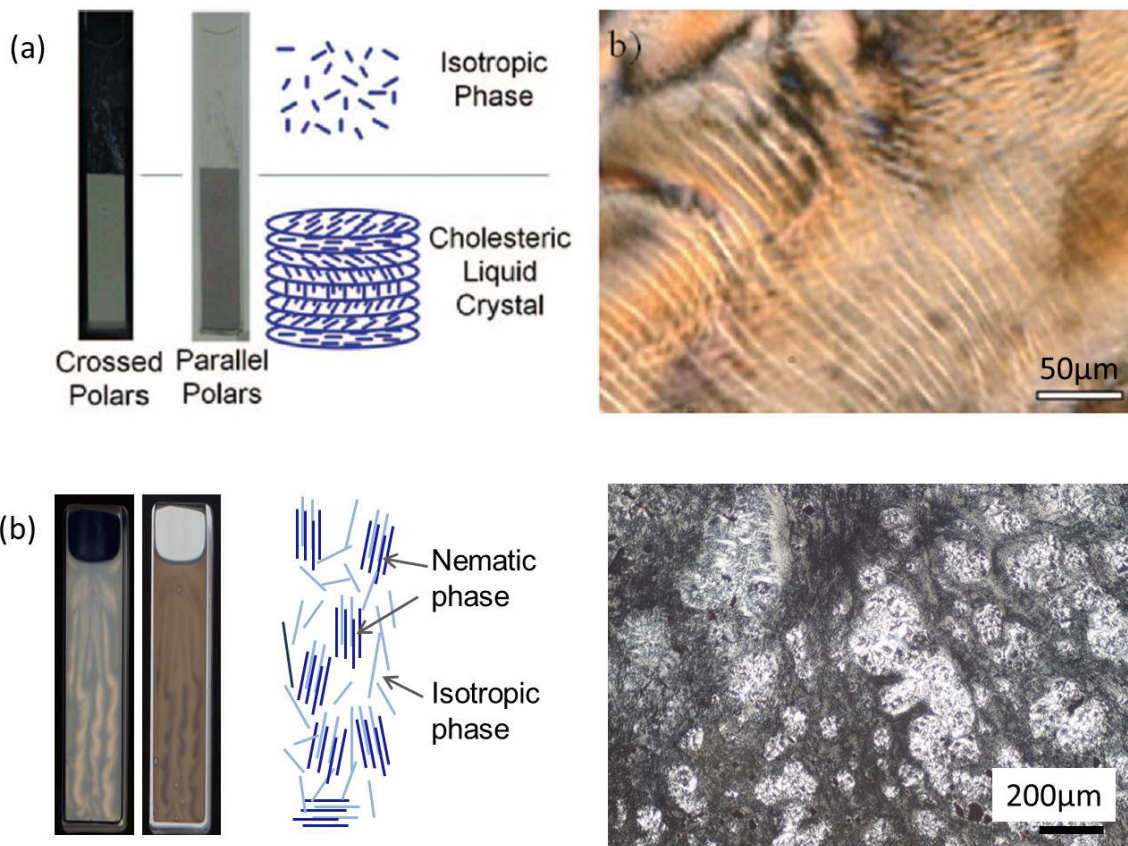


Figure 1.8 Phase behavior of CNC suspensions. (a) Sulfuric acid-synthesized CNC 9.5 % (w/v) cholesteric LC phase separation and polarized microscopy. Reprinted with permission from ref. 36. Copyright 2012 Taylor and Francis. (b) Acetic acid-synthesized CNC 8.5% (w/v) nematic LC suspended phase and polarized microscopy

Cellulose Nanocrystals as a Reinforcement Filler

The first fiber-reinforced materials were developed at the beginning of the 1900s using cellulose in phenolic and urea.³⁷ However, it was not until 20 years ago that the first investigation using nanocellulose for polymer reinforcement was proposed by Favier et al.¹⁴ Since then, much research attention has been placed on exploring the reinforcing mechanisms, cost-effective production, broadening the range of applications, and

developing modifications to take advantage of the excellent mechanical properties of cellulose.^{2, 8, 38-41}

The advantages of using cellulose nanocrystals over other nanorod fillers, such as carbon nanotubes and nanoclays, include the attractive mechanical properties of the CNCs as presented previously in Table 1.2, as well as the renewability, biocompatibility, biodegradability and abundance of cellulose.^{2, 8, 39, 40, 42} However, nanocellulose may not be able to compete with nanoclays and carbon nanotubes in some areas of application. For example, carbon nanotubes have shown to increase, among other properties, the flame retardation and electromagnetic shielding of nanocomposites, which are of interest for a variety of applications from consumer electronic devices to security products.⁴² For nanoclay composites, their increased UV protection and gas and vapor barrier properties provide to this filler an advantage in the food packaging fields.⁴³ Although previous research in this area has demonstrated the ability of CNC to reduce gas permeability,⁴⁴ nanoclays have been found to be more effective for polymers than nanocellulose fillers.⁴⁵ CNCs can provide such added advantages as good transparency and optical properties, both of which are advantageous properties in the packaging field, as well as for electronic devices including displays, solar cells and organic light emitting diodes.^{42, 46} Furthermore, cellulose biocompatibility and biodegradability increase potential applicability in the biomedical and tissue engineering fields.⁴⁷

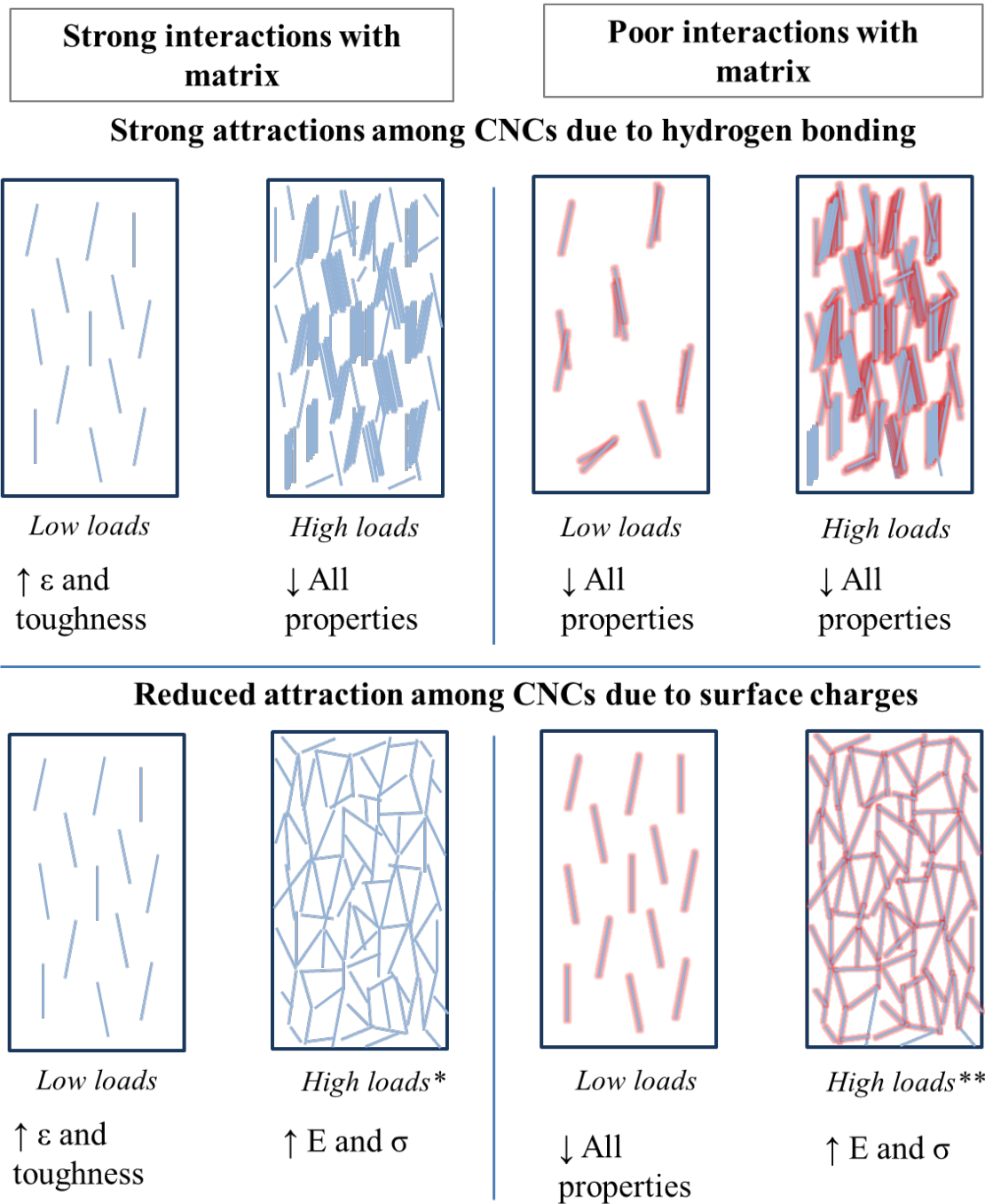


Figure 1.9 Schematic representation of the reinforcement mechanisms for CNC composites with low aspect ratios. E= modulus; σ =strength; ϵ =elongation at break. Red color indicates poor adhesion with the matrix. *Network may form at higher concentrations; **Network may phase separate if extremely incompatible, resulting in reduction of properties. Low loads: $<\sim 10\%$; high loads: $10\%-30\%$

Reinforcement Mechanisms

The mechanical properties of CNC composites vary depending on a number of factors such as functionality, polydispersity, nanocrystal morphology, and the processing conditions.¹⁰ The two possible mechanical enhancements produced by CNCs reported in the literature are on one hand the strength and modulus, and in the other the elongation at break and toughness.⁸ The reinforcement mechanisms for each case seem to be dependent, among other variables such as the viscoelasticity of the polymer,⁴⁸ on the filler-filler and filler-matrix interactions as illustrated in Figure 1.9.

Influence of CNC functionality

Tensile strength and elastic modulus typically increase at high CNC filler concentration (>~10% depending of the aspect ratio) due to a percolation network formed.⁸ The percolation is a statistical theory that applies to species that are likely to connect with one another. The goal of this theory is to predict the behavior of this set of objects by taking into account various parameters such as particle interaction, orientation, and aspect ratio.⁴⁹ The concentration at which the percolation network forms is referred to as the percolation threshold or the critical percolation volume fraction (X_{PN}). This concentration depends mainly on the aspect ratio of the fillers, but is also influenced by the filler-matrix interactions. Favier et al.⁵⁰ proposed an equation to estimate this volume fraction for cylindrical-shaped particles as a function of their aspect ratio, $X_{PN}=0.7/A$, where $A=L/w$ (length/width). As an example, CNCs with an average length of 250 nm and width of 30 nm, begins the network formation at approximately 8.4 vol.%.

If the percolation network is formed for CNCs, the strong filler-filler interactions, resulting from the hydrogen bonding of the cellulose, are responsible for the stress transfer, increasing the strength and modulus even when low filler-matrix interactions exist.¹⁰ However, CNCs with only hydroxyl groups on the surface tend to form agglomerates due to the strong attractive interactions. In contrast, partially surface-charged CNCs have shown to exhibit good balance between electrostatic repulsion and hydrogen bonding for the percolation network to form without significant agglomerations. On the negative side, composites with this reinforcement mechanism exhibit reduced toughness due to the rigid nature of both CNCs and the percolation network.

However, if the filler-matrix interactions are of the same order or stronger than the filler-filler interaction, an enhancement of the elongation at break and toughness of composites at low filler contents is usually observed.¹⁰ At higher concentrations (~5%), this reinforcement effect can decrease due to the formation of agglomerates,^{51, 52} which is an effect that has been attributed to a lack of surface charge.⁵³ This behavior is primarily observed in hydrophobic composites since steric repulsions are required for improved compatibility, rather than electrostatic interactions. For surface-charged particles, toughening can occur at higher concentrations (10-15%) without agglomerations but before the critical percolation network. Many theories have been proposed explaining the toughening of polymers with rigid nanorods. Among these are the formation of microvoids,⁵⁴ crack bifurcation and crack path alteration,⁵⁵ interfacial debonding,⁵⁶ and

shear yielding resulting from the difference between the Young's moduli of the filler and the matrix.⁵⁷

Influence of the CNC morphology

As shown in Table 1.2, the modulus of CNC is much higher than other fillers and polymeric materials. Therefore, it is expected that the modulus of the nanocomposites may also be increased. The modulus enhancement depends significantly on the aspect ratio of the filler and on the strong filler-matrix interactions, resulting in an efficient stress transfer. According to the Halpin-Tsai model,⁵⁸ only nanorods with aspect ratios larger than 50 can guarantee an efficient reinforcement effect on the composites. CNC aspect ratios vary depending on the source and the type of synthesis as presented in Table 1.1. As this table shows, the aspect ratios for most nanocrystals are less than 40, indicating that the addition of CNCs may not have a significant impact on the modulus of the composite at low concentrations.

The nanofiller morphologies are determining factors in the enhancement of nanocomposites mechanical properties. Recent studies have demonstrated that higher aspect ratios, or nanofibers compared to nanocrystals, can increase the three properties of tensile strength, modulus and toughness.^{56, 59} The increase of the modulus was attributed to the long aspect ratios with strong filler-matrix interactions that effectively transferred the stresses. On the other hand, higher tensile strength and elongations at break were attributed to relatively dispersed entanglements (below 7%) that were shown to bridge and craze at multiple locations, thus dissipating the energy at break. However, for the

same functionality, nanocrystals were shown to increase the elongation at break more than the nanofibers.⁵⁶

Influence of the processing method

The processing method also plays a significant role in determining the properties of the nanocomposites. Film casting with evaporation yields the best performance when the goal is to form the percolating network, since CNCs have adequate time to interconnect during this slow evaporation process. In contrast, when hot pressing is used, the high melt viscosities may reduce the random movements of CNCs, limiting the formation of the network. In addition, the shear stresses that occur during extrusion processing induce filler alignments in the matrix and further limit the interconnections of the CNCs, retarding the formation of the percolation network.⁶⁰ Therefore, in addition to considering the filler-matrix interactions and CNC morphology, the correct processing method must also be chosen to target the enhancement of specific properties.

Biomimicry

Another important parameter for the reinforcement of composites is the nanoscale structural orientation of cellulose. Previous research in our group has found that the mechanical properties can be influenced by a spiral orientation of the CNCs in the composite.³⁶ This behavior was found to be similar to the nanostructures observed in natural cellulose fibers, which also seem to control the strength and flexibility of various trees and plants.⁶¹ Studying these structure-property relationships are of significant

interest in tailoring the nanofiller assembly for the development of composites with processing-induced tunable properties.

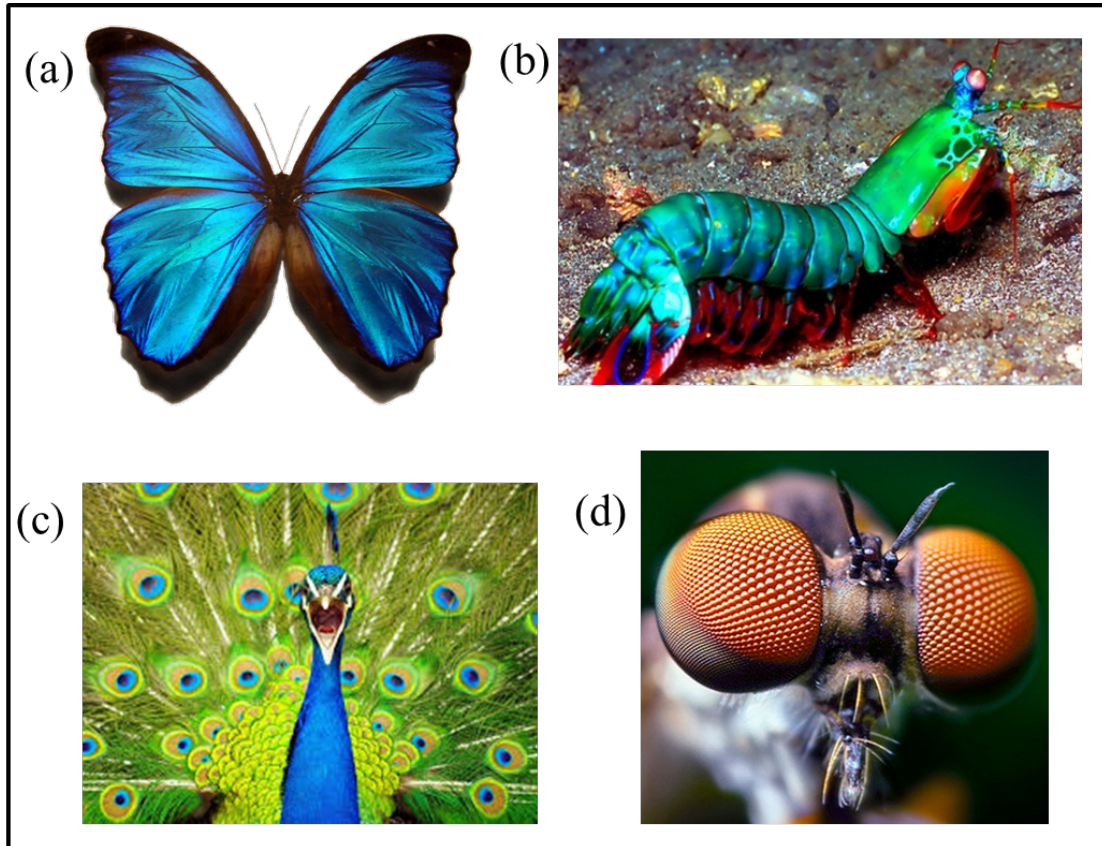


Figure 1.10. Examples of colors observed in nature due in part or completely to ordered structures. (a) Butterfly wings; (b) mantis shrimp eyes and exoskeleton; (c) peacock feathers; (d) moth eyes.

This concept of seeking motivation and insight from nature is referred to as biomimicry (from *bios*, meaning life, and *mimesis*, meaning to imitate) and includes the emulation of nature, its systems, models, processes, and elements to solve human problems. There are many every day examples of this in science, including the emulation of shark skin in the fabrication of swimming suits or the burr structure in the invention of Velcro, among others. Another interesting property that nature offers is a variety of

optical effects due to arrangements and structures of materials ranging from the nano- to macroscale level and that are produced by physical and chemical methods.⁶ Examples of these structures are presented in Figure 1.10. For instance, the colors in butterfly wings and moth eyes are produced by either thin-film interference or diffraction, both of which depend on ordered microstructures. In thin-film interference, coloration is due to alternating layers of high and low refractive index materials.⁶² This behavior is also observed in other animals such as peacocks and mantis shrimp, which is considered one of the animals best able to perceive light.

The self-assembly of CNCs has been shown to exhibit such optical properties due to the micro-scale arrangements in suspension and nanocomposites. These optical properties and structural color appear to emulate those found in nature, and therefore, it becomes important to study the structures that nature has perfected for many years and learn from them in order to design new materials with analogous properties. Some of the potential applications of these new materials can range from security papers to decorative coatings. Nanocomposites having such nanoscale structures produced with bio-based, biodegradable matrices have the potential to offer added advantages for the development of sustainable advanced materials.

Biodegradable Polymers

Although petroleum-based polymers are an invaluable invention that have revolutionized our society over the last century, a result is an annual production of approximately 280 million tons of plastic for a variety of applications (Figure 1.11).⁶³

The resistance of these synthetic polymers to chemical, physical and biological degradation has raised concerns in the medical, agricultural and environmental fields, due to the amount of waste and degradation issues. This has provided motivation for the use of and research on alternative materials that can satisfy the conditions of biodegradability, low toxicity degradation products and biocompatibility without compromising on performance.⁵

Biodegradable polymers are by definition polymeric substances susceptible to degradation through biological activity that lowers the molecular weight of the macromolecules forming the material.⁴ However, this definition has been broadened to include other polymers that undergo complete degradation by other means such as hydrolysis.

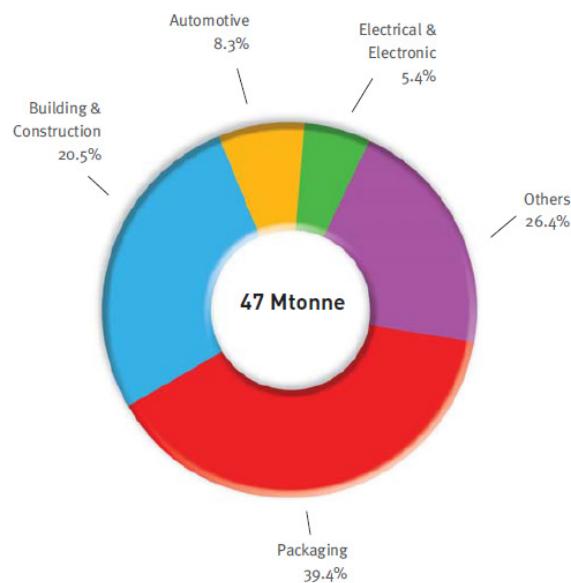


Figure 1.11. End-use applications of plastics in Europe in 2011.⁶³

The market for biodegradable polymers has been gradually increasing because of the various improvements and modifications over the last twenty years. In 2011, the production of biodegradable polymers reached approximately 490,000 metric tons, a 64% increase from the 2010 production.⁶⁴ Even though these numbers appear to be significant, the total bioplastic production only represents approximately 0.2% of the total market of synthetic plastics worldwide in 2011.⁶³ Polylactic acid is the most widely used biopolymer, accounting for 38% of the biopolymers market in the same year.⁶⁴

Polylactic Acid

Polylactic acid (PLA), a biodegradable, aliphatic polyester derived from lactic acid,⁶⁵ has received much research attention as a potential alternative to traditional petroleum-based plastics due to its high tensile strength and tensile modulus, both of which are comparable to conventional polymers such as PET (Table 1.3).⁶⁶ In addition, PLA has been confirmed to naturally degrade in soil and compost, resulting in non-toxic degradation products.⁶⁷

PLA was first developed in 1893 and was first marketed in 1954 for medical applications such as sutures and implants. The commercial production of PLA began in 1992 in Japan by Kanebo Gohsen, Ltd., under the name Lactron, followed by other countries such as France and the US. In 2002, Cargill Dow, LCC, began commercial production of PLA from starch in the USA.⁶⁹ Later in 2005, this segment of Cargill Dow became NatureWorks™, and is currently the major PLA manufacturer in the world.⁷⁰ The

approximately 187,00 tons of PLA produced worldwide are primarily used in short-lived applications such as packaging, bottles and disposable cups and plates.⁶⁴

Table 1.3. Representative properties of common petroleum-based polymer and PLA.⁶⁸

Polymer	Density	Tensile Modulus (GPa)	Tensile Strength (MPa)	Elongation at Break (%)
Polyethylene (LDPE)	0.92	0.2-0.3	8-30	100-900
Polyethylene (HDPE)	0.96	0.8-1.5	28-32	10-300
Polypropylene	0.9	1.1-1.5	25-33	50-300
Polystyrene (general purpose)	1.05	3.3-3.4	34-36	1-2
PVC (unplasticized)	1.4	2.8-3.0	50-55	60
PET	1.4	3.0	50-75	60-300
Nylon 6/6 (PA 6.6)	1.1	2.9	60-80	60-80
ABS	1.04	2.1-2.4	20-55	8
Polycarbonate	1.2	2.3-2.4	60-110	100-110
PLA	1.24	3.0-3.5	26-144	3.5-8.1

PLA offer many advantages, including i) the production through fermentation of renewable sources such as corn; ii) non-toxic degradation products and the ability to recycle back to lactic acid through hydrolysis; iii) reduction of landfill volume; iv) the ability to tailor physical properties through material modifications; v) a reduction of the manufacturing energy needed compared to conventional polymers; and vi) the reduction of net greenhouse gas emissions.⁷¹ PLA decreases the net emissions of CO₂ to the environment, which is believed to be the most important contributor to global climate change.⁷² The net greenhouse gas emission, calculated as the total emissions from the cradle to factory gate minus the CO₂ needed for the corn production, is negative for the

current PLA production.⁷³ This value is estimated to be approximately (-) 0.7 kg of CO₂ eq./kg of polymer compared to the (+) 2.0 and higher for conventional polymers.⁷⁴ In addition, its production requires 25-55% less energy than petroleum-based polymers because of its relatively lower melting temperature, resulting in important economic benefits as well.^{69, 75}

Modification of Polylactic Acid

Despite many advantages, PLA production and applications are still limited by its brittleness and low gas barrier properties.⁷⁶ To solve these problems, a number of additives and modifications have been applied to PLA in recent years such as plasticizers^{77, 78}, fillers^{41, 79} and grafted polymers.^{80, 81} Frequently, one type of modification may enhance one property but decrease another one. For instance, the addition of plasticizers is known to significantly improve the elongation at break and toughness, but it also reduces the tensile strength and modulus. Finding an appropriate combination is key for the reinforcement of the mechanical properties without the significant reduction of the others. Furthermore, retaining the biodegradable and biocompatible properties is highly desirable.

The combination of PLA with nanorod fillers has been shown to significantly increase the PLA properties needed for food packaging, medical and tissue engineering applications.⁷² Nanoclays, carbon nanotubes and cellulose nanocrystals are among the most explored materials, and as discussed before, each offers different advantages. PLA-CNC composites may exhibit advantages compared to other fillers due to complete

biodegradability, biocompatibility, and desirable optical properties, among others. CNCs have been shown to increase various properties depending on their morphology. Among these properties are tensile strength and modulus,⁸²⁻⁸⁴ toughness,⁵⁹ crystallinity,^{83, 85} and gas barrier.⁸⁶ The use of CNC in the reinforcement of PLA is still an area of opportunity and much research is needed to obtain a fundamental understanding of the structure-property relationships as well as more efficient CNC incorporation, reduction of agglomerates in the composite, and improved compatibilities.⁸⁷ New findings in the area of nanocomposites are of significant importance for the advancement of biopolymers in a very competitive polymer market.

Biomaterials Obtained from Animal By-products

Biopolymers can not only be synthesized from carbohydrates such as corn in the case of PLA, but also from proteins due to the repeating amino acid sequence.⁸⁸ Although protein-based polymers are not studied in this work, a more efficient separation of fat from proteins obtained from inedible animal parts is explored. The inedible by-products of animals are used for a variety of applications ranging from biofuels and fertilizers to consumer and industrial products: thus more efficient separations are of interest to the rendering industry.

CO₂ Extraction of Rendered Materials

Rendered materials (RM) are produced from the inedible parts of animals produced for human consumption, which constitutes one third to one half of the total animal

mass.⁸⁹ In 2009, for example, the US produced 33 million cattle, 113 million hogs, 245 million turkeys and 8.6 billion chickens for human consumption. The inedible parts were processed in more than 200 rendering plants in North America, producing approximately 18 billion pounds of RMs, composed of 52% fats and the remaining 48% representing protein meals such as meat-and-bone and poultry meals.^{90, 91} The prices of these value-added materials have increased significantly since 2006 due to higher demands in the pet food and biofuels industry.⁷⁸ For example, meat and bone meal, which has the highest meal production, increased in price by 125% between 2006 and 2011, while inedible fats increased approximately 196% in the same period.^{91, 92}

RMs are used primarily as animal feed ingredients with 85% of the total production, including a fraction of the extracted fats, used for this purpose. The rest is used in a diversity of industries with nearly 3,000 applications identified.⁸⁹ Much of the fat not used for animal feed is used in the manufacture of soaps and personal care products; however, since 2010 the biofuels industry, which has shown record production, has placed a significant demand on the fat from the rendering industry, more than doubling the amount of rendered fats used for biodiesel production and thus driving up the price.⁹²

In addition to bringing economic benefits to the meat industry, the rendering of inedible materials is also considered a green and environmentally friendly industry. This rendering process reduces the amount of waste, and recycles carbon and energy into valuable feed ingredients instead of ending in the landfills.^{91 93} The disposal and accumulation of unprocessed animal waste also represents a large source of potential

hazards for animal and public health, thus providing another significant benefit of the rendering industry.

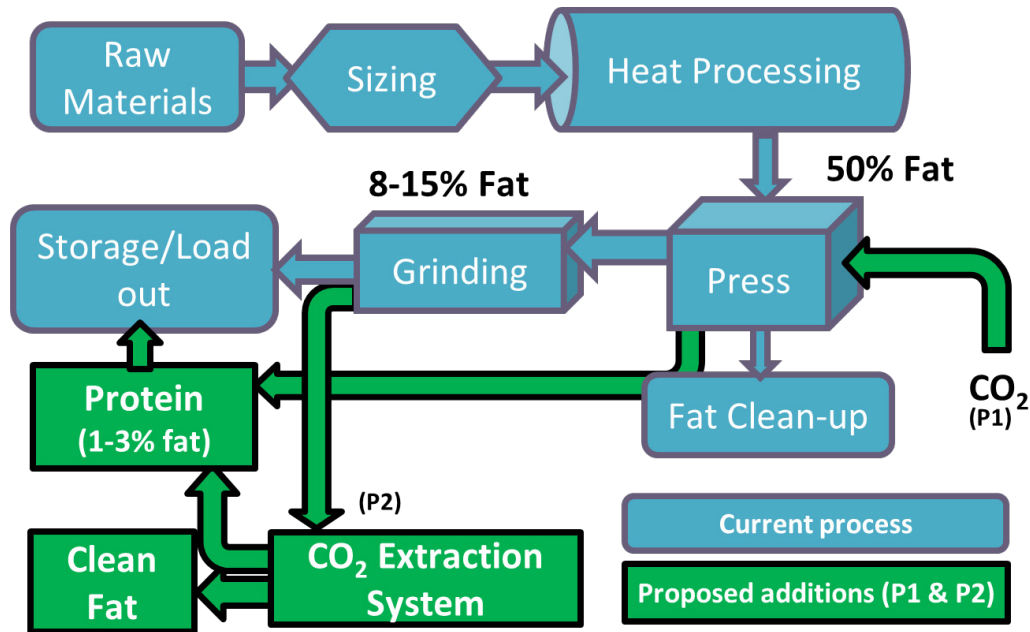


Figure 1.12 Schematic diagram of the current industrial production of rendered material and fat separation (blue) and the proposed methods investigated in this dissertation (green)

Rendering Industry Process

The current rendering process involves the application of heat, the extraction of moisture, and the separation of fat as depicted in Figure 1.12.⁹⁰ First, the raw materials are ground to a consistent size and cooked with steam at temperatures ranging from 115°C to 145°C for 40 to 90 min.⁹⁰ Moisture is boiled off, and the fat associated with the solids is then mechanically removed by screw presses while the moisture associated with the extracted fat is separated using centrifuges in the fat clean-up. The two primarily

products of this process are the fats (greases, tallow, lard and poultry fat) and the protein meals, which contain 8-15% residual fat.

Screw press separations offer the advantages of producing uncontaminated fats and low capital and operational costs, but this process has limited efficiencies, leaving valuable residual fat in the protein matrix. Extraction with organic solvents, e.g., hexane, is a well-known method for separating fats with more than 99% extraction yields, but produces low quality fat due to remaining traces of solvent, requiring refining for feed ingredients, and thus increasing costs and lowering the gate quality.⁹⁴ Developing methods to increase extraction yields of high quality fat and protein meals can bring important economic benefits to the industry, especially with the increasing demand for fat for biofuels. Moreover, these low fat content proteins can potentially broaden applications, which include organic fertilizers, protein-based polymers, and low-fat pet foods.

An alternative method attracting considerable attention for the separation of fats, oils, and other organic compounds is extraction with liquid or supercritical carbon dioxide (LCO₂ or SCCO₂).⁹⁵⁻⁹⁷ Past research has shown that SCCO₂ extraction of flaxseed oil yields approximately 28% more fat than screw expression and only 9% less than hexane extraction.⁹⁸ CO₂ has the added advantages of facile CO₂ recycling and complete fat separation with an FDA approved solvent, which leads to high-quality products for a diversity of value-added products.

Extractions with High Pressure CO₂

CO₂ is a non-toxic, non-flammable, and relatively inexpensive solvent that has been used for a wide variety of applications including separations, reactions, and materials processing.^{97, 99} For example, the use of supercritical fluids in the food industry is widely established.⁹⁹⁻¹⁰¹ The first commercial supercritical CO₂ extraction was performed in 1978 by Hag A.G in Germany to decaffeinate green coffee beans.¹⁰² Since then, commercial extractions with CO₂ have expanded to decaffeination of tea, extraction of natural colors, natural flavorings, antioxidants, nutraceuticals, and hops, as well as the extraction of lipids and cholesterol from egg yolks, milk fat, beef and pork.⁹⁹ The supercritical extraction of fats for the production of biodiesel is also a promising and expanding research area.^{96, 103}

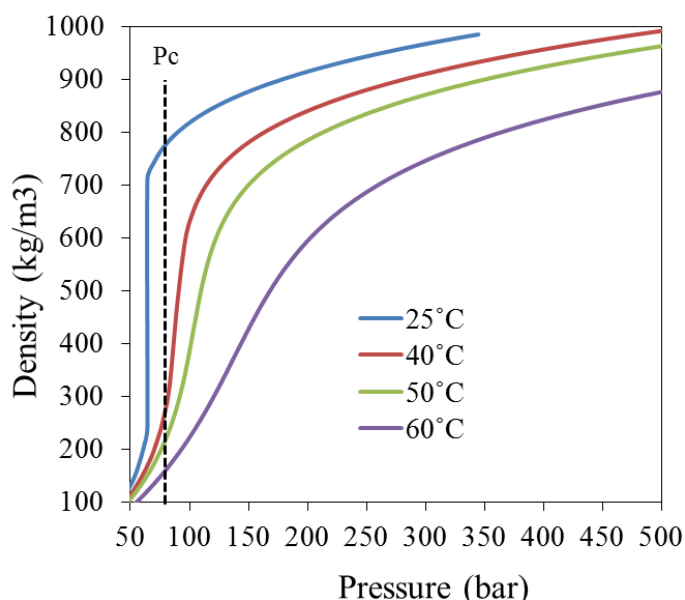


Figure 1.13. Density of CO₂ as a function of pressure. Critical point: 73.8 bar and 31.1 °C. Data obtained from NIST Chemistry Webbook.¹⁰⁴

SCCO₂ is more frequently used than LCO₂ because of the potentially better transport properties. The diffusivity of SCCO₂ is one to two orders of magnitude higher than the liquid and the viscosity is on the order of a gas. Moreover, the density of SCCO₂ is on the order of a liquid at pressures well above the critical pressure (P_c) as seen in Figure 1.13. The diffusivity and viscosity allow for better penetration throughout the matrices while the density, together with the fat volatility, determines the solubility of the fat in CO₂. However, when there are no mass transfer limitations in the systems, i.e., SCCO₂ and LCO₂ have the same power of penetration, the extraction yields are primarily controlled by the fluid density and solute volatility.

For many supercritical extraction systems, a retrograde solubility phenomenon may occur, where decreased solubility of the solute occurs at elevated temperatures for a given pressure. This phenomenon, which occurs below a pressure referred to as the “cross-over” point, is the result of reduced solvent strength caused by reduced density in the high compressibility region of the fluid (i.e., close to the critical point) as seen in Figure 1.13. The increased solute volatility due to the higher temperatures cannot compensate for the reduced solvation power due to lowered densities of certain types of solutes,¹⁰² resulting in higher solubility at the lower temperatures. This phenomenon affords the advantage of using LCO₂ at lower temperatures and pressures for extractions, a benefit for capital and operating costs as well as for the recovery of volatile and thermally labile components.¹⁰⁵

Despite the advantages, high pressure CO₂ extractions generally require a large volume of fluid because of the relatively low fat solubilities, between 0.491 to 6.474 g/L for rendering fats depending on pressure and temperature.¹⁰⁶ To further increase the extraction efficiency, a process that combines mechanical pressure with high pressure CO₂ has been shown to significantly reduce the required amount of this green solvent.⁹⁵ Gas-assisted mechanical expression (GAME) was first introduced by Venter et al. for the separation of cocoa butter.¹⁰⁷

In GAME, a gas-expanded liquid is formed by saturating CO₂ in the oil or fat, significantly reducing the viscosity of the mixture compared to pure fat.¹⁰⁸ This reduction in the viscosity allows for an increase in the expression yield compared to conventional mechanical pressing, as the fats are drained more easily through the compressed bed.¹⁰⁹ Moreover, this reduction in viscosity is also accompanied by a reduction in the energy required for the pressing process.⁹⁵ This process has been shown to have higher yields than conventional expression⁹⁵ and requires less CO₂ since the solubility of CO₂ in the oils have been observed to be up to 50% higher than the solubility of oil in CO₂.^{110, 111}

The schematic in Figure 1.12 shows schematically two proposed additions/modifications to the current rendering process for a more efficient extraction of fat based on the two methods, LCO₂ and SCCO₂ extractions (P2), and GAME (P1), which are investigated in this dissertation.

Dissertation Outline

The goal of this dissertation is to investigate the properties of new bio-based materials for the production of advanced materials with novel properties, intellectually contributing to the understanding of CNC reinforcement of conventional and bio-derived polymers. This area of CNC nanocomposites is a field of expanding opportunities, and much research is needed to obtain efficient CNC incorporation, reduction of agglomerates and improved compatibilities. The investigation of the structure-property relationships can also provide insight on the reinforcement mechanisms of these nanocomposites, all aspects covered in this work. Furthermore, in the second half of this dissertation (Chapters 5 and 6), two methods using high pressure CO₂ are reported for a more efficient and greener fat separation of rendered materials, potentially opening new areas of application for these bio-based materials with new characteristics.

As a first step, Chapter 2 reports on the surface functionalization of hydrophilic CNCs by surfactants in order to increase the compatibility with non-polar matrices. The surfactants decylamine, cetyltrimethyl-ammonium bromide (CTAB) and tetrahexyl-ammonium bromide (THAB) were investigated in different organic solvents. These surfactants have been used with other nanomaterials such as in the stabilization of gold nanoparticles,¹¹² but they have not been fully investigated for the stabilization of acetylated CNC. The goal of the surfactant is to reduce the CNC hydrophilicity for easier incorporation and enhanced compatibility with hydrophobic solvents and polymers. The dispersion stability and self-assembly of modified CNCs in these solvents were

examined, obtaining important information about the molecular interactions and the degree of stability, knowledge which may be a key for the prediction of the reinforcement of polymers upon CNCs addition.

The second step was to add the surface-modified CNCs to a biodegradable polymer to enhance its mechanical properties and to understand the effect of the CNC functionality. As discussed in this introduction, PLA is a versatile polymer with properties that need to be improved such as toughness to broaden its applications. In Chapter 3, surface-modified CNCs were compounded with PLA in concentrations between 1 and 10 wt.% and the nanocomposite mechanical properties were tested. Decylamine- and CTAB-modified CNC were used for the reinforcement of the PLA because of their good stability in organic solvents. The orientation of the CNCs on the PLA films was studied under polarized-light microscopy. The results obtained through these observations contribute to the understanding of the effect of the orientation of CNC on the mechanical properties of the composites.

To further understand the reinforcement mechanisms of CNCs and to find other alternatives for the enhancement of PLA, a stiff and more hydrophilic polymer, polyacrylic acid (PAA), was grafted onto PLA and the effects of CNC addition were investigated. These results are presented in Chapter 4 for CNC concentrations between 1 and 5 wt.% in the nanocomposite films. In addition, high molecular weight polyethylene glycol (PEG) was also added to PLA-PAA to compare the plasticizing effects obtained by using both modifying agents. Mechanical testing and polarized-light microscopy were

used again to study their properties. Differential scanning calorimetry was also conducted on these polymers obtaining their crystallinity percentage and the shift in glass transition temperature (T_g).

In Chapter 5, liquid and supercritical CO_2 were used for the extraction of the remaining fat from rendered poultry meal. This extraction offers higher efficiencies with potential ecological and economic benefits for the rendering industry. A continuous-flow extraction unit was used to investigate the effect of pressure (69-345 bar), temperature (25°C , 40°C and 50°C), flow rate, and mass of CO_2 on the extraction yield and the fat solubility. High fat extraction yields were obtained, and liquid CO_2 was observed to be more effective than supercritical CO_2 for the extraction of rendered fats under the conditions tested.

For the purpose of decreasing the amount of CO_2 used in the extraction and to better suit to the process already used in the industry, gas-assisted mechanical expression (GAME) is explored in Chapter 6. A combination of mechanical pressure (300 to 2,000 bars), temperature (25 to 100°C), and high pressure CO_2 (69 to 241 bar) were evaluated and compared to conventional mechanical expression.

Lastly, work that is currently under investigation and that has a significant potential for future research is presented in Chapter 7. The application of CNCs as a substitute of silicon for the fabrication of microelectromechanical devices is proposed, and the preliminary results are included in this chapter. In addition, PLA composites with high concentrations of CNCs were found to display a colorful birefringence when observed

between cross-polarized films, and these colors were found to vary as a function of thickness or number of film layers. These findings have potential applications for security papers, decorative coatings, and materials that required optical properties.

References

1. Goodwin N, Nelson JA, Ackerman F, Weisskopf T. Consumption and the consumer society. *Retrieved December*. 2008;15:2008.
2. Khalil H, Bhat AH, Yusra AFI. Green composites from sustainable cellulose nanofibrils: A review. *Carbohydr Polym*. Jan 2012;87(2):963-979.
3. Mohanty A, Misra M, Drzal L. Sustainable bio-composites from renewable resources: opportunities and challenges in the green materials world. *Journal of Polymers and the Environment*. 2002;10(1-2):19-26.
4. Vert M, Doi Y, Hellwich K-H, et al. Terminology for biorelated polymers and applications (IUPAC Recommendations 2012). *Pure and Applied Chemistry*. 2012 2012;84(2):377-408.
5. Luckachan GE, Pillai C. Biodegradable polymers-a review on recent trends and emerging perspectives. *Journal of Polymers and the Environment*. 2011;19(3):637-676.
6. Xia F, Jiang L. Bio-Inspired, Smart, Multiscale Interfacial Materials. *Advanced Materials*. 2008;20(15):2842-2858.
7. Eichhorn SJ. Cellulose nanowhiskers: promising materials for advanced applications. *Soft Matter*. 2011 2011;7(2):303-315.
8. Eichhorn SJ, Dufresne A, Aranguren M, et al. Review: current international research into cellulose nanofibres and nanocomposites. *Journal of Materials Science*. Vol 45; 2010: 1-33.

9. Klemm D, Heublein B, Fink H-P, Bohn A. Cellulose: Fascinating Biopolymer and Sustainable Raw Material. *ChemInform*. 2005;36(36):no-no.
10. Habibi Y, Lucia LA, Rojas OJ. Cellulose Nanocrystals: Chemistry, Self-Assembly, and Applications. *Chemical Reviews*. Jun 2010;110(6):3479-3500.
11. Lavoine N, Desloges I, Dufresne A, Bras J. Microfibrillated cellulose – Its barrier properties and applications in cellulosic materials: A review. *Carbohydr Polym*. 2012;90(2):735-764.
12. Rånby BG. Fibrous macromolecular systems. Cellulose and muscle. The colloidal properties of cellulose micelles. *Discussions of the Faraday Society*. 1951;11:158-164.
13. Battista O, Coppick S, Howsmon J, Morehead F, Sisson WA. Level-off degree of polymerization. *Industrial & Engineering Chemistry*. 1956;48(2):333-335.
14. Favier V, Chanzy H, Cavaille JY. Polymer nanocomposites reinforced by cellulose whiskers. *Macromolecules*. Aug 1995;28(18):6365-6367.
15. Azizi Samir MAS, Alloin F, Dufresne A. Review of Recent Research into Cellulosic Whiskers, Their Properties and Their Application in Nanocomposite Field. *Biomacromolecules*. 2005/03/01 2005;6(2):612-626.
16. Sturcova A, Davies GR, Eichhorn SJ. Elastic modulus and stress-transfer properties of tunicate cellulose whiskers. *Biomacromolecules*. Mar-Apr 2005;6(2):1055-1061.
17. Moon RJ, Martini A, Nairn J, Simonsen J, Youngblood J. Cellulose nanomaterials review: structure, properties and nanocomposites. *Chemical Society Reviews*. 2011;40(7):3941-3994.
18. Urena-Benavides EE, Ao GY, Davis VA, Kitchens CL. Rheology and Phase Behavior of Lyotropic Cellulose Nanocrystal Suspensions. *Macromolecules*. Nov 2011;44(22):8990-8998.

19. Araki J, Wada M, Kuga S, Okano T. Flow properties of microcrystalline cellulose suspension prepared by acid treatment of native cellulose. *Colloid Surf A-Physicochem Eng Asp.* Nov 1998;142(1):75-82.
20. Braun B, Dorgan JR. Single-Step Method for the Isolation and Surface Functionalization of Cellulosic Nanowhiskers. *Biomacromolecules.* Feb 2009;10(2):334-341.
21. Habibi Y, Chanzy H, Vignon MR. TEMPO-mediated surface oxidation of cellulose whiskers. *Cellulose.* Dec 2006;13(6):679-687.
22. Denooy AEJ, Besemer AC, Vanbekkum H. Highly selective tempo mediated oxidation of primary alcohol groups in polysaccharides. *Recl Trav Chim Pays-Bas-J Roy Neth Chem Soc.* Mar 1994;113(3):165-166.
23. Lasseguette E. Grafting onto microfibrils of native cellulose. *Cellulose.* 2008;15(4):571-580.
24. Fukuzumi H, Saito T, Okita Y, Isogai A. Thermal stabilization of TEMPO-oxidized cellulose. *Polym Degrad Stabil.* Sep 2010;95(9):1502-1508.
25. Roman M, Winter WT. Effect of sulfate groups from sulfuric acid hydrolysis on the thermal degradation behavior of bacterial cellulose. *Biomacromolecules.* 2004;5(5):1671-1677.
26. Johnson RK, Zink-Sharp A, Glasser WG. Preparation and characterization of hydrophobic derivatives of TEMPO-oxidized nanocelluloses. *Cellulose.* Dec 2011;18(6):1599-1609.
27. Onsager L. The effects of shape on the interaction of colloidal particles. *Annals of the New York Academy of Sciences.* 1949;51(4):627-659.
28. Marchessault R, Morehead F, Walter N. Liquid crystal systems from fibrillar polysaccharides. 1959.

29. Revol J-F, Bradford H, Giasson J, Marchessault R, Gray D. Helicoidal self-ordering of cellulose microfibrils in aqueous suspension. *International journal of biological macromolecules*. 1992;14(3):170-172.
30. Olympus MRC. Polarized Light Microscopy. Available at: <http://www.olympusmicro.com/primer/techniques/polarized/polarizedhome.html>.
31. Araki J. Electrostatic or steric? - preparations and characterizations of well-dispersed systems containing rod-like nanowhiskers of crystalline polysaccharides. *Soft Matter*. 2013;9(16):4125-4141.
32. Davis VA. Liquid crystalline assembly of nanocylinders. *Journal of Materials Research*. Jan 2011;26(2):140-153.
33. A. GEAAISO. Glossary of Nanotechnology and Related Terms- Liquid crystal *Rusnano*, 2013.
34. Araki J, Wada M, Kuga S, Okano T. Birefringent glassy phase of a cellulose microcrystal suspension. *Langmuir*. Mar 2000;16(6):2413-2415.
35. Heux L, Chauve G, Bonini C. Nonflocculating and chiral-nematic self-ordering of cellulose microcrystals suspensions in nonpolar solvents. *Langmuir*. Oct 17 2000;16(21):8210-8212.
36. Urena-Benavides EE, Kitchens CL. Cellulose Nanocrystal Reinforced Alginate Fibers-Biomimicry Meets Polymer Processing. *Molecular Crystals and Liquid Crystals*. 2012;556:275-287.
37. Mohanty AK, Misra M, Hinrichsen G. Biofibres, biodegradable polymers and biocomposites: An overview. *Macromol Mater Eng*. Mar 2000;276(3-4):1-24.
38. Kalia S, Dufresne A, Cherian BM, et al. Cellulose-Based Bio- and Nanocomposites: A Review. *International Journal of Polymer Science*. 2011 2011.

39. Ramires EC, Dufresne A. A review of cellulose nanocrystals and nanocomposites. *Tappi J.* Apr 2011;10(4):9-16.
40. Pandey JK, Ahn SH, Lee CS, Mohanty AK, Misra M. Recent Advances in the Application of Natural Fiber Based Composites. *Macromol Mater Eng.* Nov 2010;295(11):975-989.
41. Siqueira G, Bras J, Dufresne A. Cellulosic Bionanocomposites: A Review of Preparation, Properties and Applications. *Polymers.* Dec 2010;2(4):728-765.
42. Reddy MM, Vivekanandhan S, Misra M, Bhatia SK, Mohanty A. Biobased Plastics and Bionanocomposites: Current Status and Future Opportunities. *Prog Polym Sci.* (0).
43. Lagaron JM, Lopez-Rubio A. Nanotechnology for bioplastics: opportunities, challenges and strategies. *Trends in food science & technology.* 2011;22(11):611-617.
44. Fukuzumi H, Saito T, Wata T, Kumamoto Y, Isogai A. Transparent and High Gas Barrier Films of Cellulose Nanofibers Prepared by TEMPO-Mediated Oxidation. *Biomacromolecules.* Jan 2009;10(1):162-165.
45. Petersson L, Oksman K. Biopolymer based nanocomposites: Comparing layered silicates and microcrystalline cellulose as nanoreinforcement. *Composites Science and Technology.* 2006;66(13):2187-2196.
46. Nogi M, Yano H. Transparent Nanocomposites Based on Cellulose Produced by Bacteria Offer Potential Innovation in the Electronics Device Industry. *Advanced Materials.* 2008;20(10):1849-1852.
47. Cherian BM, Leão AL, de Souza SF, et al. Cellulose nanocomposites with nanofibres isolated from pineapple leaf fibers for medical applications. *Carbohydr Polym.* 2011;86(4):1790-1798.
48. Mathew AP, Oksman K, Sain M. Mechanical properties of biodegradable composites from poly lactic acid (PLA) and microcrystalline cellulose (MCC). *Journal of Applied Polymer Science.* 2005;97(5):2014-2025.

49. Kechrakos D. Handbook of Nanophysics: Nanoparticles and Quantum Dots, edited by K. Sattler. Taylor & Francis, Honolulu; 2010.
50. Favier V, Canova GR, Shrivastava SC, Cavaille JY. Mechanical percolation in cellulose whisker nanocomposites. *Polymer Engineering and Science*. Oct 1997;37(10):1732-1739.
51. Ng CB, Ash BJ, Schadler LS, Siegel RW. A study of the mechanical and permeability properties of nano- and micron-TiO₂ filled epoxy composites. *Adv Compos Lett*. 2001;10(3):101-111.
52. Bulota M, Vesterinen AH, Hughes M, Seppala J. Mechanical behavior, structure, and reinforcement processes of TEMPO-oxidized cellulose reinforced poly(lactic) acid. *Polym Compos*. Feb 2013;34(2):173-179.
53. Rusli R, Shanmuganathan K, Rowan SJ, Weder C, Eichhorn SJ. Stress Transfer in Cellulose Nanowhisker Composites-Influence of Whisker Aspect Ratio and Surface Charge. *Biomacromolecules*. Apr 2011;12(4):1363-1369.
54. Knauert ST, Douglas JF, Starr FW. The effect of nanoparticle shape on polymer-nanocomposite rheology and tensile strength. *Journal of Polymer Science Part B-Polymer Physics*. Jul 2007;45(14):1882-1897.
55. Kim JK, Robertson RE. Toughening of thermoset polymers by rigid crystalline particles. *Journal of Materials Science*. Jan 1992;27(1):161-174.
56. Xu XZ, Liu F, Jiang L, Zhu JY, Haagenson D, Wiesenborn DP. Cellulose Nanocrystals vs. Cellulose Nanofibrils: A Comparative Study on Their Microstructures and Effects as Polymer Reinforcing Agents. *ACS Appl Mater Interfaces*. Apr 2013;5(8):2999-3009.
57. Liang JZ, Li RKY. Rubber toughening in polypropylene: A review. *Journal of Applied Polymer Science*. Jul 2000;77(2):409-417.
58. Halpin JC, Kardos JL. Halpin-tsai equations - review. *Polymer Engineering and Science*. 1976;16(5):344-352.

59. Bulota M, Kreitsmann K, Hughes M, Paltakari J. Acetylated microfibrillated cellulose as a toughening agent in poly(lactic acid). *Journal of Applied Polymer Science*. Oct 25 2012;126:E448-E457.
60. Hajji P, Cavaille JY, Favier V, Gauthier C, Vigier G. Tensile behavior of nanocomposites from latex and cellulose whiskers. *Polym Compos*. Aug 1996;17(4):612-619.
61. Barnett J, Bonham VA. Cellulose microfibril angle in the cell wall of wood fibres. *Biological reviews*. 2004;79(2):461-472.
62. Srinivasarao M. Nano-optics in the biological world: beetles, butterflies, birds, and moths. *Chemical Reviews-Columbus*. 1999;99(7):1935-1962.
63. Europe P. *Plastics – the Facts 2012*: Plastics Europe; 2012.
64. Bioplastics E. Bioplastics facts and figures Available at: <http://en.european-bioplastics.org/>. Accessed 06/06/2013, 2013.
65. Ahmed J, Varshney SK. Polylactides-Chemistry, Properties and Green Packaging Technology: A Review. *Int J Food Prop*. 2011;14(1):37-58.
66. Anderson KS, Schreck KM, Hillmyer MA. Toughening polylactide. *Polym Rev*. 2008;48(1):85-108.
67. Fukushima K, Abbate C, Tabuani D, Gennari M, Camino G. Biodegradation of poly(lactic acid) and its nanocomposites. *Polym Degrad Stabil*. Oct 2009;94(10):1646-1655.
68. Tolinski M. *Plastics and Sustainability - Towards a Peaceful Coexistence between Bio-Based and Fossil Fuel-Based Plastics*. Wiley - Scrivener: 81.
69. Rasal RM, Janorkar AV, Hirt DE. Poly (lactic acid) modifications. *Prog Polym Sci*. 2010;35(3):338-356.

70. Abdel-Rahman MA, Tashiro Y, Sonomoto K. Recent advances in lactic acid production by microbial fermentation processes. *Biotechnology Advances*. (0).
71. Dorgan JR, Lehermeier H, Mang M. Thermal and rheological properties of commercial-grade poly(lactic acid)s. *Journal of Polymers and the Environment*. Jan 2000;8(1):1-9.
72. Jamshidian M, Tehrani EA, Imran M, Jacquot M, Desobry S. Poly-Lactic Acid: Production, Applications, Nanocomposites, and Release Studies. *Compr Rev Food Sci Food Saf*. Sep 2010;9(5):552-571.
73. Bogaert JC, Coszach P. Poly(lactic acids): A potential solution to plastic waste dilemma. *Macromol Symp*. Mar 2000;153:287-303.
74. Vink ETH, Rabago KR, Glassner DA, Gruber PR. Applications of life cycle assessment to NatureWorks (TM) polylactide (PLA) production. *Polym Degrad Stabil*. Jun 2003;80(3):403-419.
75. Auras RA, Lim L-T, Selke SE, Tsuji H. *Poly (lactic acid): synthesis, structures, properties, processing, and applications*. Vol 10: Wiley; 2011.
76. Nampoothiri KM, Nair NR, John RP. An overview of the recent developments in polylactide (PLA) research. *Bioresource Technology*. Nov 2010;101(22):8493-8501.
77. Sungsanit K, Kao N, Bhattacharya SN. Properties of linear poly(lactic acid)/polyethylene glycol blends. *Polymer Engineering and Science*. Jan 2012;52(1):108-116.
78. Martin O, Averous L. Poly(lactic acid): plasticization and properties of biodegradable multiphase systems. *Polymer*. Jun 2001;42(14):6209-6219.
79. Ray SS. Polylactide-Based Bionanocomposites: A Promising Class of Hybrid Materials. *Accounts of Chemical Research*. Nov 2012;45(10):1710-1720.

80. Oyama HI. Super-tough poly(lactic acid) materials: Reactive blending with ethylene copolymer. *Polymer*. Jan 2009;50(3):747-751.
81. Theryo G, Jing F, Pitet LM, Hillmyer MA. Tough Polylactide Graft Copolymers. *Macromolecules*. Sep 2010;43(18):7394-7397.
82. Liu DY, Yuan XW, Bhattacharyya D, Eastal AJ. Characterisation of solution cast cellulose nanofibre - reinforced poly(lactic acid). *Express Polym Lett*. Jan 2010;4(1):26-31.
83. Lin N, Huang J, Chang PR, Feng JW, Yu JH. Surface acetylation of cellulose nanocrystal and its reinforcing function in poly(lactic acid). *Carbohydr Polym*. Feb 2011;83(4):1834-1842.
84. Pandey J, Chu W, Kim C, Lee C, Ahn S. Bio-nano reinforcement of environmentally degradable polymer matrix by cellulose whiskers from grass. *Composites Part B: Engineering*. 2009;40(7):676-680.
85. Pei A, Zhou Q, Berglund LA. Functionalized cellulose nanocrystals as biobased nucleation agents in poly(L-lactide) (PLLA) - Crystallization and mechanical property effects. *Composites Science and Technology*. May 2010;70(5):815-821.
86. Fortunati E, Peltzer M, Armentano I, Torre L, Jiménez A, Kenny JM. Effects of modified cellulose nanocrystals on the barrier and migration properties of PLA nano-biocomposites. *Carbohydr Polym*. 2012;90(2):948-956.
87. Hassan A, Balakrishnan H, Akbari A. Polylactic Acid Based Blends, Composites and Nanocomposites. *Advances in Natural Polymers*: Springer; 2013: 361-396.
88. Tirrell JG, Tirrell DA. Synthesis of biopolymers: proteins, polyesters, polysaccharides and polynucleotides. *Current Opinion in Solid State and Materials Science*. 1996;1(3):407-411.
89. Meeker DL. North American Rendering - processing high quality protein and fats for feed. *Revista Brasileira De Zootecnia-Brazilian Journal of Animal Science*. Jul 2009;38:432-U443.

90. Meeker DL. Essential Rendering - All About The Animal By-Products Industry. . In: Association NR, ed. Arlington; 2006.
91. NRS. National Renderers Association. Available at: <http://nationalrenderers.org/>. Accessed March 2012, 2012.
92. Swisher K. Market Report: Industry savors record prices and growing global demand. *Render Magazine*; 2012: 10-18.
93. Gooding CH. Data for the Carbon Footprinting of Rendering Operations. *Journal of Industrial Ecology*. Apr 2012;16(2):223-230.
94. Willems P, Kuipers NJM, de Haan AB. Gas assisted mechanical expression of oilseeds: Influence of process parameters on oil yield. *J Supercrit Fluids*. Jul 2008;45(3):298-305.
95. Voges S, Eggers R, Pietsch A. Gas assisted oilseed pressing. *Sep Purif Technol*. Oct 2008;63(1):1-14.
96. Min JA, Li SF, Hao J, Liu NH. Supercritical CO₂ Extraction of Jatropha Oil and Solubility Correlation. *Journal of Chemical and Engineering Data*. Sep 2010;55(9):3755-3758.
97. Brunner G. Applications of Supercritical Fluids. In: Prausnitz JMDMFSMA, ed. *Annual Review of Chemical and Biomolecular Engineering, Vol 1*. Vol 1; 2010: 321-342.
98. Pradhan RC, Meda V, Rout PK, Naik S, Dalai AK. Supercritical CO₂ extraction of fatty oil from flaxseed and comparison with screw press expression and solvent extraction processes. *Journal of Food Engineering*. Jun 2010;98(4):393-397.
99. Sahena F, Zaidul ISM, Jinap S, et al. Application of supercritical CO₂ in lipid extraction - A review. *Journal of Food Engineering*. Nov 2009;95(2):240-253.

100. Catchpole OJ, Tallon SJ, Eltringham WE, et al. The extraction and fractionation of specialty lipids using near critical fluids. *J Supercrit Fluids*. Jan 2009;47(3):591-597.
101. Brunner G. Supercritical fluids: technology and application to food processing. *Journal of Food Engineering*. Mar 2005;67(1-2):21-33.
102. Palmer MV, Ting SST. Applications for supercritical fluid technology in food processing. *Food Chemistry*. 1995;52(4):345-352.
103. Halim R, Danquah MK, Webley PA. Extraction of oil from microalgae for biodiesel production: A review. *Biotechnology Advances*. May-Jun 2012;30(3):709-732.
104. (NIST) NIST Chemistry WebBook -Thermophysical Properties of Fluid Systems. Available at: <http://webbook.nist.gov/chemistry/>. Accessed October 2011.
105. Rout PK, Naik S, Rao YR. Liquid CO₂ extraction of flowers of pandanus fascicularis lam. And fractionation of floral concrete and comparative composition of the extracts. *Journal of Food Biochemistry*. Apr 2011;35(2):500-512.
106. Orellana JL, Smith TD, Kitchens CL. Liquid and Supercritical CO₂ Extraction of Fat from Rendered Materials. *The Journal of Supercritical Fluids*. 2013.
107. Venter MJ, Willems P, Kuipers NJM, de Haan AB. Gas assisted mechanical expression of cocoa butter from cocoa nibs and edible oils from oilseeds. *J Supercrit Fluids*. May 2006;37(3):350-358.
108. Jenab E, Temelli F. Viscosity measurement and modeling of canola oil and its blend with canola stearin in equilibrium with high pressure carbon dioxide. *The Journal of Supercritical Fluids*. 2011;58(1):7-14.
109. Pietscha A, Eggers R. Gas-assisted oilseed pressing - Design of and tests with a novel high-pressure screw press. In: Saravacos G, Taoukis P, Krokida M, et al.,

- eds. *11th International Congress on Engineering and Food*. Vol 1. Amsterdam: Elsevier Science Bv; 2011: 1381-1387.
110. Bharath R, Inomata H, Adschiri T, Arai K. Phase-equilibrium study for the separation and fractionation of fatty oil components using supercritical carbon-dioxide. *Fluid Phase Equilib*. Dec 1992;81(1-2):307-320.
 111. Eggers R, Sievers U. Processing of oilseed with supercritical carbon-dioxide. *J Chem Eng Jpn*. Dec 1989;22(6):641-649.
 112. Von White G, II, Provost MG, Kitchens CL. Fractionation of Surface-Modified Gold Nanorods Using Gas-Expanded Liquids. *Industrial & Engineering Chemistry Research*. Apr 11 2012;51(14):5181-5189.

CHAPTER TWO
PHASE BEHAVIOR AND DISPERSIBILITY OF SURFACE MODIFIED
CELLULOSE NANOCRYSTALS IN ORGANIC SOLVENTS BY MEANS OF
SURFACTANTS

Introduction

Cellulose nanocrystals (CNCs) have attracted much attention for a diversity of applications such as nanocomposites, smart coatings, pharmaceutical applications, and electronic materials, due to their unique chemical, mechanical and optical properties.¹ They can be isolated via acid hydrolysis from a variety of sources including cotton, tunicate, and bacteria.² Through this process, disordered regions of cellulose are preferentially hydrolyzed, while the crystalline regions resist the acid catalyzed hydrolysis, resulting in a crystalline, high performance material with nanoscale dimensions and unique morphology. These characteristics and others such as low density, low toxicity, abundance, and renewability make CNCs a prime material for advanced materials applications.²

One of these applications is as potential reinforcement filler for polymeric matrices, which has attracted much attention in the last two decades due to the notable mechanical properties, high aspect ratios, and surface areas of the CNCs.³⁻⁷ CNCs, theoretically, have a higher elastic modulus than Kevlar and higher tensile strength than steel wire, while only having a fraction of the weight.⁸ Nanocomposites are a potential market for the production of cellulose, which is estimated to be between 10^{10} to 10^{11} tons each year,

which is mainly destined for paper, textiles, construction materials and chemical industries.⁹ Evidence of the potential increase in the field of cellulose nanomaterials is the opening of the first nanocellulose plant in the U.S. in 2012, which is predicted to contribute \$600 billion to the economy by 2020.¹⁰ However, some challenges still exist for the application of CNCs in different areas. One of these challenges is the reduction of the hydrophilicity of cellulose for a better compatibilization and dispersion of CNCs in non-polar polymeric matrices.

The surface functionality of CNCs is initially determined by the nature of the acid used for the isolation of the nanocrystals. For instance, isolation with sulfuric acid, which is one of the most used in the literature, introduces charged sulfate groups,¹¹ while a synthesis with hydrochloric acid only yields hydroxyl groups on the surface.¹² Functionalization after the isolation process presents the challenge of only altering the surface of the crystals and preserving the morphology and integrity of them. Many surface modifications have been successfully conducted in the literature, such as silylation, polymer grafting, acetylation, oxidation, and non-covalent modification, i.e. adsorption of surfactants.²

A widely studied modification is the TEMPO-mediated oxidation which introduces negatively charged carboxyl entities that provide electrostatic stabilization of the CNCs in water.^{13, 14} Despite their stable dispersion in aqueous media, CNCs obtained by the TEMPO and sulfuric acid synthesis show low thermal stabilities, which are a disadvantage for the processing of nanocomposites.¹⁵⁻¹⁷ An alternative modification was

recently proposed by Braun and Dorgan who isolated CNCs by a combination of acetic and hydrochloric acid, producing more hydrophobic CNCs while maintaining a high thermal stability.¹⁸ These acetylated CNCs have a moderate stability in organic solvents that can be further increased by the addition of surfactants.

The use of surfactants offers advantages such as ease of addition and inalterability of the nanocrystal morphology. The hydrophilic headgroup of the surfactant interacts with the surface of the cellulose while the hydrophobic tail has affinity for the organic solvent. The steric repulsion of the surfactant, coupled with the hydrophobic properties, make the cellulose more stable in non-polar substances. This concept was first introduced by Heux et al.,¹⁹ using esters of phosphoric acid as surfactants for cellulose microcrystals, obtaining improved dispersibility and self-organization in toluene and cyclohexane. Other modifications with surfactants were later conducted successfully.²⁰⁻²³ More recently, alkylamines¹⁷ and different quaternary salts²⁴ have been absorbed into TEMPO-oxidized CNCs, obtaining good dispersions in non-polar and aprotic solvents. However, the fractions of these surfactants added to CNCs are usually high, ranging from 0.5:1 to 4:1 (surfactant to CNC ratio). It is believed that high amounts of these additives can potentially affect the properties of the polymer matrix; therefore it is crucial to find better alternative surfactants.^{20 21}

The dispersion stability or phase behavior of CNCs in organic media is a key aspect for the understanding of the interactions of cellulose with both hydrophilic and hydrophobic matrices, and for the prediction of the enhancements to the mechanical

properties of nanocomposites. For example, Rojas et al. found that the addition of surfactants to CNCs enhanced the dispersion in THF and it correlated with favorable dispersions in polystyrene.²¹ The phase behavior of the CNC suspensions depends on many parameters such as polydispersity, surface functionality and aspect ratio. Acetylated CNCs with low degrees of substitution have the tendency to aggregate due to intermolecular hydrogen bonding²⁵ and lack of surface charge.²⁶ The addition of surfactants will alter the surface functionally and increase the steric repulsion, thus reducing the degree of flocculation.

On the other hand, the ability of CNCs to self-assemble is also important for composite applications, and it is an indication of a favorable dispersion and solvent compatibility. There is an appreciable volume of literature that focuses on the self-assembly of sulfuric acid and TEMPO-synthesized CNCs, which exhibit chiral-nematic ordering above a critical concentration.^{11, 27-29} However, further investigation is needed for other types of environmentally-friendly, thermally-stable CNC synthesis in order to understand their phase behavior and self-organization in organic media.

In this work, the dispersibility of acetylated CNCs (CNC-AA) was investigated in three different solvents: tetrahydrofuran (THF), chloroform and ethyl acetate. Furthermore, decylamine (DA), cetyltrimethyl-ammonium bromide (CTAB) and tetrahexyl-ammonium bromide (THAB) surfactants were used to increase the dispersion stability of CNCs in the organic solvents. The amount of surfactant found to be required for the stabilization of CNC-AA was much lower than the surfactants that have been

utilized in the literature. The self-assembly of CNC-AA in organic solvents was investigated by visual examination of bulk samples in 2 mm path length cuvettes and using polarized microscopy with a red plate filter. CNCs showed the ability to self-assemble in the stationary and shearing states when dispersed in organic solvents.

Materials and Methods

Materials

Cotton ashless clippings filter aids from WhatmanTM were used as the cellulose source for the CNC synthesis. Glacial acetic acid, hydrochloric acid 37% w/v (HCl), tetrahydrofuran (THF), chloroform and ethyl acetate were all ACS grade products obtained from VWR. The surfactants decylamine (95% purity) and tetrahexyl-ammonium bromide (THAB) (99% purity) were ACS grade reagents obtained from Sigma Aldrich, and high purity grade cetyltrimethyl-ammonium bromide (CTAB) was obtained from Amresco.

Synthesis of Cellulose Nanocrystals

CNCs were isolated by both acid hydrolysis with HCl (CNC-HCl), and with a mixture of HCl and acetic acid (CNC-AA) as described in the literature.¹⁸ In the latter, a Fischer esterification reaction occurs between the hydroxyl groups and the acetic acid during the hydrolysis, introducing carbonyl groups onto the surface of the cellulose and resulting in the acetylated CNCs. In short, 15 g of cotton was soaked overnight in either 300 mL of deionized water (DI) to prepare CNC-HCl or in 338 mL of acetic acid to

prepare CNC-AA. For the CNC-HCl, 79.5 mL of 37% HCl was added to obtain a concentration of 2.5 M of HCl, and the mixture was heated to 103 °C for 60 min. For CNC-AA, 36.8 mL of DI water and 1.2 mL of 37% HCl was added and heated for 10 h at 105 °C. When the reaction was finished, the mixtures were cooled in an ice bath and poured into 50 ml centrifuge tubes for a washing process. Three washes with DI water were carried out via centrifugation using 8,600 rpm for 3 min to completely precipitate the cellulose. These suspensions were recombined and sonicated in an ice bath with a Fisher Scientific 550 Sonic Dismembrator for 35 min (7 min pulse, 2 min rest, 5 cycles). The suspensions were washed again two more times or until a cloudy supernatant appears. This supernatant and the supernatant from a 2nd and 3rd additional wash/centrifugation steps are kept as the dispersed nanocrystals. The residue at the bottom of the tubes is discarded at the end of the separations.

In order to transfer the CNCs to an organic solvent, aqueous suspension of CNC were precipitated at 14,000 rpm for 10 min and washed with acetone twice. For each wash, the cellulose precipitate was agitated in acetone using a vortex mixer (Vortex-Genie 2 Scientific Industries, Inc.) until the CNCs re-suspended in acetone and then centrifuged. After the third precipitation, the desired solvent was added, and the suspension was vortex mixed for about 40 min until all of the CNCs were well dispersed. The surfactant was added at the desired concentration, and the suspensions were agitated again until no agglomerations were observed. For CNCs without surfactant, it would usually take longer periods of time to completely disperse in the organic solvent. CNC suspensions at higher

concentrations were made by evaporating the solvent to the desired volume to reach specific concentrations.

Transmission Electron Microscopy (TEM)

TEM images were obtained using a Hitachi 7600 with an accelerating voltage of 120 kV. TEM samples were prepared using a nebulizer to spray 10 times diluted CNC suspensions (~0.01% w/v) onto a formvar carbon coated copper TEM grid (Ted Pella), followed by air drying at ambient conditions.

Thermal stability

Thermal gravimetric analysis (TGA) was performed on different cellulose materials using a TA instruments SDT Q600 at a heating rate of 10 °C/min. CNCs were first heated to 110°C for 25 min to eliminate any residual water and cooled again to 80 °C before ramping to 650°C. The run was carried out under nitrogen atmosphere (100mL/min) and then switched to oxygen for a ramp from 650°C to 800°C.

Determination of the Dispersion Stability

Suspensions of 1% (wt/vol) of CNC-AA were prepared and placed in scintillation vials to study the phase separation over time. This was determined by visual examination, taking pictures periodically over the course of 4 weeks and measuring the relative height of the separated phase. Different concentrations of surfactant ranging from 1 to 20 wt. %

were added to the CNC suspensions in order to evaluate the effect of the surfactant concentration on the dispersion stability. This effect was studied by both visual examination and gravimetric analysis of the supernatant, or stable suspension, after centrifugation at 29 xg for 90 min.

CNC Self-Assembly

Imaging of bulk samples between cross-polarized films at various concentrations of CNC-AA were performed on suspensions held in 2 mm path length sealed cuvettes. An 8 Watt fluorescent light box was used as the light source in a dark room for a better quality of the images. Shear-induced liquid crystals were studied using diluted concentrations of CNC-AA in scintillation vials and sheared with a magnetic stir bar. The CNC-AA suspensions and dried films were also characterized with an Olympus BX-60 optical microscope using polarized filters and a 530 nm first order red plate (U-TP530). The suspensions were introduced in flat-sided capillary tubes (0.2 mm path length and 4 mm wide) obtained from Electron Microscopy Sciences and sealed with PVA-based glue.

Results and discussion

Morphology of isolated CNC

The nanoscale dimensions of the CNCs are very important for many applications including the mechanical reinforcement of polymers. Figure 2.1 shows a TEM micrograph of CNCs dried from THF after the addition of DA, where the isolation of nanocrystals can be observed. The size distribution cannot be estimated due to the

agglomerate nature of the CNCs as observed in Figure 2.1, but an approximate average size was estimated to be 250 nm long and 35 nm wide. This result is close to the average crystal size (269 nm x 45 nm) reported in the literature for acetylated CNCs in aqueous suspension.¹⁸ The cellulose network formed after drying is expected to be reduced in suspensions if a good compatibility with the solvent is achieved. In general, it can be observed that the synthesis of CNCs was conducted successfully and that the addition of surfactants did not alter the morphology.

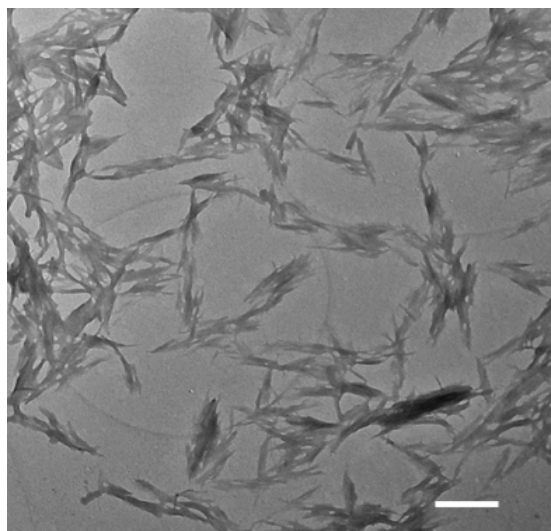


Figure 2.1. TEM micrograph of decylamine stabilized CNC-AA. Scale bar: 500 nm

Thermal stability

The thermal stability of cellulose is an important parameter for the production of CNC-based materials, especially in the reinforcement of thermoplastic polymers.³⁰ Figure 2.2 shows the TGA analysis of various types of CNCs compared to un-hydrolyzed cellulose. The degradation temperature did not decrease significantly after the reaction with acetic and hydrochloric acid compared to un-hydrolyzed cellulose, which has a

degradation temperature of 339.24 °C. The addition of surfactants did not affect the thermal stability of cellulose, showing a degradation temperature of approximately 331°C with the addition of DA. On the other hand, CNCs synthesized via sulfuric acid showed a very low degradation temperature as is reported elsewhere, and it was shown to vary depending of the degree of sulfate group surface modification.¹⁶ Degradation temperatures as low as 120 °C have been reported for this type of modification.³¹ Significant reduction of the degradation temperature for the TEMPO-oxidized CNCs has also been reported elsewhere,¹⁵ and it has been attributed to the decarbonation of previously formed anhydroglucuronic acid groups.¹⁷ From these results (Figure 2.1 and Figure 2.2), it can be demonstrated that the integrity of CNC-AA does not vary and that the high thermal stability of native cellulose is retained, which is requisite for the reinforcement of nanocomposites undergoing melt processing.

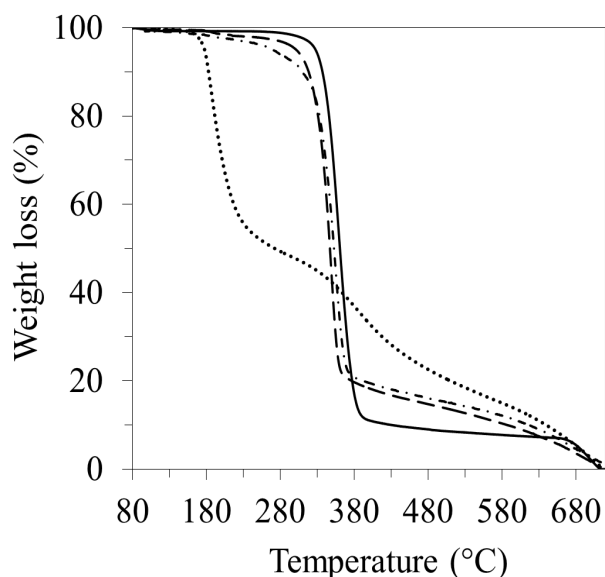


Figure 2.2. Thermal gravimetric analysis of unhydrolyzed cellulose (solid line), acetylated CNC (long dash), acetylated CNC modified with surfactant (dash dot) and sulfuric acid synthesized CNC (dots)

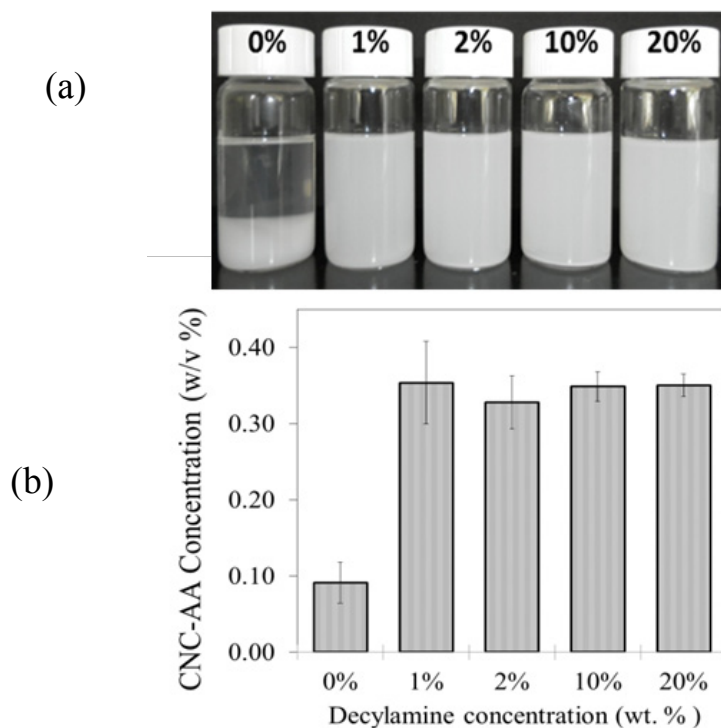


Figure 2.3. Effect of the fraction of surfactant on the stability of CNC-AA suspensions in THF. (a) visual examination after 4 weeks; and (b) concentration of the CNC-AA supernatant (stable suspension) after 90 min of centrifugation at 29 x G where initial total concentration was 0.56% (w/v)

Suspension Stability

Initially the surfactants were added to both CNC-HCl and CNC-AA to determine the increased stability in organic solvents. CNC-HCl contains only hydroxyl groups on the surface while CNC-AA contains carbonyl groups introduced by the reaction with acetic acid. It was found that the surfactants did not improve the stability of CNC-HCl in organic solvents perhaps because of to the strong interactions and agglomerations resulting from the hydrogen bonding of the hydroxyl groups.²⁵ Thus, the results of the CNC-HCl suspensions are not shown, and the phase behavior was not further investigated. On the other hand, CNC-AA showed a significant improvement in the

suspension stability upon the addition of surfactants. It is believed that the carbonyl groups attached to the CNC-AA surface reduces the hydrogen bonding and allows the surfactant to be adsorbed more effectively on the surface.

The amount of surfactant was varied from 0 to 20 wt.% with respect to cellulose in order to determine the effect of the surfactant concentration on the stability and the minimum amount required for stabilization. Figure 2.3 demonstrates that as little as 1.0 wt.% DA was required to significantly enhance the CNC-AA stability in organic solvents. The enhanced suspensions remained visually stable for a period of weeks, while CNC-AA without surfactant started phase separating after the first few hours. This behavior was also demonstrated by determining the concentration of the stable supernatant after centrifugation at 29 xg for 90 min as it can be observed in Figure 2.3b. The use of a small amount of surfactant provides an advantage over other systems that use higher proportions of surfactants to increase the stability of cellulose in organic solvents.^{21, 32}

The settling rate of the CNC-AA was studied using three types of surfactants and three solvents in order to understand the behavior and the interactions with different organic media. For all of the suspensions, the degree of sedimentation (F) was measured. F is defined as the height of the flocculated suspension after a time t divided by the initial height of the suspension. Figure 2.3 shows the degree of sedimentation (F) for the different combinations studied in this work. A stable suspension in Figure 2.4 has an $F=1$, which means that no settling is observed and the separated phase occupies the entire

volume of the suspension. This stable suspension is assumed to be close to equilibrium in terms of flocculation, and it is considered to be a stable form. This is sometimes referred as the “sedimentation paradox” because this definition is in some way in contradiction with colloidal science, which considers flocculated suspensions as unstable.³³

Figure 2.4 shows the settling behavior of the suspensions using the 3 different surfactants. DA surfactant provides the greatest enhancement of suspension stability of CNCs in both THF (Figure 2.4a) and ethyl acetate (Figure 2.4b). CTAB and THAB surfactants also increased the stability of these suspensions to a certain extent compared to pure CNCs but not as much as DA. On the other hand, Figure 2.4c shows that CTAB makes CNCs the most stable in chloroform compared to CNCs without surfactant. THAB did not have any effect, while DA in this case reduced the stability of CNCs in chloroform.

THF and ethyl acetate are polar, aprotic solvents while chloroform is a non-polar, protic solvent. CNC-AA has a predominant H-acceptor surface due to the carbonyl groups. Hence, CNC-AA would tend to have a higher stability in chloroform than in aprotic solvents as shown in the phase separation results in Figure 2.4. The addition of the surfactants, all proton donors, improved the stability of CNCs in all of the cases, except when using DA with chloroform. The reason for the reduction upon addition of DA can be attributed to the reduction of the small electrostatic attraction that existed initially between CNCs and chloroform. On the other hand, the addition of DA introduces steric stabilization between CNCs and the aprotic solvent, where there were initially no favorable interactions.

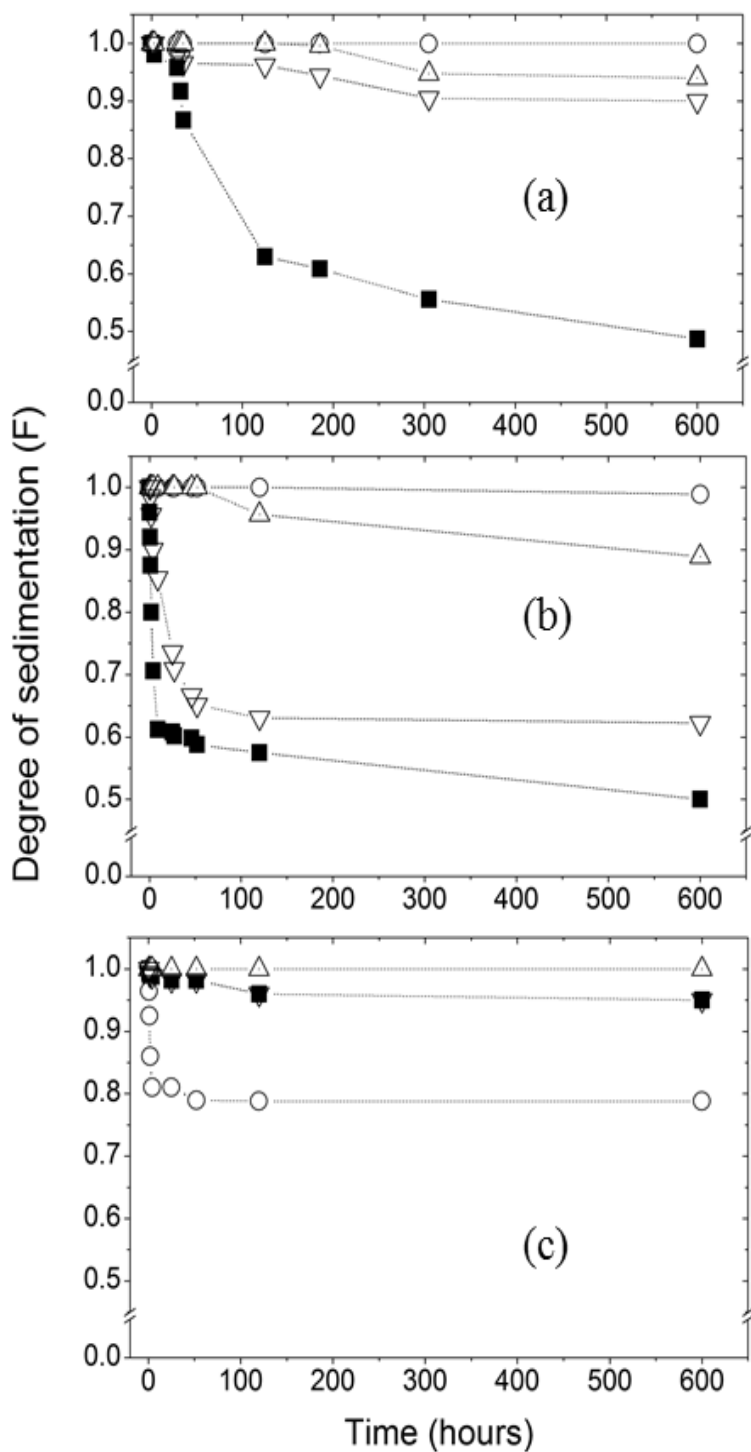


Figure 2.4. Phase separation of CNC-AA 1 wt/v% suspensions in: a) THF; b) ethyl acetate and c) chloroform. CNC-AA ■ without surfactant; ○ with DA; △ with CTAB and ▽ with THAB.

CNC Self-Assembly

The self-assembly of CNCs was studied using DA as a surfactant in THF and ethyl acetate suspensions, while CTAB was added in the chloroform ones as these were the most stable combinations according to the results presented above. Bulk observation of the CNC suspensions through crossed polarized films (Figure 2.5) does not show the strong, uniform bright phase that is frequently observed in chiral-nematic formations but rather shows birefringent patterns when using THF and chloroform solvents. In the case of THF, the birefringence patterns are clearly evident at 2.0 wt. % CNCs with and without surfactant, while for chloroform the onset of weaker birefringence is observed at higher CNC concentration. These patterns indicate that CNCs are locally organized into oriented domains likely with a nematic organization.^{34, 35} The birefringence domains remained stable for at least two weeks in the 2 mm path length cuvettes, indicating a good stability of the ordered structures. For ethyl acetate suspensions, no visible birefringence patterns were observed but a slight bright phase can still be seen through the cuvette, indicating the existence of smaller ordered domains in suspensions.

The characteristic fingerprint texture was not observed in the CNC-AA suspensions under polarized microscopy, indicating that chiral-nematic order was not observed. The chiral-nematic liquid crystals are commonly characteristic and well-studied for the sulfuric acid and TEMPO-synthesized CNCs.^{11, 24, 27, 28} However, other syntheses such as the HCl and acetic acid may not produce this organization but rather birefringence patterns of locally ordered liquid crystals, demonstrating partial orientation

of the CNCs.¹² Among the possible reasons of not achieving chiral-nematic organization are high polydispersity of CNC dimensions, high viscosity of the suspensions, low colloidal stability, and synthesis does not produce a screw shaped nanocrystal.^{13, 36} The flocculated nature of CNC-AA may also prevent the unrestricted CNC organization into the more ordered structures. The viscosity of the CNC-AA suspensions seems to increase rapidly, achieving a maximum concentration of approximately 7 wt.% before gelling. This is compared to the 20 wt.% for sulfuric acid synthesized CNCs in water.¹¹

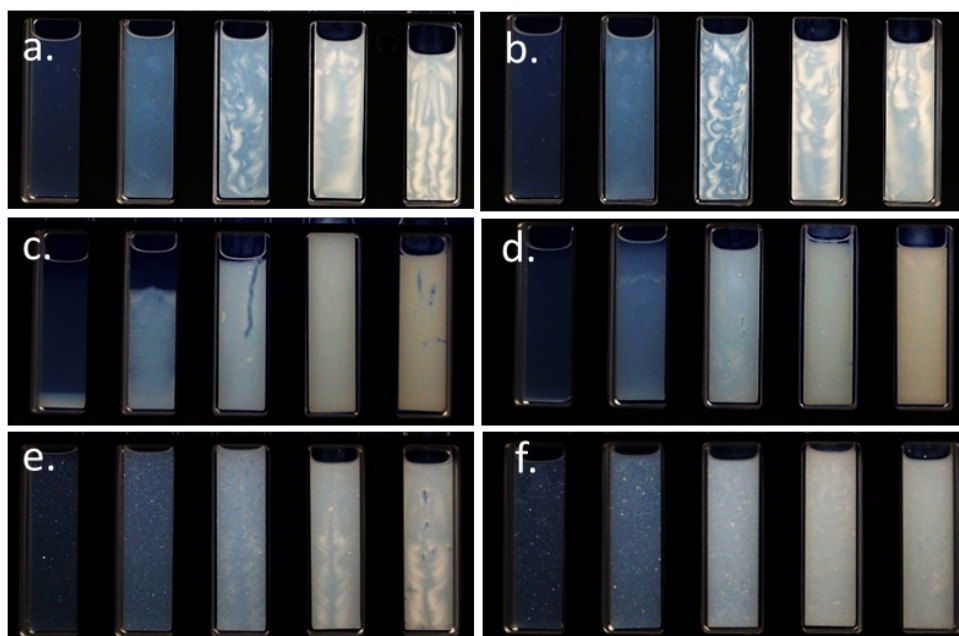


Figure 2.5. Birefringence of CNC-AA suspensions in THF (a, b), ethyl acetate (c, d), and chloroform (e, f); Suspensions are also without surfactant (a, c, e) and with 1 wt. % surfactant with respect to cellulose (b, d, f). The concentrations in each image from left to right are 0.5, 1.0, 2.0, 3.0, 4.0, and 5.0 wt. % CNCs.

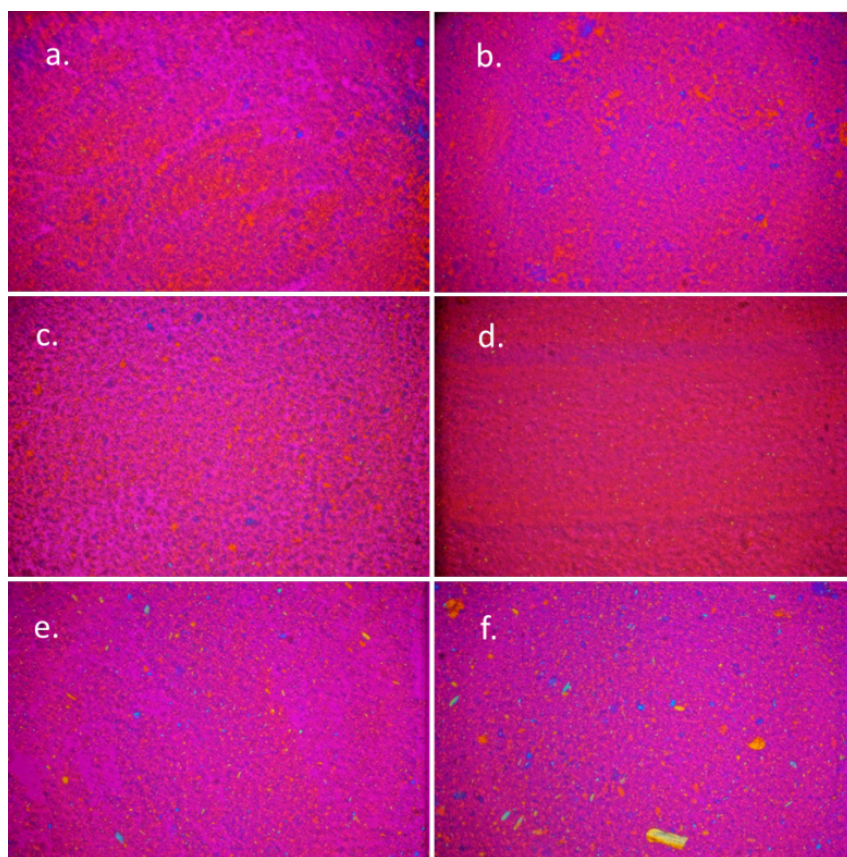


Figure 2.6. Polarized microscopy of 4% CNC-AA suspensions in THF (a, b), ethyl acetate (c, d), and chloroform (e, f). Left micrographs are CNC-AA without surfactant (a, c, e) and the right micrographs are CNC-AA with surfactant (b, d, f). Length of the longer side of each image: 1.5 mm

Polarized microscopy revealed the appearance of organized domains without significant agglomerations in THF and ethyl acetate suspensions with and without surfactants. These domains are microscopically very similar to each other as observed in Figure 2.6. However, for ethyl acetate these domains were not observed in the cuvettes, indicating that they are not long-range enough for visual observation of birefringence patterns. For the suspensions in chloroform, some agglomerates can be observed in the bulk suspensions and with polarized microscopy (Figure 2.6e-f). Since some birefringence patterns were observed a 3% or higher concentrations in the macro-scale, it

may indicate that the organized domains in chloroform exist and grow with concentration, but the agglomerations may delay their visible appearance. This appearance of agglomerates may be due to residual water present on the CNCs that cannot be dispersed because of the insolubility with chloroform.

The dispersion stability of CNCs does not seem to be strongly related to the appearance of birefringence as it has been shown previously in the literature.¹⁷ CNC-AA without any modification shows a birefringence pattern in THF but it phase separates within a few hours. Stabilization with DA increased the stability but did not affect the birefringence significantly. The observation of these patterns is very qualitative, and therefore, it becomes difficult to estimate small enhancements on the self-organization. It seems that the assembly of CNC-AA is more affected by the morphology of CNCs and the type of solvent than by the addition of the surfactants.

Another important parameter that suggests the favorable interactions of CNC-AA with the solvents is the appearance of flow birefringence. This occurs when liquid crystals form upon shearing at relatively low concentrations of CNC suspensions. Figure 2.7 shows that CNC-AA has the ability to assemble into liquid crystals when the suspensions are stirred. Flow birefringence was observed with higher intensity in THF suspensions, followed by ethyl acetate and lastly by chloroform, which showed the lowest intensity. The modification with surfactants does not significantly impact the flow birefringence observed as was the case with stationary birefringence. Chloroform suspensions did show some birefringence patterns in the stationary observation, but it did

not with the application of shear. This may be due to the degree of agglomeration, reducing the amount of single crystals that have the ability to align with the flow at lower CNC concentration.

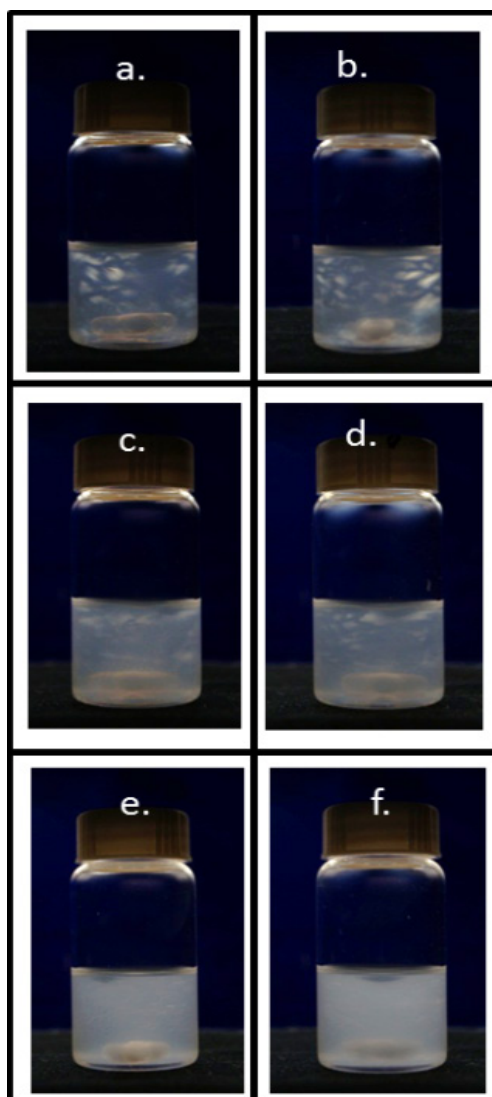


Figure 2.7. Flow birefringence of 0.1% CNC-AA suspensions. Left micrographs: CNC-AA without surfactant (a,c,e); right micrographs: CNC-AA with surfactant (b,d,f). Solvents: (a and b) THF; (c and d) Ethyl acetate; (e and f) chloroform

Conclusions

The addition of surfactants to acetylated cellulose nanocrystals (CNC-AA) increased the dispersion stability in organic solvents. DA surfactant was successful in increasing the stability in THF and ethyl acetate solvents while cetyltrimethyl-ammonium bromide (CTAB) surfactant increased the stability of CNC-AA in chloroform. The minimum amount of surfactant shown to enhance the stability of CNC-AA in organic solvents was only 1wt.% with respect to cellulose weight. The suspensions remained stable in the solvent for weeks until phase separation was observed, in contrast to non-surfactant-modified CNCs, which would phase separate within a few hours after dispersion. CNC-AA showed the ability to self-assemble in specific organic solvents in the stationary and shearing state. For both states, the addition of surfactants did not affect the self-assembly of CNCs significantly.

The chiral-nematic assembly was not observed for any of the suspensions but birefringence patterns were observed in THF and chloroform suspensions. These patterns were stable with time and are thought to be organized domains that are produced by the assembly of non-agglomerated CNC-AA. Suspensions in ethyl acetate did not show these patterns but it showed assembly in the microscopic level, indicating that the organized domains were too small to be observed as birefringence patterns. Finally, the flow birefringence showed the ability for CNC-AA to assemble upon shearing for suspension in THF and ethyl acetate. These results are of great significance for the nanocomposite field, since an improved compatibility of CNCs plus the ability to align

upon shear can potentially enhance the mechanical and optical properties of hydrophobic polymeric matrices.

References

1. Eichhorn SJ. Cellulose nanowhiskers: promising materials for advanced applications. *Soft Matter*. 2011;7(2):303-315.
2. Habibi Y, Lucia LA, Rojas OJ. Cellulose Nanocrystals: Chemistry, Self-Assembly, and Applications. *Chemical Reviews*. Jun 2010;110(6):3479-3500.
3. Urena-Benavides EE, Brown PJ, Kitchens CL. Effect of Jet Stretch and Particle Load on Cellulose Nanocrystal-Alginate Nanocomposite Fibers. *Langmuir*. Sep 2010;26(17):14263-14270.
4. Eichhorn SJ, Dufresne A, Aranguren M, et al. Review: current international research into cellulose nanofibres and nanocomposites. *Journal of Materials Science*. Vol 45; 2010: 1-33.
5. Khalil H, Bhat AH, Yusra AFI. Green composites from sustainable cellulose nanofibrils: A review. *Carbohydr Polym*. Jan 2012;87(2):963-979.
6. Ramires EC, Dufresne A. A review of cellulose nanocrystals and nanocomposites. *Tappi J*. Apr 2011;10(4):9-16.
7. Siqueira G, Bras J, Dufresne A. Cellulosic Bionanocomposites: A Review of Preparation, Properties and Applications. *Polymers*. Dec 2010;2(4):728-765.
8. Moon RJ, Martini A, Nairn J, Simonsen J, Youngblood J. Cellulose nanomaterials review: structure, properties and nanocomposites. *Chem Soc Rev*. 2011;40(7):3941-3994.
9. Lavoine N, Desloges I, Dufresne A, Bras J. Microfibrillated cellulose – Its barrier properties and applications in cellulosic materials: A review. *Carbohydr Polym*. 2012;90(2):735-764.

10. FPL FPL. Nanocellulose Pilot Plant to be Unveiled at Forest Products Lab. Available at: <http://www.fpl.fs.fed.us/news/newsreleases/releases/20120716.shtml>.
11. Urena-Benavides EE, Ao GY, Davis VA, Kitchens CL. Rheology and Phase Behavior of Lyotropic Cellulose Nanocrystal Suspensions. *Macromolecules*. Nov 2011;44(22):8990-8998.
12. Araki J, Wada M, Kuga S, Okano T. Flow properties of microcrystalline cellulose suspension prepared by acid treatment of native cellulose. *Colloid Surf A-Physicochem Eng Asp*. Nov 1998;142(1):75-82.
13. Habibi Y, Chanzy H, Vignon MR. TEMPO-mediated surface oxidation of cellulose whiskers. *Cellulose*. Dec 2006;13(6):679-687.
14. Denooy AEJ, Besemer AC, Vanbekkum H. Highly selective tempo mediated oxidation of primary alcohol groups in polysaccharides. *Recl Trav Chim Pays-Bas-J Roy Neth Chem Soc*. Mar 1994;113(3):165-166.
15. Fukuzumi H, Saito T, Okita Y, Isogai A. Thermal stabilization of TEMPO-oxidized cellulose. *Polym Degrad Stabil*. Sep 2010;95(9):1502-1508.
16. Roman M, Winter WT. Effect of sulfate groups from sulfuric acid hydrolysis on the thermal degradation behavior of bacterial cellulose. *Biomacromolecules*. 2004;5(5):1671-1677.
17. Johnson RK, Zink-Sharp A, Glasser WG. Preparation and characterization of hydrophobic derivatives of TEMPO-oxidized nanocelluloses. *Cellulose*. Dec 2011;18(6):1599-1609.
18. Braun B, Dorgan JR. Single-Step Method for the Isolation and Surface Functionalization of Cellulosic Nanowhiskers. *Biomacromolecules*. Feb 2009;10(2):334-341.
19. Heux L, Chauve G, Bonini C. Nonflocculating and chiral-nematic self-ordering of cellulose microcrystals suspensions in nonpolar solvents. *Langmuir*. Oct 17 2000;16(21):8210-8212.

20. Petersson L, Kvien I, Oksman K. Structure and thermal properties of poly(lactic acid)/cellulose whiskers nanocomposite materials. *Composites Science and Technology*. Sep 2007;67(11-12):2535-2544.
21. Kim J, Montero G, Habibi Y, et al. Dispersion of Cellulose Crystallites by Nonionic Surfactants in a Hydrophobic Polymer Matrix. *Polymer Engineering and Science*. Oct 2009;49(10):2054-2061.
22. Zhou Q, Brumer H, Teeri TT. Self-Organization of Cellulose Nanocrystals Adsorbed with Xyloglucan Oligosaccharide-Poly(ethylene glycol)-Polystyrene Triblock Copolymer. *Macromolecules*. Aug 11 2009;42(15):5430-5432.
23. Bondeson D, Oksman K. Dispersion and characteristics of surfactant modified cellulose whiskers nanocomposites. *Composite Interfaces*. 2007;14(7-9):617-630.
24. Salajkova M, Berglund LA, Zhou Q. Hydrophobic cellulose nanocrystals modified with quaternary ammonium salts. *Journal of Materials Chemistry*. 2012 2012;22(37):19798-19805.
25. Bulota M, Kreitsmann K, Hughes M, Paltakari J. Acetylated microfibrillated cellulose as a toughening agent in poly(lactic acid). *Journal of Applied Polymer Science*. Oct 25 2012;126:E448-E457.
26. Rusli R, Shanmuganathan K, Rowan SJ, Weder C, Eichhorn SJ. Stress Transfer in Cellulose Nanowhisker Composites-Influence of Whisker Aspect Ratio and Surface Charge. *Biomacromolecules*. Apr 2011;12(4):1363-1369.
27. Marchessault R, Morehead F, Walter N. Liquid crystal systems from fibrillar polysaccharides. 1959.
28. Revol J-F, Bradford H, Giasson J, Marchessault R, Gray D. Helicoidal self-ordering of cellulose microfibrils in aqueous suspension. *International journal of biological macromolecules*. 1992;14(3):170-172.
29. Araki J, Wada M, Kuga S, Okano T. Birefringent glassy phase of a cellulose microcrystal suspension. *Langmuir*. Mar 2000;16(6):2413-2415.

30. Pandey JK, Ahn SH, Lee CS, Mohanty AK, Misra M. Recent Advances in the Application of Natural Fiber Based Composites. *Macromol Mater Eng*. Nov 2010;295(11):975-989.
31. Kim DY, Nishiyama Y, Wada M, Kuga S. High-yield carbonization of cellulose by sulfuric acid impregnation. *Cellulose*. 2001;8(1):29-33.
32. Elazzouzi-Hafraoui S, Putaux JL, Heux L. Self-assembling and Chiral Nematic Properties of Organophilic Cellulose Nanocrystals. *Journal of Physical Chemistry B*. Aug 2009;113(32):11069-11075.
33. Mollet H, Grubenmann A. *Formulation technology*: Wiley-Vch; 2008.
34. Davis VA. Liquid crystalline assembly of nanocylinders. *Journal of Materials Research*. Jan 2011;26(2):140-153.
35. Song W, Windle AH. Isotropic-nematic phase transition of dispersions of multiwall carbon nanotubes. *Macromolecules*. 2005;38(14):6181-6188.
36. Orts WJ, Godbout L, Marchessault RH, Revol JF. Enhanced ordering of liquid crystalline suspensions of cellulose microfibrils: A small angle neutron scattering study. *Macromolecules*. Aug 1998;31(17):5717-5725.

CHAPTER THREE
REINFORCEMENT OF POLYLACTIC ACID FILMS WITH SURFACE MODIFIED
CELLULOSE NANOCRYSTALS

Introduction

Poly(lactic acid) (PLA) is a biodegradable polymer that has the potential to serve as a sustainable alternative to petroleum-derived plastics, becoming one of the most widely used biopolymers on the market.¹ The production of PLA, which represents 38% of the bioplastic total market, increased 64% from 2010 to approximately 187,000 metric tons in 2011 and is estimated to climb to 271,000 metric tons by 2015.² PLA is synthesized from lactic acid made from corn starch or sugar cane,³ and its production requires 25 - 55% less energy than petroleum-based polymers due to its relatively lower melting point (T_m),^{4, 5} therefore reducing the net CO₂ emission to the environment compared to these polymers.^{6, 7} Moreover, PLA has received much research attention in the last two decades due to its high tensile properties, transparency, and low toxicity, resulting in an improved material at a reduced cost that has emerged in a highly competitive polymer market.⁸⁻¹² On the other hand, its brittleness and low vapor and gas barrier are potential limitations in extending its applications, thus representing areas of current development.¹

One alternative for addressing these limitations is the reinforcement of PLA with cellulose nanocrystals (CNCs). This nanofiller has attracted attention as a polymer reinforcement material due to its exceptional mechanical properties, ability for surface functionalization, abundance, and renewability.¹³ Similar to other nanofillers, CNCs

exploit properties not found in macro-sized materials, specifically their high surface areas, aspect ratios, and multi-functionalities. These nanocrystals can be isolated from a variety of sources such as cotton, wood pulp, tunicate, or bacteria usually by acid hydrolysis.¹⁴ Through this process, non-crystalline regions of the cellulose are hydrolyzed, while the highly crystalline ones resist acid attack, resulting in a crystalline, high performance material. Crystalline cellulose has been estimated to possess a higher elastic modulus than Kevlar and higher tensile strength than steel wire, with 80% less weight.^{15, 16} However, to incorporate the mechanical property benefits of CNCs in polymer nanocomposites, the CNC surface needs to be modified to enhance compatibility with the desired polymer matrix.

Surface modifications such as acetylation, silylation, oxidation, polymer grafting, and absorption of surfactants, among others have been reported in the literature.¹⁴ For example, a single-step method for the acetylation of CNCs, proposed by Dorgan and Braun,¹⁷ is one method for successful dispersion of CNCs in organic solvents. Moreover, it is believed that CNC acetylation enhances the adsorption of surfactants, promoting a better dispersion of CNCs in an organic matrix without compromising the cellulose degradation temperature. Recent research suggests that the adsorption of surfactants and long-chain molecules have shown to be effective in the compatibilization of CNCs with hydrophobic polymers, increasing the toughness of the composites.¹⁴ However, it is usually observed that a high amount of surfactant addition ranging from 0.5:1 to 4:1 surfactant to CNC mass ratio is required for compatibilization, thus restricting the nanocomposite properties and performance.¹⁸ For this reason, it is important to explore

surfactants having similar effects but that required lower proportions. In this study, we investigate decylamine (DA) and cetyltrimethyl-ammonium bromide (CTAB) for solution compatibilization within PLA-CNC film nanocomposites.

The reinforcement of polymers varies as a function of the nanocrystal morphology, functionality, polydispersity, and processing conditions.¹⁴ Therefore, the results reported in the literature differ considerably, suggesting that future research is needed to identify the variables and the mechanisms of reinforcement. Past research indicates that good dispersibility of CNCs within the matrix is important for composite reinforcement.¹⁹ Interestingly, some hydrophobic matrices have been reinforced using hydrophilic CNCs,²⁰ while in other cases, surface-modified CNCs have not exhibited the expected enhancement in the mechanical properties that would be expected from enhanced compatibility with rigid fillers.²¹ These behaviors can be attributed to different stress transfer mechanisms. A percolating network can be formed at a critical filler concentration, in which stress transfer is facilitated by filler-filler interactions, usually increasing the tensile strength and modulus of the composites.²² On the other hand, at low filler concentrations the stress transfer is mainly through filler-matrix interactions, for which good compatibility usually results in increased toughness.¹⁴ Additionally, fillers with larger aspect ratios tend to increase the tensile properties, while smaller sizes, such as the nanocrystals, have been observed to enhance toughness.²³

The aim of this work is to enhance the toughness of PLA by the addition of acetylated CNCs that had been further modified with surfactants. We have previously

shown that the introduction of surfactants improves the CNCs stability and self-assembly in organic solvents, indicating a good dispersion of nanocrystals in the solvents. For this work, PLA-CNC nanocomposite films (0, 1, 3, 5 and 10 wt.% CNCs) were extruded and mechanically tested using an Instron testing machine. An increase in toughness was observed at low CNCs concentrations when using DA surfactant, while the tensile strength and modulus remained constant compared to neat PLA. The crystallinity of nanocomposites was not significantly affected, allowing the improvement of toughness and limiting the typical reduction of strength and modulus. The CNC orientation and nanocomposite self-organization was studied using polarized-light microscopy, demonstrating significant organization which was observed to increase with CNC concentration.

Materials and Methods

Materials

Commercially available PLA from NatureWorks 2003D (95% L-PLA and 5% D-PLA) was used as the polymer matrix. Ashless clippings filter aids from Whatman™ were used as the starting material for the CNC synthesis. The reactants used for the synthesis (glacial acetic acid and hydrochloric acid 37% w/v) were ACS grade chemicals obtained from VWR. Chloroform and decylamine were ACS grade reagents obtained from Sigma Aldrich. High purity grade cetyltrimethyl-ammonium bromide (CTAB) was obtained from Amresco.

Synthesis and characterization of CNCs

CNCs were synthesized by the method of Dorgan¹⁷ and following the steps provided here in brevity. This isolation reaction introduces carbonyl groups on the CNC surface, reducing the hydrogen bonding and thus increasing the ability to disperse in organic solvents. CNCs were reacted with a mixture of hydrochloric acid and acetic acid for 10 h at 105 °C. Cellulose cotton filters (10 g) were soaked overnight with 225 mL of acetic acid. A total of 0.8 mL of hydrochloric acid (37%) and 24.5 mL of deionized water were added and the reaction time started when the final temperature was reached. After the reaction, a purification step was performed to remove excess acid and separate the unhydrolyzed cellulose. This procedure consisted of the precipitation of cellulose by centrifugation, removal of supernatant, addition of deionized water and vigorous mixing for redispersion. After 3 purification steps, CNCs were sonicated using a Fisher Scientific 550 Sonic Dismembrator for 5 cycles of 7 min in an ice bath. The suspensions were purified again until a cloudy supernatant was observed. The aqueous suspension of isolated acetylated CNCs was obtained by combining the following 2 - 3 supernatants. The nanocrystals were transferred to an organic solvent by separating the water via centrifugation and washing the precipitates with acetone at least twice. Vigorous mixing was performed using a Vortex-Genie 2 (Scientific Industries, Inc.). At least 40 min of mixing is required to minimize visible signs of agglomeration in the resulting suspension. The desired surfactant (decylamine or CTAB) was subsequently added to the suspension and mixed for 5 – 10 min. (See complete procedure in Appendix B.1)

The nanocrystals dimensions were measured by Transmission Electron Microscopy (TEM) using a Hitachi 7600 TEM with an accelerating voltage of 120 kV. CNCs samples were prepared by nebulizing a diluted CNC suspension of about ~0.01% (w/v) onto a formvar carbon coated copper grid (Ted Pella). Thermal gravimetric analysis (TGA) (TA instruments SDT Q600) was performed to determine the degradation temperature of CNC. A sample from the organic suspension was dried and the remaining powder was placed in the TGA alumina pans. The nanocrystals were first heated to 110 °C for 25 min to minimize any residual solvent and cooled again to 80 °C before ramping at heating rate of 10 °C/min to 650°C. The TGA run was carried out under nitrogen atmosphere (100 mL/min) and then switched to oxygen from 650 °C to 800 °C.

Preparation of PLA-CNC Nanocomposites

PLA nanocomposites were made by blending a 5% (w/v) solution of PLA in chloroform with a 1% (w/v) CNC suspension using an overhead stirrer. These PLA-CNC solutions, with CNC contents of 1, 3, 5 and 10 wt.%, were allowed to dry overnight at room conditions in a Pyrex container. The films were placed under vacuum at 70 °C for 12 h and then raised to 120 °C for 1 h to remove any residual solvent. Approximately 15 g of nanocomposite films were diced and extruded using a DSM Xplore co-rotating twin-screw microcompounding extruder. The composite was fed and compounded for about 10 min at a temperature of 195 °C. The extruder was set to a constant force at the die of 500 N, allowing the equipment to vary the screw rotation to obtain a constant melt flow. The

polymer melt was then extruded through a rectangular cross-sectional shape die while it was cooled with ambient nitrogen gas and collected on a chill roll with a take-up speed of 120 rpm. These films were cut into 95 mm x 12.5 mm strips using a hydraulic press and a custom-made metal die. A total of 6 to 8 samples were prepared for each CNC composite loading and type of surfactant. The thicknesses of the films were taken at 4 different sections of the films and an average of 0.18 ± 0.02 mm was obtained. Some of the nanocomposites prepared and their respective names in this work are displayed in Table 3.1 for an easier visualization.

Nanocomposite characterization

Tensile testing of the nanocomposites was performed using an Instron 1125 tensile testing instrument. The initial grip separation was 45 mm and set to a separation rate of 4 mm/min. Information on displacement and force exerted in the stretching of the films was obtained in stress – strain curves and used to determine tensile strength, tensile modulus, and toughness of each film.

Perkin-Elmer Pyris 1 differential scanning calorimetry (DSC) was used to determine the crystallinity of the nanocomposites. Between 5 and 6 mg of sample was carefully sealed inside an aluminum pan. The samples were heated to 210 °C at 20 °C/min under nitrogen atmosphere and maintained at a constant temperature for 2 min prior to cooling at a rate of 20 °C/min. The crystallinity of PLA-CNC films was calculated by measuring the areas under the melting and crystallization curves and using Eq.1 as follows,

$$X_c [\%] = \frac{\Delta H_m - \Delta H_{cc}}{(\Delta H_m^\infty) * X_{PLA}} * 100\% \quad \text{Eq. 1}$$

Where ΔH_m and ΔH_{cc} are the enthalpies of melting and crystallization, respectively, as measured by the DSC scans. X_{PLA} is the fraction of PLA in the composites as described in the Table 3.1.²⁰ The theoretical enthalpy of fusion of 100% crystalline PLA, ΔH_m^∞ , was taken to be 93.0 J/g.²⁴

The optical properties of the films and orientation of the CNCs in the nanocomposite were studied using an optical polarized-light microscope (Olympus BX-60) in transmission mode with a polarizer in the bottom of the sample and the analyzer rotated 90° in the top. The films were directly placed on glass slides and analyzed at 10X magnification without any further modification by rotating the stage from 0 to 135°. Observations were also made adding a first-order red plate inserted at 45° between the polarizer and analyzer. Adobe Photoshop was used to increase the contrast for display purposes and to measure the percentage of color.

Table 3.1. Nomenclature and fractions of the PLA-CNC nanocomposites prepared in this work

Sample Name	CNC (%)	PLA (%)	Surfactant (1 wt. % with respect to CNC weight)
PLA	0	100	-
PLA-CNC(1%)-UM	1	99	-
PLA-CNC(5%)-UM	5	95	-
PLA-CNC(1%)-DA	1	99	Decylamine
PLA-CNC(5%)-DA	5	95	Decylamine
PLA-CNC(1%)-CTAB	1	99	CTAB
PLA-CNC(5%)-CTAB	5	95	CTAB

Results and Discussion

Characterization of Cellulose Nanocrystals

The nanoscale dimension and high aspect ratio of the CNCs are exceptionally important in the enhancement of mechanical properties of polymers. The high surface area to volume ratio enables good molecular level interactions with different matrices,¹⁷ and a high aspect ratio ensures a enhanced stress transfer to the nanocrystals.¹⁹ Figure 3.1 shows a representative TEM micrograph of CNCs dried from a THF suspension, confirming the successful isolation of the nanocrystals. These nanocrystals are observed to have the tendency to aggregate after drying which is likely due to the lack of surface charge for the acetylated CNCs.¹⁹ It is expected that the introduction of compatibilized CNCs into an organic media will reduce the tendency to agglomerate due to enhanced filler-matrix interactions. A rough estimate of the size of the isolated crystals was

measured to be around 250 nm long and 35 nm wide, which is in agreement to reported values in the literature.¹⁷

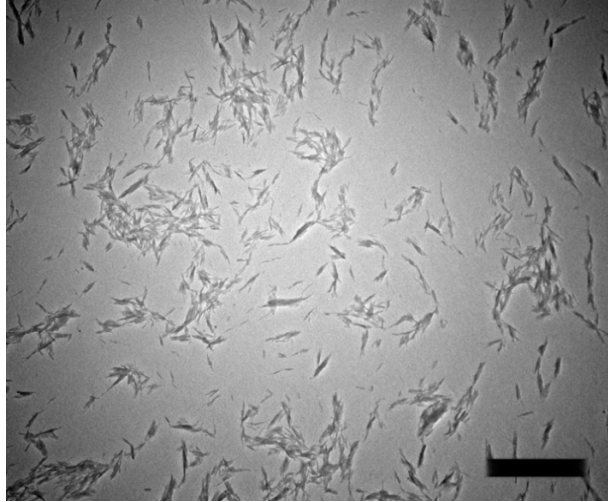


Figure 3.1. TEM image of cellulose nanocrystals synthesized using acetic acid and stabilized with decylamine surfactant. Bar: 2 μm .

The thermal stability of nanofillers is an important parameter for nanocomposite processing due to the relatively high melting point and temperatures required for melt compounding for most of the polymers. Figure 3.2 shows the degradation temperatures of CNCs without surfactant and with decylamine (DA), demonstrating the excellent thermal stability of the nanocrystals. The onset degradation temperature was observed to be approximately 331 °C for acetylated CNCs with and without surfactant, which is well above the processing temperature of the PLA (190 °C). This CNC modification, as shown by Dorgan,¹⁷ has the advantage of keeping the thermal stability of native cellulose, contrary to other common modifications which significantly reduce the degradation temperature of cellulose.²⁵⁻²⁷

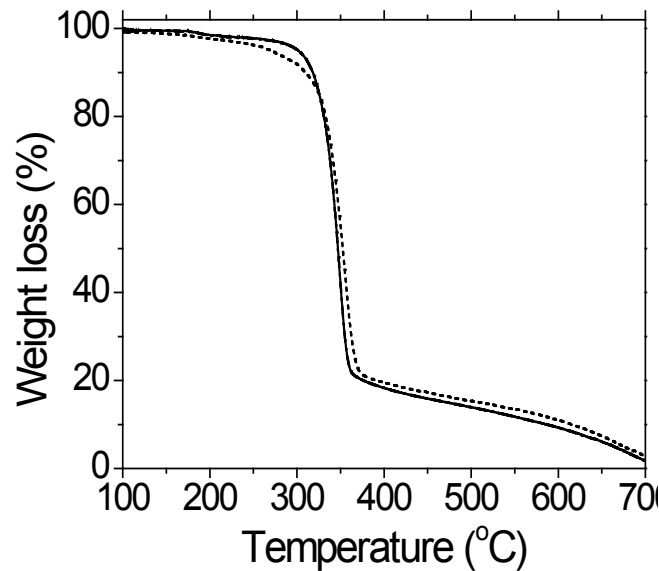


Figure 3.2. TGA weight loss as a function of temperature for the acetylated CNC without surfactant (solid line) and with decylamine surfactant (dashes).

Mechanical Properties of the Nanocomposite Films

The mechanical properties of the nanocomposite films calculated from the stress-strain curves are presented in Figure 3.3. The energy at break or toughness of PLA-CNC nanocomposites exhibited a maximum enhancement at 1% CNC content before decreasing with increasing loading. This maximum enhancement occurred for the nanocomposites with DA surfactant and represented a 61% increase with respect to neat PLA. For the 3% DA-modified CNC composites a slight enhance of 8% was exhibited, while for the 5 and 10% composites the toughness was decreased with respect to neat PLA. The unmodified (UM) and CTAB-modified nanocomposites exhibited a decreased toughness compared to PLA and to PLA-CNC-DA at each CNC concentration. The composites at 10% CNC load were more brittle, demonstrating a reduced toughness up to 95% less of that for the PLA. The decrease in toughness in nanocomposites has been

attributed to large agglomerations of nanofillers.^{19, 28} These agglomerations can act as stress concentrators, which facilitates spreading of the defects generated at the interface. These defects can grow larger than the critical crack size, resulting in film failure.

A maximum in the reinforcement of toughness is frequently observed when good dispersions occur at low filler concentrations^{29, 30} as it was found for the PLA-CNC(1%)-DA composites. This improvement can therefore be the result of favorable dispersions and better interfacial compatibility of CNC-DA with PLA compared to UM- and CTAB-modified CNCs.^{31 32} There are a few toughening mechanisms with rigid fillers discussed in the literature; however, this discussion seems inconclusive for CNC nanocomposites. Toughening mechanisms include the formation of microvoids,³³ crack bifurcation and crack path alteration,³⁴ interfacial debonding,²³ assembly into spiral orientation,³⁵ and shear yielding resulting from the difference on the Young's moduli of the filler and the matrix.³⁶ In our previous work (Chapter 2), the addition of DA improved the CNC compatibility with aprotic solvents compared to plain CNC, which agrees with the enhanced mechanical properties obtained when using this surfactant in the present work.

The tensile strength and modulus of the composites followed similar trends as it can be observed in Figure 3.3b-c, remaining fairly constant up to 3% CNC load but decreasing drastically after 5%. At a 10% load, the mechanical properties were deteriorated obtaining at best a 45% and 32% reduction for the strength and modulus, respectively. This behavior follows the same trend as the energy at break for the 10% films and may be indicative of CNC agglomeration.

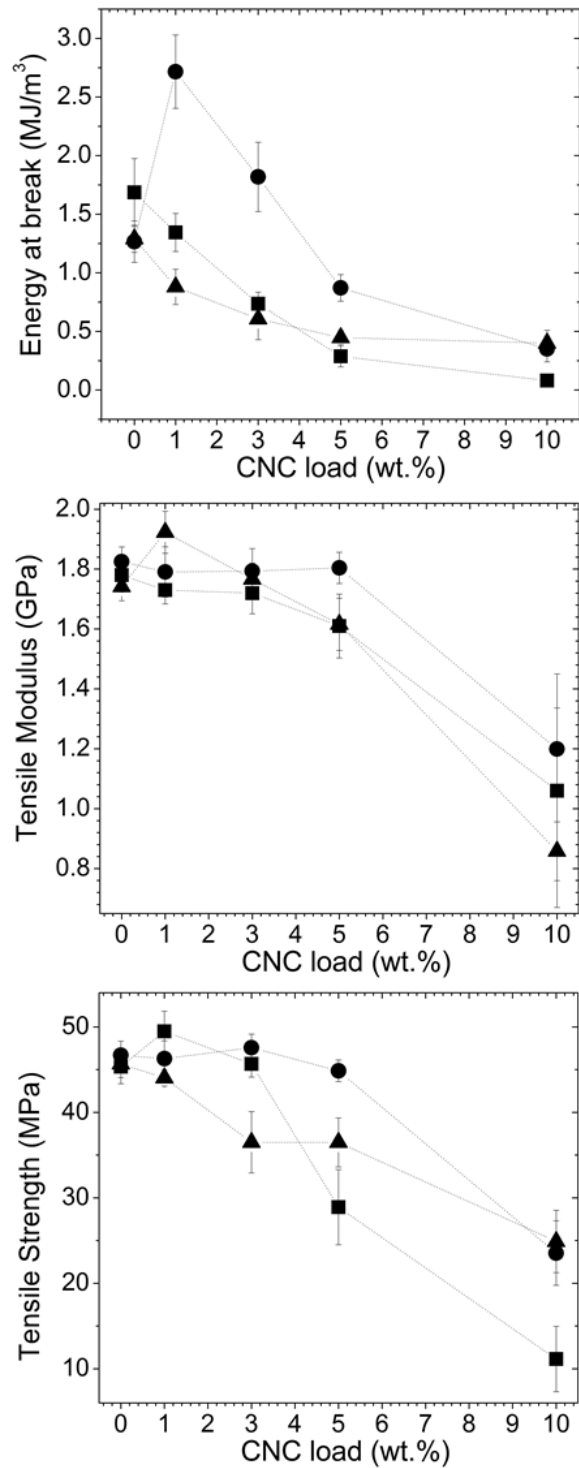


Figure 3.3. Mechanical Properties of PLA-CNC composites using different surfactants.
 ■, -UM; ●, -DA; ▲, -CTAB

It has been demonstrated that one mechanism occurring in the reinforcement of the tensile properties of CNC nanocomposites is the formation of a percolating network, which transfers the stresses effectively throughout the nanocomposite when high concentrations of filler are added.^{14, 22} This mechanism has been often observed with hydrophilic or surface-charged CNC when the filler-filler interactions are stronger than the filler-matrix ones and they do not tend to easily aggregate.^{37, 38} In non-surface-charged nanocrystals, such as the acetylated CNCs in this work, a percolating network is more difficult to form without the formation of agglomerates, introducing defects and thus reducing polymer reinforcement.¹⁹ Therefore, the reinforcement exhibited at low filler concentrations can be attributed to the stress transfer through filler-matrix interactions. However, the relatively low aspect ratios of the CNCs, which are estimated to be approximately 6 to 12, may not enable a perfect transfer of the stresses, reducing the effect of the good compatibility provided by the surfactant.²² According to the Halpin-Tsai model for short-fiber composites, only nanofillers with aspect ratios larger than 50 can guarantee an efficient reinforcement of the elastic modulus.³⁹

The addition of surfactants does not seem to significantly affect the tensile strength and modulus of the films as observed in Figure 3.3b-c. However, DA-modified composites possess overall slightly higher values compared to the other two modified composites, which may also confirm the enhancement of the filler-matrix interactions. Even though these tensile properties were not significantly increased, they were not reduced for the toughened composites (PLA-CNC(1%)-DA), which is frequently a disadvantage in the toughening of polymers. These tensile properties are already good for

PLA compared to other petroleum-based polymers; therefore enhancing toughness without compromising other properties becomes an integral step in the reinforcement of PLA.

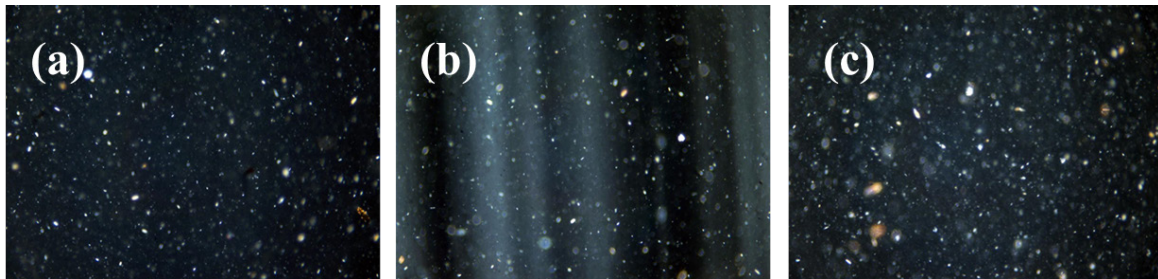


Figure 3.4. Polarized-light microscopy images demonstrating the agglomeration level on the 3% CNC nanocomposites. a) UM; b) DA; c) CTAB. Length of the longest side of each image: 1.5mm

Alignment of CNC and agglomerations

The level of CNC agglomeration in all of the 3% CNC loaded nanocomposites was observed by employing polarized-light microscopy (Figure 3.4). All of the composites appear to have relatively large agglomerates; however, for PLA-CNC(3%)-UM (Figure 3.4a) these agglomerates are considerably more than for DA (Figure 3.4b), but less than the CTAB composites (Figure 3.4c). This confirms that using DA enhances the interfacial interaction and increases the nanocrystal dispersion in the composite. Moreover, this also endorses the proposed idea that the detriment of the mechanical properties occurs due to agglomerations forming at high concentrations as a result of insufficient compatibility. PLA-CNC(3%)-DA also displayed white bands that are attributed to liquid crystal formation which may be due to local CNC alignment within the composite.

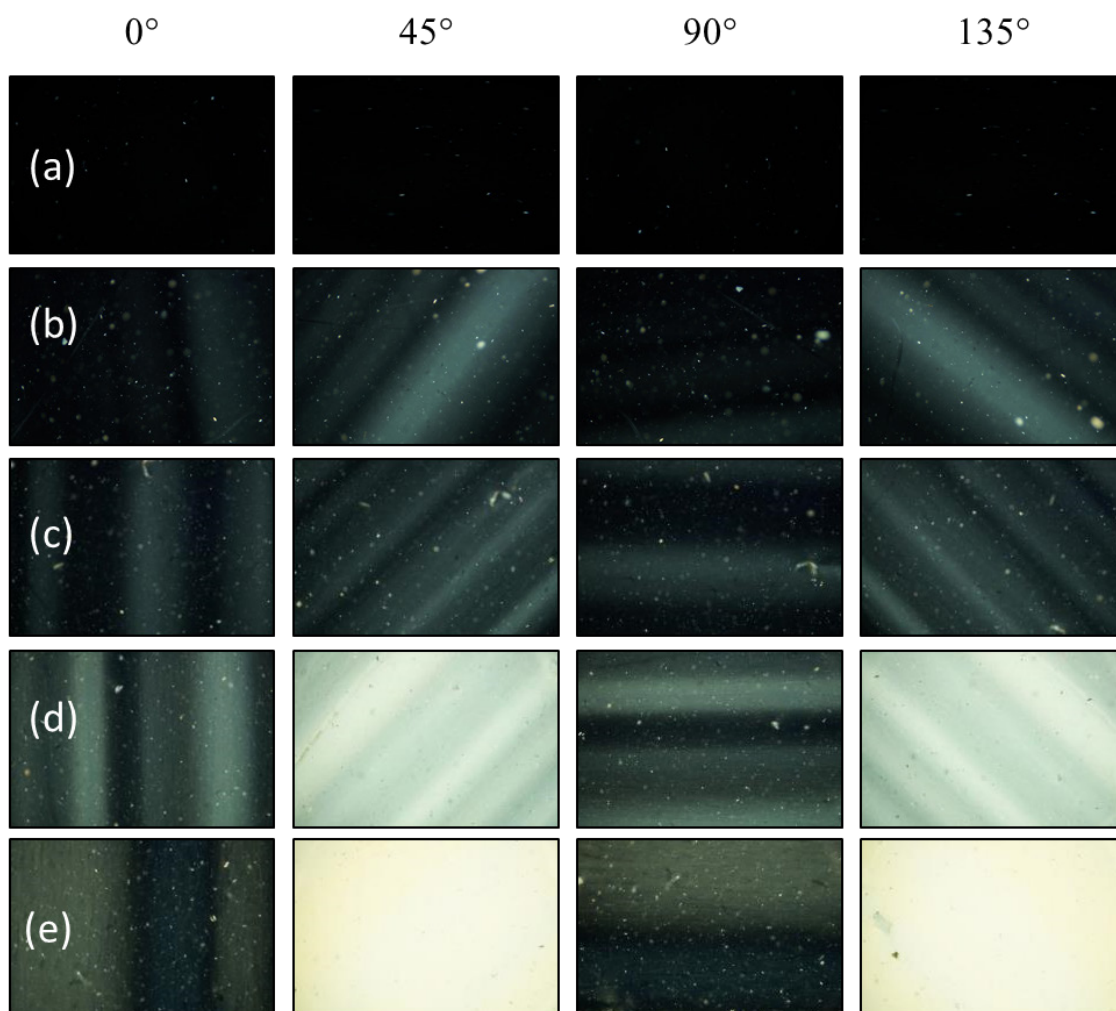


Figure 3.5. Polarized-light microscopy images of PLA-CNC-DA composites at different CNC loads: a, 0; b, 1; c, 3; d,5; and e, 10% CNC. At different rotating angles 0°, 45°, 90° and 135°. Images demonstrate the increasing formation of liquid crystals in the composites. Length of the longest side of each image: 1.5mm

The alignment and self-assembly of the nanocomposite films was studied using polarized-light microscopy. Figure 3.5 provides evidence of liquid crystal formation in the PLA composites at different CNC loads and rotation angles. A liquid crystal or anisotropic phase is formed when molecules or crystals assemble into a semi-organized structure, changing the refraction of the incident light and allowing the transmission of light between crossed polarized films. The brightness or birefringence observed on the

composites (especially at 45° and 135°) in Figure 3.5, increases with CNC concentration, indicating a higher level of crystal organization in the films. In this case, the polarizer and analyzer are fixed at 0° and 90° , respectively as observed in Figure 3.6. Crystals aligned in the 0° or 90° direction (or non-oriented crystals) will not diffract light since they possess the same angle of the polarized light. As a result, a bright phase will appear when crystals are oriented at 45° or 135° from the polarizer. For example, at 45° rotation angles in Figure 3.5, the bright phase indicates that the crystals are oriented either at 45° and 135° , indicating that the crystals are oriented parallel or perpendicular to the film extrusion.

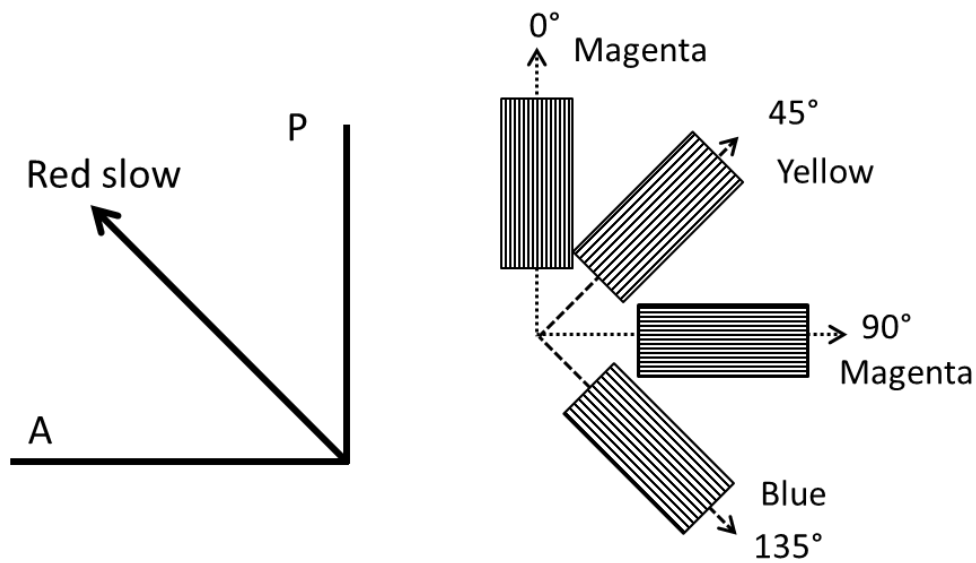


Figure 3.6. Schematics of the filter orientations in the polarized-light microscope. A) polarizer (P), analyzer (A) and first order red plate (red slow direction); and B) colors observed when liquid crystals are oriented in the corresponding angles of rotation.

A first order red plate was added between the polarizer and analyzer (Figure 3.6) in order to better elucidate the direction of the crystals, also called sign of the birefringence. The direction of the slow red axis of the filter is oriented at 135° as shown

in Figure 3.6. Therefore, liquid crystals oriented at 135° will appear blue due to the added effects resulting from coincidence of the angles of the slow axes of the liquid crystal (or larger refractive index) and the red plate. Crystals oriented in the 45° direction will appear yellow due to the lower interference colors resulting from the slow axes being perpendicular. On the other hand, crystals oriented in at 0° and 90° , as well as non-oriented crystals, will appear magenta as discussed above for polarized microscopy. The red order first plate is designed for low retardation crystals which appear as gray scale in crossed polars. This will rule out the possibility to properly analyze the 5% and 10% CNC composites since their brightness is strong as shown in Figure 3.5.

Figure 3.7 shows the polarized-light microscopy images with the red plate for neat PLA and the composites at 3% CNC load. As discussed above, the level of agglomeration for the UM- and CTAB-modified composites are evident, correlating also with the low crystal assembly on the films. On the other hand, DA films clearly display a change of color between the angles of rotation, indicating that the crystals are oriented in varying directions. As an example, for the DA composites at 0° rotation, blue and yellow indicate a crystal orientation of 45° and 135° , respectively, while magenta would be non-oriented, 0° , and 90° orientation. When the sample is rotated 45° , yellow indicates crystals oriented perpendicular to the direction of the extrusion (45°), while blue will be perpendicular (135°). Therefore, the total area occupied by the oriented crystals can be calculated theoretically by adding the colors blue and yellow from the 0° and 45° angle images.

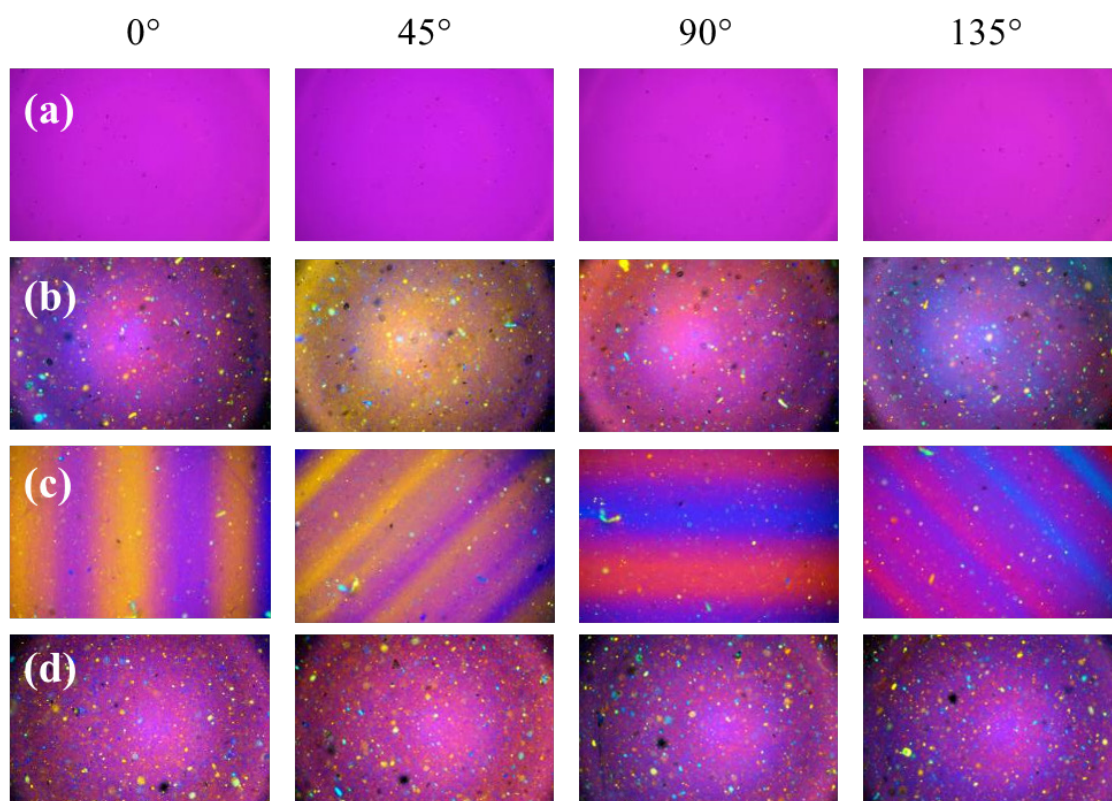


Figure 3.7. Polarized-light microscopy images of the 3% CNC loaded nanocomposites using a first order red filter; a, Neat PLA; b, UM; c, DA; d, CTAB. At 0°, 45°, 90° and 135° rotation angles. Length of the longest side of each image: 1.5mm

Image analysis was performed using Photoshop in order to quantify the percentage of colors magenta, blue and yellow from the entire area of the images. The 1 and 3% CNC loaded composites were analyzed at 0° and 45° angles as observed in Table 3.2. The estimated oriented area was calculated by adding the blues and yellows at 0° and 45°. For neat PLA, the orientation is negligible resulting in 0% oriented area. However, as the CNC load increases the total calculated oriented area increases in different proportion for each of the composites. For example, the orientation in the DA composites goes from ~97% to ~100%, while for the UM goes from ~70% to ~100% (108% was actually measured) with increasing CNC content. Such results indicate a better

organization for DA composites at low concentrations as discussed above. The assembly of crystals for the CTAB composites is the lowest among all (0% and 8% for PLA-CNC(1%)-CTAB and PLA-CNC(3%)-CTAB, respectively), correlating correctly with the poor mechanical properties obtained for those composites.

The high level of assembly for the DA composites does not necessarily mean well-oriented filler in the direction of the extrusion. Indeed, the DA composites only have ~26% of their organized crystals oriented parallel to the extrusion of the flow, ~14% perpendicular, and around 60% is distributed between 45° and 135° with respect to the extrusion direction. In the case of UM composites, an unexpected high orientation of the crystals was observed in the direction of extrusion (~89% for PLA-CNC(3%)-UM). Poor oriented crystals cannot necessarily be translated to poor mechanical properties. It has been suggested in the literature that a lower degree of CNC orientation may enhance the nanocomposite toughness, although a reduced tensile modulus is accompanied.³⁵ Therefore, it can be thought that this distribution of crystal orientation may change the path of the crack sufficiently enough to dissipate energy and increase toughness. The ability for acetylated CNCs to self-assemble in organic media in stationary and shear states was studied in our previous work, agreeing with the self-assembly observed in the nanocomposites in the present study.

Table 3.2. Approximate Percentage of colors of PLA-CNC composites observed under polarized-light microscopy with a first order red plate.

	0°			45°			Estimated oriented area
	Magenta	Yellow	Blue	Magenta	Yellow	Blue	
PLA	100%	0%	0%	100%	0%	0%	0%
PLA-CNC(1%)-UM	53%	42%	5%	77%	22%	1%	70%
PLA-CNC(3%)-UM	92%	3%	5%	0%	89%	11%	100%
PLA-CNC(1%)-DA	43%	23%	34%	59%	26%	14%	97%
PLA-CNC(3%)-DA	40%	38%	21%	60%	26%	14%	100%
PLA-CNC(1%)-CTAB	100%	0%	0%	100%	0%	0%	0%
PLA-CNC(3%)-CTAB	97%	1%	2%	95%	2%	3%	8%

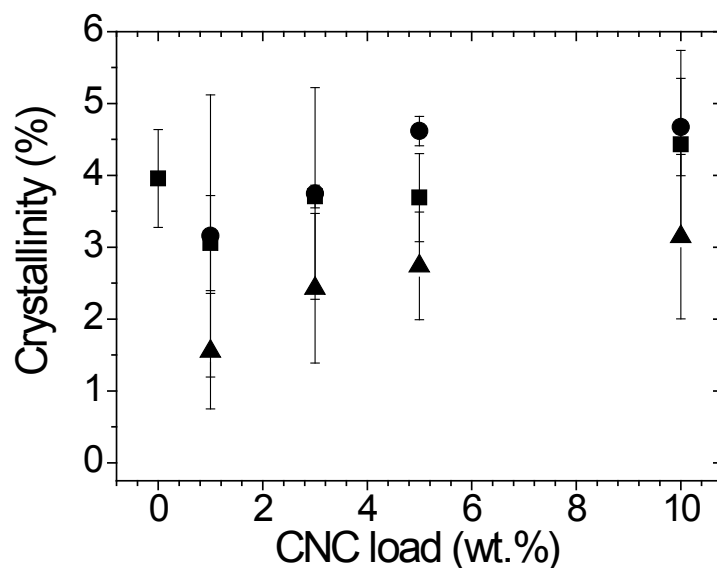


Figure 3.8. Crystallinity of PLA-CNC composites estimated by DSC. ■, -UM; ●, -DA; ▲, -CTAB

Crystallinity of Nanocomposite Films

PLA-CNC nanocomposite crystallinity was determined by DSC, and the results are shown in Figure 3.8. Neat PLA was determined to have low crystallinity, which is likely due to the enantiomer composition, L (95%) and D (5%). It is observed that the addition of CNCs did not significantly affect PLA crystallinity, which is advantageous to the enhancement of toughness and elongation at break. However, the slightly highest crystallinity occurs for the DA composites, which were observed to be the least agglomerated and most oriented of the 3 modifications studied in this work. DSC analysis also revealed a double melting peak for PLA which occurs at specific conditions of cooling and heating rates.⁴⁰ The double peaks have been attributed to a melting-recrystallization mechanism of PLA, in which small and imperfect crystallites change into more stable crystals during the melting of the polymer.⁴¹

Transparency

The transparency of some of the nanocomposite films decreased with CNC addition as observed in Figure 3.9. However, even at 5% loads there is significant optical transparency compared to neat PLA. Transparency is an important property for food packaging applications among others, and it may be enhanced with other additives.

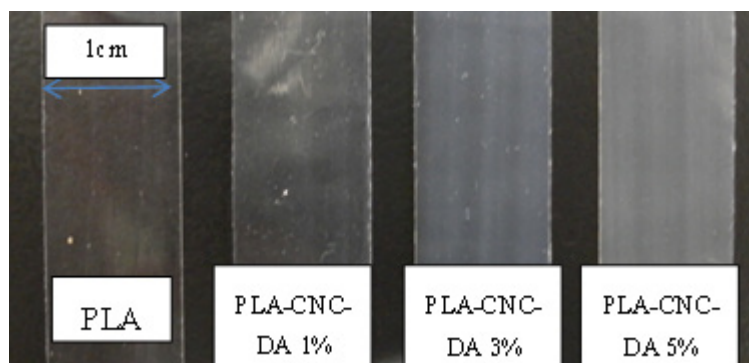


Figure 3.9. Example of the transparency of PLA-CNC-DA composites

Conclusions

Surfactant-modified CNCs were added into PLA as reinforcement fillers, resulting in enhanced mechanical and optical properties of extruded films. The toughness of the PLA composites was enhanced 61% compared to neat PLA when using 1% of DA-modified CNCs. As the CNC concentration increased higher than 1%, toughness gradually decreased to very low values for 10% CNCs. For unmodified and CTAB-modified CNCs, toughness decreased with concentration worsening the properties of PLA. The increase in toughness was attributed to a relatively good dispersion and good interfacial adhesion between the CNC and the matrix. Tensile strength and modulus remained fairly similar compared to neat PLA, but as CNC concentration increased these

properties decreased more than 45% for the 10% CNC composites. The relatively low aspect ratio of the CNC may not enable a perfect stress transfer and therefore reducing the effect on the modulus. The lack of surface charge also forbids CNC to form a percolating network that has been shown to greatly increase the tensile properties.

Polarized-light microscopy images revealed liquid crystal formation of the CNC nanocomposites, which was found to be oriented in different directions within the polymeric matrix. It was shown that a better dispersion of CNC would present a higher organization in the composites, especially in the ones modified with DA. However, the degree of alignment was found to be relatively low with CNC orientation pointing along multiple directions around the extrusion line for the toughened composites, which can be attributed to the inherent spiral assembly of cellulose as reported in the literature.³⁵ The crystallinity of the nanocomposites was not increased by the addition of the CNCs, which also facilitated the toughening of the composites by the addition of the filler. Overall, this work shows the ability to increase PLA toughness without compromising the good strength and modulus of PLA by the addition of a low percentage of acetylated CNCs further functionalized with surfactants.

References

1. Nampoothiri KM, Nair NR, John RP. An overview of the recent developments in polylactide (PLA) research. *Bioresource Technology*. Nov 2010;101(22):8493-8501.
2. Bioplastics E. Bioplastics facts and figures Available at: <http://en.european-bioplastics.org/>. Accessed 06/06/2013, 2013.

3. Pang X, Zhuang X, Tang Z, Chen X. Polylactic acid (PLA): research, development and industrialization. *Biotechnology Journal*. 2010;5(11):1125-1136.
4. Rasal RM, Janorkar AV, Hirt DE. Poly (lactic acid) modifications. *Prog Polym Sci*. 2010;35(3):338-356.
5. Auras RA, Lim L-T, Selke SE, Tsuji H. *Poly (lactic acid): synthesis, structures, properties, processing, and applications*. Vol 10: Wiley; 2011.
6. Bogaert JC, Coszach P. Poly(lactic acids): A potential solution to plastic waste dilemma. *Macromol Symp*. Mar 2000;153:287-303.
7. Vink ETH, Rabago KR, Glassner DA, Gruber PR. Applications of life cycle assessment to NatureWorks (TM) polylactide (PLA) production. *Polym Degrad Stabil*. Jun 2003;80(3):403-419.
8. Ahmed J, Varshney SK. Polylactides-Chemistry, Properties and Green Packaging Technology: A Review. *Int J Food Prop*. 2011;14(1):37-58.
9. Balakrishnan H, Hassan A, Imran M, Wahit MU. Toughening of Polylactic Acid Nanocomposites: A Short Review. *Polym-Plast Technol Eng*. 2012;51(2):175-192.
10. Jamshidian M, Tehrany EA, Imran M, Jacquot M, Desobry S. Poly-Lactic Acid: Production, Applications, Nanocomposites, and Release Studies. *Compr Rev Food Sci Food Saf*. Sep 2010;9(5):552-571.
11. Liu HZ, Zhang JW. Research Progress in Toughening Modification of Poly(lactic acid). *Journal of Polymer Science Part B-Polymer Physics*. Aug 2011;49(15):1051-1083.
12. Ray SS. Polylactide-Based Bionanocomposites: A Promising Class of Hybrid Materials. *Accounts of Chemical Research*. Nov 2012;45(10):1710-1720.

13. Ramires EC, Dufresne A. A review of cellulose nanocrystals and nanocomposites. *Tappi J.* Apr 2011;10(4):9-16.
14. Habibi Y, Lucia LA, Rojas OJ. Cellulose Nanocrystals: Chemistry, Self-Assembly, and Applications. *Chemical Reviews.* Jun 2010;110(6):3479-3500.
15. Sturcova A, Davies GR, Eichhorn SJ. Elastic modulus and stress-transfer properties of tunicate cellulose whiskers. *Biomacromolecules.* Mar-Apr 2005;6(2):1055-1061.
16. Moon RJ, Martini A, Nairn J, Simonsen J, Youngblood J. Cellulose nanomaterials review: structure, properties and nanocomposites. *Chem Soc Rev.* 2011;40(7):3941-3994.
17. Braun B, Dorgan JR. Single-Step Method for the Isolation and Surface Functionalization of Cellulosic Nanowhiskers. *Biomacromolecules.* Feb 2009;10(2):334-341.
18. Kim J, Montero G, Habibi Y, et al. Dispersion of Cellulose Crystallites by Nonionic Surfactants in a Hydrophobic Polymer Matrix. *Polymer Engineering and Science.* Oct 2009;49(10):2054-2061.
19. Rusli R, Shanmuganathan K, Rowan SJ, Weder C, Eichhorn SJ. Stress Transfer in Cellulose Nanowhisiker Composites-Influence of Whisker Aspect Ratio and Surface Charge. *Biomacromolecules.* Apr 2011;12(4):1363-1369.
20. Liu DY, Yuan XW, Bhattacharyya D, Eastal AJ. Characterisation of solution cast cellulose nanofibre - reinforced poly(lactic acid). *Express Polym Lett.* Jan 2010;4(1):26-31.
21. Grunert M, Winter WT. Nanocomposites of cellulose acetate butyrate reinforced with cellulose nanocrystals. *Journal of Polymers and the Environment.* Apr 2002;10(1-2):27-30.
22. Eichhorn SJ, Dufresne A, Aranguren M, et al. Review: current international research into cellulose nanofibres and nanocomposites. *Journal of Materials Science.* Vol 45; 2010: 1-33.

23. Xu XZ, Liu F, Jiang L, Zhu JY, Haagenonson D, Wiesenborn DP. Cellulose Nanocrystals vs. Cellulose Nanofibrils: A Comparative Study on Their Microstructures and Effects as Polymer Reinforcing Agents. *ACS Appl Mater Interfaces*. Apr 2013;5(8):2999-3009.
24. Pei A, Zhou Q, Berglund LA. Functionalized cellulose nanocrystals as biobased nucleation agents in poly(L-lactide) (PLLA) - Crystallization and mechanical property effects. *Composites Science and Technology*. May 2010;70(5):815-821.
25. Johnson RK, Zink-Sharp A, Glasser WG. Preparation and characterization of hydrophobic derivatives of TEMPO-oxidized nanocelluloses. *Cellulose*. Dec 2011;18(6):1599-1609.
26. Roman M, Winter WT. Effect of sulfate groups from sulfuric acid hydrolysis on the thermal degradation behavior of bacterial cellulose. *Biomacromolecules*. 2004;5(5):1671-1677.
27. Kim DY, Nishiyama Y, Wada M, Kuga S. High-yield carbonization of cellulose by sulfuric acid impregnation. *Cellulose*. 2001;8(1):29-33.
28. Hossain KMZ, Ahmed I, Parsons AJ, et al. Physico-chemical and mechanical properties of nanocomposites prepared using cellulose nanowhiskers and poly(lactic acid). *Journal of Materials Science*. Mar 2012;47(6):2675-2686.
29. Ng CB, Ash BJ, Schadler LS, Siegel RW. A study of the mechanical and permeability properties of nano- and micron-TiO₂ filled epoxy composites. *Adv Compos Lett*. 2001;10(3):101-111.
30. Bulota M, Vesterinen AH, Hughes M, Seppala J. Mechanical behavior, structure, and reinforcement processes of TEMPO-oxidized cellulose reinforced poly(lactic) acid. *Polym Compos*. Feb 2013;34(2):173-179.
31. Urena-Benavides EE, Kitchens CL. Cellulose Nanocrystal Reinforced Alginate Fibers-Biomimicry Meets Polymer Processing. *Molecular Crystals and Liquid Crystals*. 2012;556:275-287.

32. Bulota M, Kreitsmann K, Hughes M, Paltakari J. Acetylated microfibrillated cellulose as a toughening agent in poly(lactic acid). *Journal of Applied Polymer Science*. Oct 25 2012;126:E448-E457.
33. Knauert ST, Douglas JF, Starr FW. The effect of nanoparticle shape on polymer-nanocomposite rheology and tensile strength. *Journal of Polymer Science Part B-Polymer Physics*. Jul 2007;45(14):1882-1897.
34. Kim JK, Robertson RE. Toughening of thermoset polymers by rigid crystalline particles. *Journal of Materials Science*. Jan 1992;27(1):161-174.
35. Urena-Benavides EE, Kitchens CL. Wide-Angle X-ray Diffraction of Cellulose Nanocrystal-Alginate Nanocomposite Fibers. *Macromolecules*. May 2011;44(9):3478-3484.
36. Liang JZ, Li RKY. Rubber toughening in polypropylene: A review. *Journal of Applied Polymer Science*. Jul 2000;77(2):409-417.
37. Tang LM, Weder C. Cellulose Whisker/Epoxy Resin Nanocomposites. *ACS Appl Mater Interfaces*. Apr 2010;2(4):1073-1080.
38. Urena-Benavides EE, Brown PJ, Kitchens CL. Effect of Jet Stretch and Particle Load on Cellulose Nanocrystal-Alginate Nanocomposite Fibers. *Langmuir*. Sep 2010;26(17):14263-14270.
39. Halpin JC, Kardos JL. Halpin-tsai equations - review. *Polymer Engineering and Science*. 1976;16(5):344-352.
40. Yasuniwa M, Tsubakihara S, Sugimoto Y, Nakafuku C. Thermal analysis of the double-melting behavior of poly(L-lactic acid). *Journal of Polymer Science Part B-Polymer Physics*. Jan 2004;42(1):25-32.
41. Tang ZB, Zhang CZ, Liu XQ, Zhu J. The crystallization behavior and mechanical properties of polylactic acid in the presence of a crystal nucleating agent. *Journal of Applied Polymer Science*. Jul 2012;125(2):1108-1115.

CHAPTER FOUR

CELLULOSE NANOCRYSTALS VERSUS POLYETHYLENE GLYCOL AS
TOUGHENING AGENTS FOR POLY(LACTIC ACID)-POLY(ACRYLIC ACID)
GRAFT COPOLYMER

Introduction

Poly(lactic acid) (PLA) is a biodegradable, bioabsorbable polymer derived from renewable resources that offers promising alternatives to traditional petroleum-based plastics.¹ PLA, which accounts for 38% of the bioplastics market,² is utilized for applications ranging from medical devices to food packaging.³ PLA has a comparable tensile strength and elastic modulus to commodity polymers such as polyethylene terephthalate (PET); however, it has a very low toughness and elongation at break, limiting its widespread application.⁴ To address these disadvantages, many additives and modifications such as plasticizers,^{5, 6} fillers,^{7, 8} and graft copolymers^{9, 10} have been investigated for PLA.

One of the primary challenges in the toughening of polymers is the corresponding reduction of tensile strength and modulus of the material, making them impractical for many of the intended applications.⁴ In addition, many plasticizers are hydrophilic, representing issues of incompatibility with non-polar matrices. Several approaches have received recent research attention, including a reactive modification of PLA with polyacrylic acid (PAA) and subsequent blending with polyethylene glycol (PEG), which successfully increased toughness without a significant loss in the tensile properties.¹¹

PEG, a hydrophilic, non-toxic, polymer, is a common plasticizer that has been shown to increase the flexibility and ductility of polymers including PLA.^{12, 13} However, the chemical incompatibility between PEG and PLA leads to low molecular weight PEG migrating and phase separating from the matrix with time, while the high molecular weight structure results in an immiscible blend.¹⁴ The miscibility of PEG in PLA can be improved by the grafting of PAA, which is more hydrophilic,¹¹ potentially allowing improved miscibility with higher molecular weight PEG. Despite best attempts to increase toughness without compromising tensile properties by enhancing chemical compatibility, the common tradeoff between these two properties cannot be avoided when using PEG as a toughening agent. An alternative approach to enhance toughness without compromising tensile strength and modulus may be through the addition of cellulose nanocrystals.¹⁵

Cellulose nanocrystals (CNC), also known as cellulose nanowhiskers, have been widely investigated as reinforcement fillers for polymeric matrices due to their remarkable mechanical properties and high aspect ratios.¹⁶⁻¹⁸ These fillers usually increase the modulus of the matrix through the addition of a rigid material and the formation of a percolating network; however, some research has reported an improvement in toughness without compromising other mechanical and thermal properties.^{19, 20} In addition, research has also shown improved crystallinity and gas barrier properties for PLA with the addition of CNCs,^{21, 22} increasing the potential applications to encompass from food packaging to biomedical applications. One of the greatest challenges in the utilization of CNCs as a reinforcement filler for hydrophobic matrices is

the hydrophilicity of native cellulose.²³ One approach to addressing this challenge is through the surface functionalization of the nanocrystals, either by covalent modification or the use of a surfactant compatibilizer.²⁴

In this work, the modulus and toughness of PLA were improved by grafting PAA at 10 wt % concentration in order to increase the stiffness and hydrophilicity, making PLA more compatible with the plasticizers. Increasing proportions of either CNCs (1, 3, and 5 wt. %) or high molecular PEG (10, 20 and 30 wt.%) were added to the PLA-PAA copolymer. CNCs were isolated from cotton and functionalized by a combination of acetic acid and hydrochloric acid. The plasticizing efficiency of PEG was evaluated by the shift of glass transition temperature (T_g). The mechanical, thermal, and optical properties of the nanocomposites and the blends were subsequently analyzed.

Materials and Methods

Materials

Poly(lactic acid) (PLA) 2002D was purchased from NatureWorks LLC ($M_w \approx 198$ kDa and $M_n \approx 76$ kDa).²⁵ Benzyl peroxide was purchased from Fluka. Acrylic acid 99% and 10 kDa polyethylene glycol (PEG) (OH-terminated) were obtained through Aldrich. Cotton ashless powder from Whatman was used as the source of cellulose. All other solvents and reactants in this work were ACS grades obtained from VWR.

Cellulose Nanocrystals Preparation

Cellulose nanocrystals were isolated by acid hydrolysis with a mixture of hydrochloric acid (HCl) and acetic acid (AA) as developed by Dorgan and co-workers.²⁶ In this reaction, a Fischer esterification reaction occurs between the hydroxyl groups and the acetic acid during the hydrolysis, introducing methylesters onto the CNC surface. For the isolation, 10 g of cotton were soaked for approximately 12 h in a round bottom flask with 225 mL of AA. The next day, 24.5 mL of DI water and 0.8 mL 37% HCl were added. The reaction was performed for 10 h at 105 °C with constant stirring. The reaction was quenched by immersing the flask in an ice bath. Three washes with DI water were carried out by sequential centrifugation (8,600 rpm for 3min) and vortex mixing to remove the remaining acid from the cellulose. The suspension was combined and ultrasonicated in an ice bath using a Fisher Scientific 550 Sonic Dismembrator for 35 min (5 cycles of 7 min pulse, 2 min rest) at a power level of 7.5. The suspension was washed again two more times and the resulting supernatant was combined and stored as the CNC master suspension. To transfer the CNCs to an organic solvent, the supernatant was precipitated by centrifugation at 14,000 rpm for 10 min, washed twice with acetone to remove bound water, and transferred to chloroform. The suspension was agitated vigorously in a vortexer until no CNC agglomerates were observed. (The complete synthesis procedure is detailed in Appendix B.1)

PLA Reactive Modification and Blending

PLA reactive modification was performed in a 1 L Parr reactor, where PAA side chains were grafted from the PLA polymer chains using benzoyl peroxide as an initiator as described by Rasal and Hirt.¹¹ Initially, the reactor was loaded with 100 g of PLA and dissolved in 750 mL of chloroform with constant agitation at 100 rpm. Benzoyl peroxide totaling 1% of the mass of PLA was added to the initial solution in the reactor. The reactor was sealed and heated to 60°C for 60 minutes. The heater was turned off and 10 g of acrylic acid was added to the solution. The reactor was resealed and heated to 100°C for 10 minutes. The heater was shut off and the reactor was allowed to cool to below 60°C before the solution was drained from the bottom of the reactor. This solution was then separated into specific portions before the desired amount of cellulose nanocrystals or PEG was added to the mixture. This solution was thoroughly blended with an overhead impeller for 10 min and then poured out in a Pyrex dish. The chloroform was allowed to evaporate in a hood overnight followed by 24 h at 80°C under vacuum. The resulting films were cut into approximately 5 mm squares in preparation for extrusion.

Film Extrusion

The polymer films were extruded using a twin-screw micro-compounder extruder (DSM Xplore) operating in co-rotating mode with 170 mm long tapered screws and a barrel volume of 15 cm³. The polymer was compounded for approximately 10 min at 180°C with the motor force set to 500 N and the rate of co-rotating screws controlled by the instrument. The polymer melt was extruded through a rectangular cross-sectional

shape die and cooled by ambient nitrogen. The resulting films were approximately 0.1 mm thick and collected on a chill roll at a take-up speed between 110 to 130 rpm depending of the viscosity of the melt. These films were diced into uniform strips 95 mm long and 12.5 mm wide on a USM hydraulic machine press by means of a metal die. The thickness of each film was measured at 4 different points with a film thickness gauge (Digimacro ME-50HA).

Characterization of the films

Tensile testing of the polymer film strips was conducted using an Instron 1125 universal testing instrument. The initial grip separation was set to 45 mm and a crosshead speed of 4 mm/min. The stress-strain curves were analyzed with Origin® software in order to determine the tensile strength, tensile modulus, and toughness of each film.

Differential Scanning Calorimetry (DSC) (TA DSC 2920) was used to measure the thermal transitions: glass transition temperature (T_g), crystallization temperature (T_c), melting temperature (T_m), and the heat of crystallization (ΔH_{cc}) and melting (ΔH_m), and percent crystallinity of the films (X_c). Aluminum pans were carefully loaded and sealed with 4 to 6 mg of the polymer sample and heated to 200 °C at a constant rate of 10°C/min under a nitrogen purge. At the end of the run, the samples were quench cooled using a metal bar previously submerged liquid nitrogen. A second run was immediately conducted on these samples under the same conditions. T_g , T_c , T_m , ΔH_{cc} and ΔH_m , were

taken from the second run after quenching. The X_c of the nanocomposites was determined from the first run before quenching using equation 4.1,

$$X_c [\%] = \frac{\Delta H_m - \Delta H_{cc}}{(\Delta H_m^\infty) \times X_{PLA}} \times 100\%$$

Eq. 4.1

where X_{PLA} is the fraction of PLA in the composites, and ΔH_m^∞ is the theoretical enthalpy of fusion of 100% crystalline PLA, which was taken to be 93.0 J/g.²¹

Optical polarized-light microscopy was performed using an Olympus BX-60 in transmission mode with a polarizer in the bottom of the sample and the analyzer rotated 90° in the top. A first order red plate (U-TP530) was also used to study the specific direction of the oriented crystals. The samples were placed on a glass microscope slide without further preparation and pictures were taken at rotating angles of 0, 45, 90 and 135° using 13X magnification.

Results and Discussion

PLA was reactively modified with acrylic acid by means of the initiator benzyl peroxide as detailed in the literature.¹¹ The reaction took place at elevated temperatures in a sealed reactor, producing a graft copolymer with 10 wt. % poly-acrylic acid (PAA), hereafter referred as PLA-PAA(10%). The copolymer was analyzed to verify the covalent attachment of PAA onto PLA using FTIR analysis after microwave extraction of the PLA-PAA(10%) in water. CNCs or PEG were added in the desired concentrations and physically mixed in solution to form the nanocomposites or polymer blends,

respectively. Nanocomposites of pure PLA were also prepared in order to compare the effects with the graft copolymer.

PLA and PLA-PAA Nanocomposites

Mechanical properties

Figure 4.1 shows the energy at break (or toughness), tensile strength, and tensile modulus of the PLA and PLA-PAA nanocomposites films. The addition of CNCs to the PLA films results in increased toughness of as observed in Figure 4.1: increasing from 1.1 MJ/m³ for neat PLA to a maximum of 2.5 MJ/m³ (125% increase) at 1% CNC load. At higher CNC loadings, the toughness progressively decreased to a lowest value of 1.6 MJ/m³ for 5% CNC, which still represented a 46% increase over the neat PLA. For the PLA-PAA, the toughness decreased as the CNC load increased, obtaining a lowest value at 5% CNC load, which represented a 75% decrease. The tensile properties (Figure 4.1b-c) for both composites possessed increasing trends with the addition of CNC concentrations studied. The tensile strength and modulus of the PLA-CNC composites were approximately the same for the 3 concentrations but increased compared to neat PLA. For the PLA-PAA nanocomposites, the strength showed a modest increase at 3% loading followed by a subsequent reduction at 5% CNCs. The modulus, on the other hand, was enhanced for all of the grafted polymer films upon the addition of CNCs, having an optimum increase at 3% CNC which represents a 159% increase.

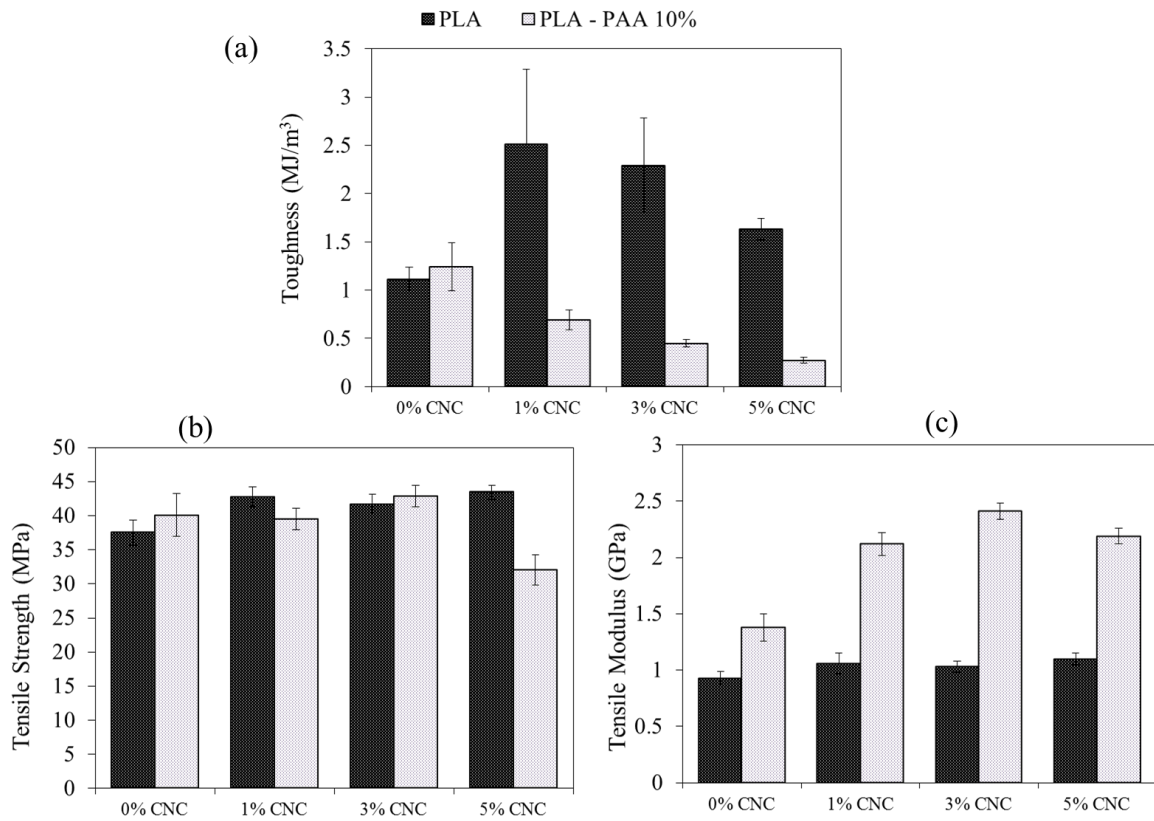


Figure 4.1. Mechanical properties of PLA and PLA-PAA CNC nanocomposites. (a) toughness, (b) tensile strength; and (c) tensile modulus.

The interfacial interactions between CNCs and the matrix play a very important role in the reinforcement of the mechanical properties, especially in the toughness, which has been shown to increase due to strong filler-matrix interactions in CNC nanocomposites. On the other hand, a lower compatibility between CNCs and the matrix allows the filler to associate with itself, forming a rigid percolating network which can be responsible for the enhancement in composite modulus.²⁴ This network is frequently formed when there is a balance of surface charge and hydrogen bonding, since strong electrostatic attractions aid the formation of agglomerates.²⁷ In addition, the theoretical critical volume fraction at which the network would begin to form is 9 vol.% (11 wt.%)

for the CNCs isolated here, as predicted by Favier et al for cylindrical shaped particles.²⁸ Therefore, it is unlikely that the modulus reinforcement of the PLA-PAA nanocomposites is due to such a network.

Another possibility for the increase of the PLA-PAA modulus is due to higher crystallinities obtained when CNCs are added to the copolymer. Several publications have reported increase of crystallinity upon addition of nanocelullose to polymers including PLA, resulting in higher tensile strength and modulus.^{21, 29} Pei et al. reported that surface-modified CNCs promoted higher crystallinities and tensile properties than unmodified CNC in PLA.²¹

Thermal properties of nanocomposites

The results in Figure 4.2 show an increase in PLA-PAA crystallinity from 32% for neat copolymer to 48% at 3% CNC load before suffering a slight reduction at 5% CNCs. These results correlate well with the enhancement of modulus as discussed above. Hence, the grafting of the hydrophilic PAA into PLA increases the compatibility with CNC,³⁰ which results in improved CNC dispersion and the nanocrystals acting as effective nucleating agents for the copolymer.

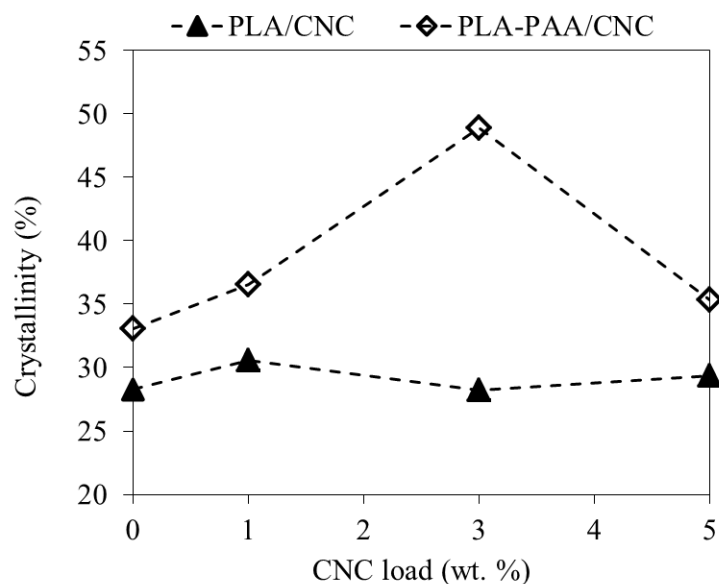


Figure 4.2. Crystallinity of PLA and PLA-PAA loaded with CNCs; X_c obtained from the first run DSC curves.

The DSC results obtained from the second run after quenching are shown in Figure 4.3. For PLA composites (Figure 4.3a), the exothermic peak attributed to the cold crystallization gradually decreased in area with increasing CNC concentration, while the peak for the PLA-PAA composites increases (Figure 4.3b). The melting temperature (T_m) and the glass transition temperature (T_g) tend to increase with CNC concentration in both cases. The values of these thermal transitions are shown in Table 4.1. The slight increase in the T_g of the PLA nanocomposites could be evidence of reduced mobility of the chains either due to increased crystallinity in the polymer or chain entanglements on the nanofiller.³¹ However, since the crystallinity of PLA composites did not increase, the latter chain entanglements are potentially occurring, which would require higher energies to obtain the same mobility of the polymer under stress. This result is in agreement with the higher toughness obtained for PLA composites as shown in Figure 4.1a.

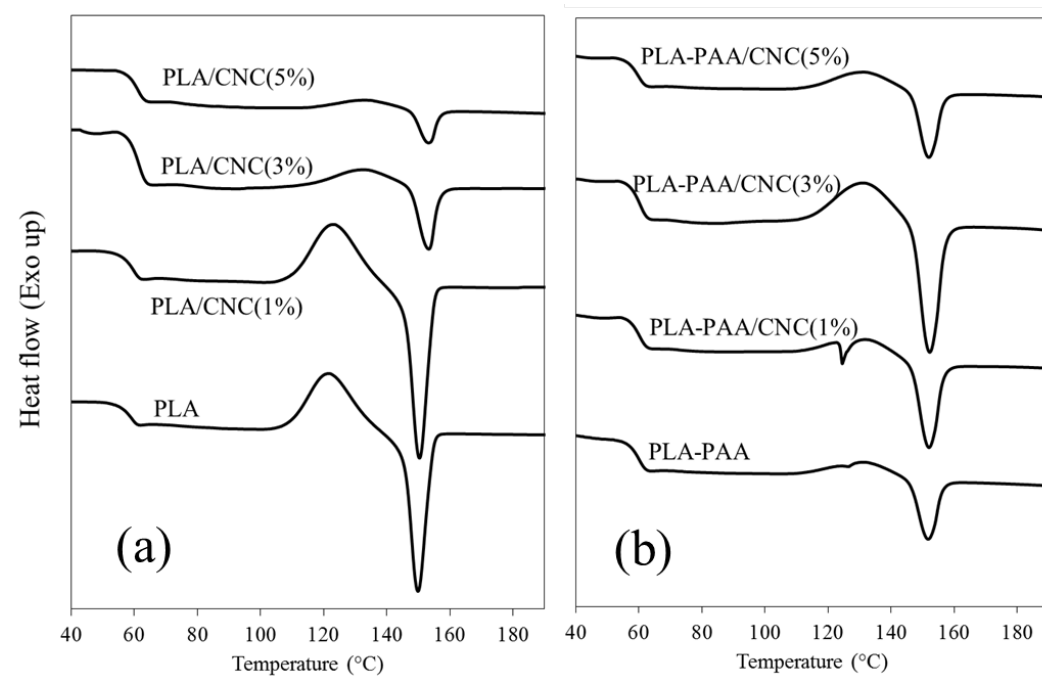


Figure 4.3. Second run DSC scan curves of PLA (a) and PLA-PAA (b) loaded with cellulose nanocrystals. The plots are offset for clarity.

The reduced mobility of PLA chains upon addition of CNCs is also reflected in the significant reduction of the second run heat of crystallization, and consequently in the heat of melting for the PLA composites. This is contrary to the PLA-PAA copolymers which increased their mobility due to an improved crystallization as observed in Table 4.1. This difference in the crystallization between both types of polymers may be based on the strength of the interactions and the starting state of the material. As observed in Table 4.1, the heat of crystallization for neat PLA is much higher than for the PLA-PAA(10%). The addition of CNCs actually disrupts the initial mobility of PLA chains, while for hydrophilic PLA-PAA, CNCs enhance the initially low crystallization of this copolymer due to an increased compatibility. Liu et al. also found that the crystallization

of PLA was more effective in the amorphous than in the crystalline composites upon the addition of CNCs.²⁹

Table 4.1. Thermal properties of PLA and PLA-PAA loaded with cellulose nanocrystals

Polymer	CNC (wt.%)	T _g (°C)	T _{cc} (°C)	T _m (°C)	ΔH _{cc} (J/g)	ΔH _m (J/g)
PLA/CNC	0	55.5	122.1	149.9	26.6	26.6
	1	55.8	123.6	150.4	26.4	26.4
	3	58.1	132.6	153.4	3.3	3.3
	5	57.9	134.9	153.3	2.9	2.8
PLA-PAA/CNC	0	56.9	132.2	147.7	6.4	6.4
	1	57.2	132.9	152.1	7.7	7.7
	3	57.1	131.2	152.3	10.7	10.7
	5	56.3	132.3	152.0	6.5	6.5

Optical Properties

Previous research has shown that the nanostructure of CNCs in nanocomposites are deterministic of the mechanical properties.³² A spiral formation was shown to contribute to the increase of toughness in the composites (for sulfuric acid synthesized CNCs), similar to the behavior observed in the fibers of plants and trees.³³ For this reason, the optical properties of the films were studied using polarized-light microscopy in the present work. The polarizer, which was placed under the sample, was aligned along the 0° angle (north-south direction), while the analyzer, which is above the sample, was at the 90° angle (east-west). Figure 4.4 shows the polarized micrographs of the PLA and PLA-PAA composites rotated at 0°, 45°, 90° and 135° angles. For the PLA composites, a bright phase or birefringence can be observed at 45° and 135° angles, indicating the formation of liquid crystals in either parallel or perpendicular to the direction of extrusion. The birefringence is significantly brighter for the 3% CNC in PLA indicating

the formation of a highly ordered liquid crystalline phase, and therefore a greater degree of CNC self-assembly within the matrix. The formation of an oriented phase in a matrix is usually a good indication of non-agglomerated nanocrystals,^{34, 35} which agrees with the increase in toughness observed in this work. On the other hand, an oriented phase is not observed for the PLA-PAA nanocomposites, which may be attributed to CNCs associating with the PAA grafts and being surrounded by stiffer PLA crystallites that inhibit orientation or self-assembly of the nanocrystals.

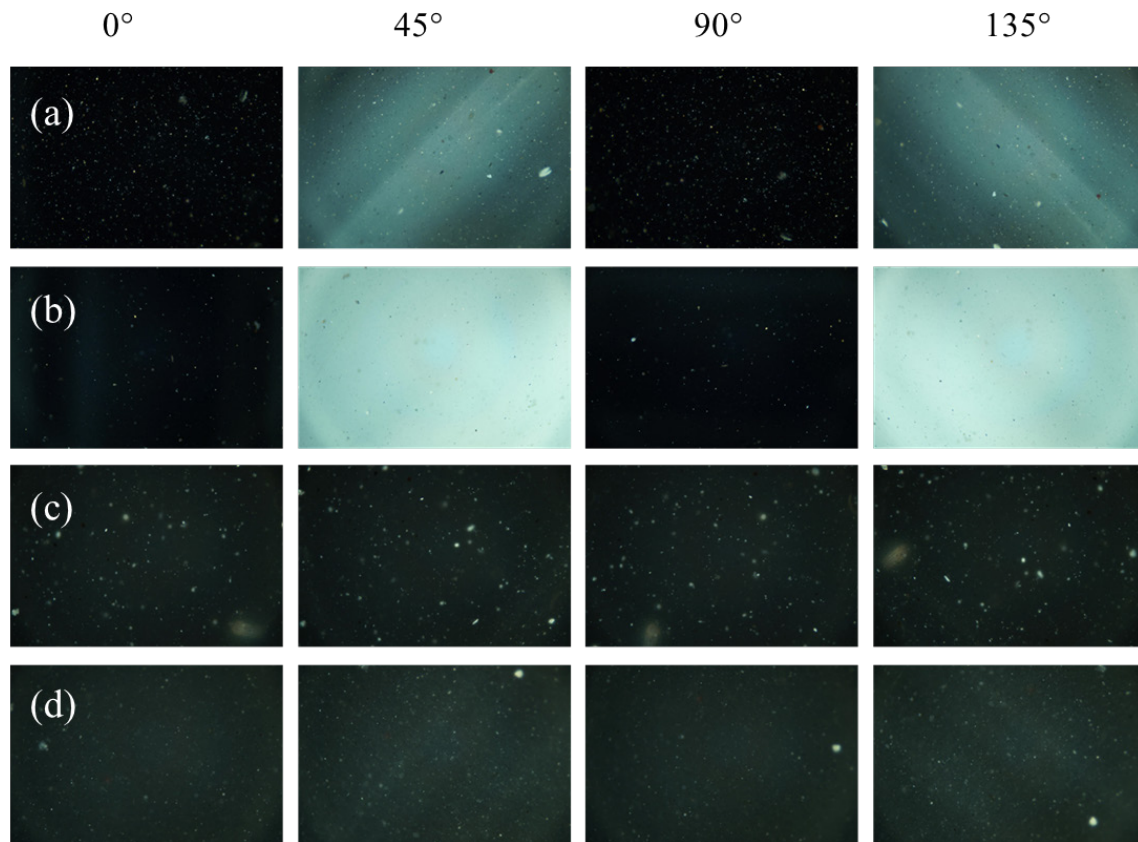


Figure 4.4. Polarized-light microscopy of PLA (a and b) and PLA-PAA (c and d) loaded with cellulose nanocrystals. (a and c) 1%; and (b and d) 3% CNC loaded nanocomposites. Length of the longer side of each image: 1.5 mm

A first order red plate was used to determine the specific orientation of the assembled crystals and the results are shown in Figure 4.5. The slow axis of the plate was placed parallel to the 135° angle (northwest-southeast), and the direction of the extrusion of the films was always parallel to the rotation angle. The appearance of the color magenta, yellow, and blue can be observed indicating the different orientations. CNCs oriented in the 135° angle will present a color blue, while the assemblies oriented in the 45° will be yellow. Magenta colors indicate the alignment at 0°, 90°, and also the un-oriented nanocrystals. Hence, the total theoretical oriented area of the films can be obtained by adding the percentage of both yellow and blue from 2 consecutive angles of rotation.

The percentage of the oriented area estimated from a centered region of the analyzed images increased from 85% to 100% for the 1% and 3% CNC loads, respectively, for the PLA composites. For the PLA-PAA composites, the oriented area only increased from 2% to 4% at 1% and 3% CNC, respectively. The directions of the crystal assemblies are predominately parallel to the direction of the extrusion, which it is demonstrated for the amount of yellow for the 45° rotation angle. For the PLA/CNC 1% films, approximately 75% of the CNCs is estimated to be oriented parallel to the line of extrusion, while for the PLA/CNC 3% the orientation is apparently more than 100%. This > 100% value however, lacks of significant meaning other than very high alignment because the birefringence of this composite is too bright as observed in Figure 4.4, and the red plate is not capable of working with this level of retardation. This relationship between the directions of the crystals and the toughness observed for the 1 and 3% CNC films, may

support the theory of the effect of the spiral formation on the increase of toughness as observed by Urena-Benavides and Kitchens in alginate fiber composites.³⁶

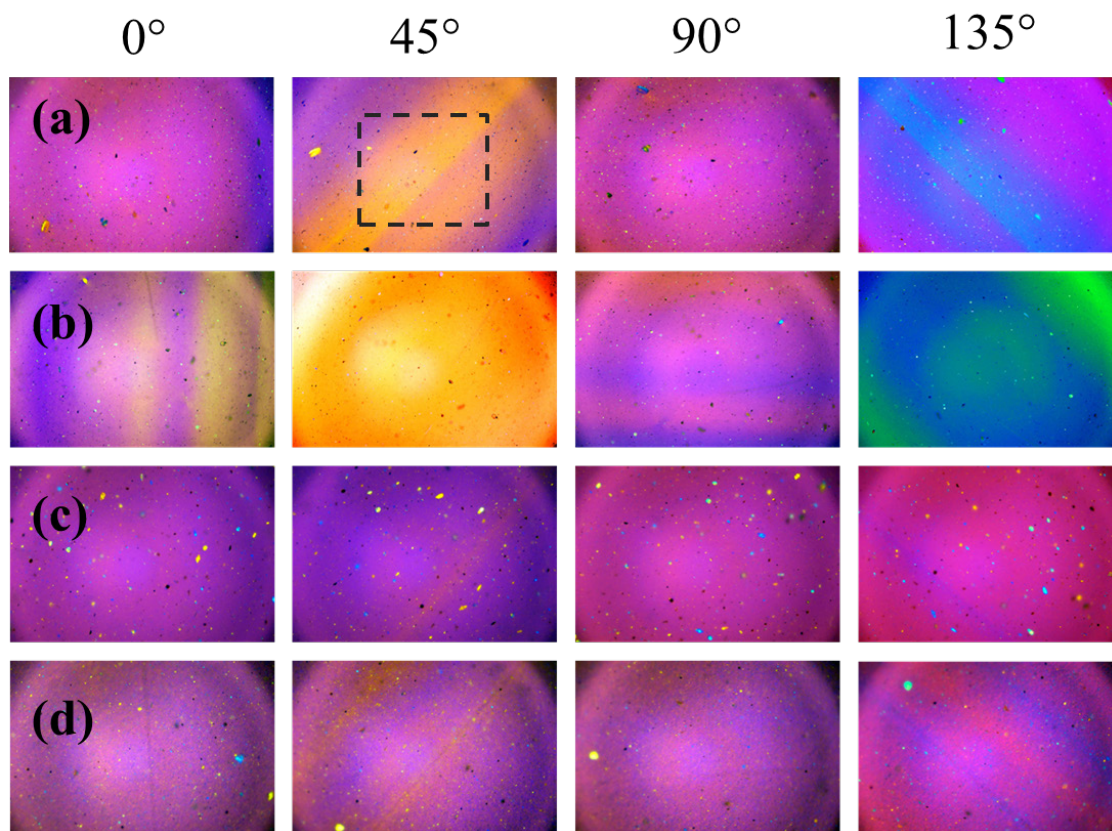


Figure 4.5. Polarized-light microscopy PLA (a and b) and PLA-PAA (c and d) loaded with cellulose nanocrystals using a first order red filter. (a and c) 1%; and (b and d) 3% CNC loaded nanocomposites. Dotted squared in the picture represents the size of the area used for the color quantification. Length of the longer side of each image: 1.5 mm

PLA-PAA copolymer blends

PEG was added to the graft copolymer in solution immediately after the reaction of acrylic acid with PLA. Neat PLA blended with PEG was not prepared since it has been already studied in the literature.^{13, 37-40} The study of low molecular weight (< 2 kDa) PEG is commonly studied because at high molecular weights phase separation¹³ and tensile

properties reduction⁴¹ occurs due to immiscibilities. However, low molecular weight plasticizers have the tendency to migrate from the host polymer due to a slow phase separation and the crystallization of PEG at room temperature.^{14, 42} This problem could be addressed by increasing the compatibility by the grafting of PAA into the hydrophobic PLA matrix.¹¹ PAA and PEG are both hydrophilic polymers and are more compatible with each other than with PLA. Previous research investigated this reactive-blend modification using a low molecular weight PEG (Mn=1.5kDa), obtaining a significant increase in toughness without compromising the tensile properties of the films.¹¹ In this work, a higher molecular weight PEG (10 kDa) was blended with the graft copolymer to explore the enhancement of PLA properties with possible reduced migration rates of the plasticizer.

Mechanical properties

The toughness of the PLA-PAA/PEG blends (0, 10, 20 and 30% PEG), which were determined by measuring the area under the stress-strain curve, are shown in Figure 4.6. It can be observed that the toughness was greatly increased as the percentage of PEG was increased in the formulation. The highest toughness was reached at 30% PEG, increasing 3497.3% with respect to neat PLA from 1.1 ± 0.1 to 39.9 ± 7.4 MJ/m³. For 10% and 20% PEG, the toughness was increased by 925.2% and 2376.4%, respectively.

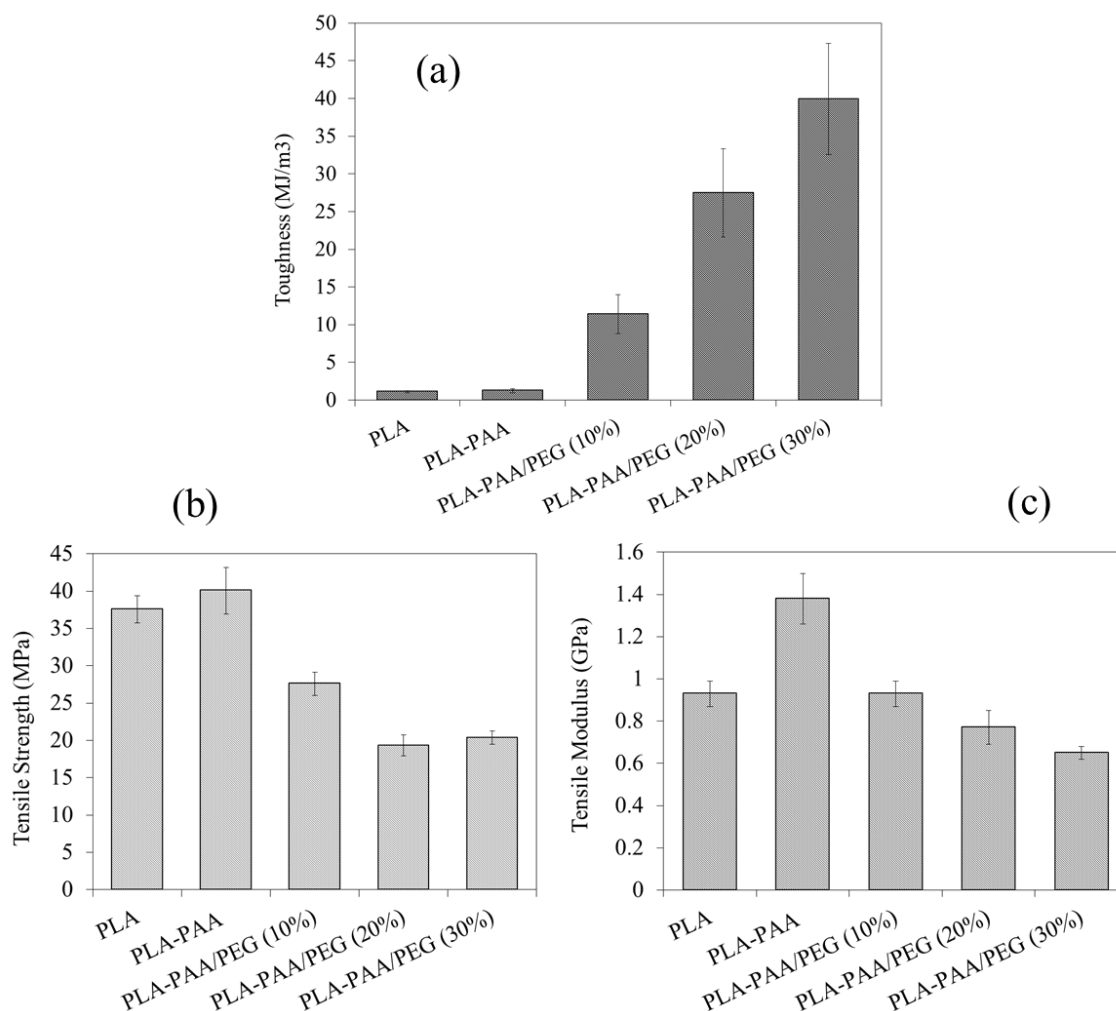


Figure 4.6. Mechanical properties of PLA-PAA/PEG blends. (a) toughness, (b) tensile strength; and (c) tensile modulus.

The tensile properties of the blends are shown in Figure 4.6b-c. PAA grafting increased the strength and the modulus of the graft copolymer by 6.7% and 48%, respectively, due to the higher stiffness of PAA. The addition of PEG decreased both the tensile strength and modulus of the films with similar trends. The tensile strength was reduced to as low as 48.5% for the 20% PEG, while the modulus decreased as low as 30.1% for the 30% PEG content, which is commonly observed in the plasticization of polymers.

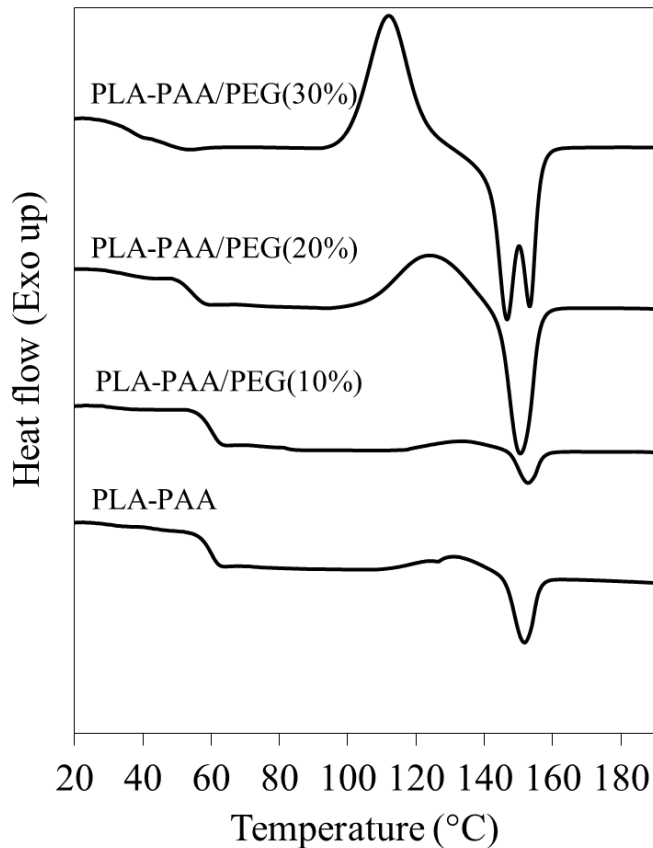


Figure 4.7. Second run DSC curves of PLA-PAA/PEG blends

Thermal properties

The DSC plots for the PLA-PAA/PEG blends are shown in Figure 4.7. The plots show the endothermic melting peaks in all of the blends and an increasing endothermic crystallization peak with increasing PEG concentration. A double peak can be observed during the melting region for the 30% PEG blend, which has been attributed to lamellar rearrangement during crystallization of PLA.⁴³ The efficiency of plasticization can be evaluated by the T_g decrease from 56.9 °C for neat PLA-PAA to 30.9 °C for a 30% PEG formulation as observed in the Table 4.2. Moreover, a reasonable miscibility of the blend is suggested by the appearance of a single T_g transition and its lowering with increasing

plasticizer content. The heat of crystallization and melting increases with the addition of PEG, demonstrating increased mobility of the PLA chains due to the plasticizing effect of PEG.⁶ This result also indicates higher crystallization rates, which are beneficial for the increase of the slow crystallization kinetics of PLA when it is cooled from the melt.⁴⁴

Table 4.2. Thermal properties of PLA-PAA blends

PEG (wt.%)	T_g (°C)	T_{cc} (°C)	T_m (°C)	ΔH_{cc} (J/g)	ΔH_m (J/g)	X_c (%)
0	56.9	132.22	147.7	4.022	6.4	32.4
10	56.4	133.09	153.3	2.403	2.3	48.0
20	50.2	123.93	150.1	14.86	14.2	36.9
30	30.9	112.05	152.3	24.26	25.5	38.2

Conclusions

The toughening of PLA was studied by the addition of either acetylated CNCs or PEG, and both were shown to act as toughening agents for PLA. Polyacrylic acid (PAA) was grafted to PLA to increase the hydrophilicity of the polymer and to improve the compatibility of the reinforcements. CNCs increased the toughness of PLA by 125% with an optimum loading of 1% without compromising the tensile properties. For the PLA-PAA composites the toughness decreased, while the modulus increased significantly with CNC concentration. This behavior was attributed to an increase of crystallinity of the PLA-PAA composites as a result of increased compatibilization between CNCs and the PAA chains.

The thermal properties of these nanocomposites revealed a lower mobility of the PLA chains as reflected by the slight increase of T_g. This reduced mobility was attributed

to the increase of crystallinity in the PLA-PAA composites, while for PLA, it was attributed to polymer chain entanglements on the nanocrystals. These two effects correspond correctly with the enhancement of mechanical properties observed in both types of polymers. PLA composites exhibited a greater degree of CNC orientation compared to PLA-PAA as observed under polarized microscopy, suggesting the self-assembly and improved alignment of the CNCs in PLA. This assembly was found to be less oriented for the 1% CNC films, which exhibited enhanced toughness, than for the 3% CNC composites of PLA.

High molecular weight PEG greatly increased the toughness of PLA-PAA copolymer by approximately 3500%, decreasing the tensile strength and tensile modulus only 49% and 30%, respectively for the same PEG content. The T_g was decreased by 26 °C demonstrating effective plasticization when using 30% PEG. Moreover, the appearance of single T_g transition indicates favorable miscibility in the blends. It can be expected that tuning the concentrations of PLA, PLA-PAA, CNCs, and PEG will enable the design of a polymer composite with desired combinations of mechanical, optical, and thermal properties, thus expanding potential application for this bio-based composite.

References

1. Ahmed J, Varshney SK. Polylactides-Chemistry, Properties and Green Packaging Technology: A Review. *Int J Food Prop.* 2011;14(1):37-58.
2. Bioplastics E. Bioplastics facts and figures Available at: <http://en.european-bioplastics.org/>. Accessed 06/06/2013, 2013.

3. Nampoothiri KM, Nair NR, John RP. An overview of the recent developments in polylactide (PLA) research. *Bioresource Technology*. Nov 2010;101(22):8493-8501.
4. Anderson KS, Schreck KM, Hillmyer MA. Toughening polylactide. *Polym Rev*. 2008;48(1):85-108.
5. Sungsanit K, Kao N, Bhattacharya SN. Properties of linear poly(lactic acid)/polyethylene glycol blends. *Polymer Engineering and Science*. Jan 2012;52(1):108-116.
6. Martin O, Averous L. Poly(lactic acid): plasticization and properties of biodegradable multiphase systems. *Polymer*. Jun 2001;42(14):6209-6219.
7. Siqueira G, Bras J, Dufresne A. Cellulosic Bionanocomposites: A Review of Preparation, Properties and Applications. *Polymers*. Dec 2010;2(4):728-765.
8. Ray SS. Polylactide-Based Bionanocomposites: A Promising Class of Hybrid Materials. *Accounts of Chemical Research*. Nov 2012;45(10):1710-1720.
9. Oyama HI. Super-tough poly(lactic acid) materials: Reactive blending with ethylene copolymer. *Polymer*. Jan 2009;50(3):747-751.
10. Theryo G, Jing F, Pitet LM, Hillmyer MA. Tough Polylactide Graft Copolymers. *Macromolecules*. Sep 2010;43(18):7394-7397.
11. Rasal RM, Hirt DE. Poly(lactic acid) Toughening with a Better Balance of Properties. *Macromol Mater Eng*. Mar 2010;295(3):204-209.
12. Liu HZ, Zhang JW. Research Progress in Toughening Modification of Poly(lactic acid). *Journal of Polymer Science Part B-Polymer Physics*. Aug 2011;49(15):1051-1083.
13. Park B-S, Song JC, Park DH, Yoon K-B. PLA/Chain-Extended PEG Blends with Improved Ductility. *Journal of Applied Polymer Science*. Feb 15 2012;123(4):2360-2367.

14. Ran X, Jia Z, Han C, Yang Y, Dong L. Thermal and mechanical properties of blends of polylactide and poly (ethylene glycol-co-propylene glycol): Influence of annealing. *Journal of Applied Polymer Science*. 2010;116(4):2050-2057.
15. Jose Luis Orellana EEU-BaCLK. Bio-Nano Reinforcement of Polylactic Acid with Surface Modified Cellulose Nanocrystals. Paper presented at: AIChE Annual Meeting, 2011; Minneapolis, MN.
16. Jamshidian M, Tehrany EA, Imran M, Jacquot M, Desobry S. Poly-Lactic Acid: Production, Applications, Nanocomposites, and Release Studies. *Compr Rev Food Sci Food Saf*. Sep 2010;9(5):552-571.
17. Eichhorn SJ, Dufresne A, Aranguren M, et al. Review: current international research into cellulose nanofibres and nanocomposites. *Journal of Materials Science*. Vol 45; 2010: 1-33.
18. Urena-Benavides EE, Brown PJ, Kitchens CL. Effect of Jet Stretch and Particle Load on Cellulose Nanocrystal-Alginate Nanocomposite Fibers. *Langmuir*. Sep 2010;26(17):14263-14270.
19. Bulota M, Kreitsmann K, Hughes M, Paltakari J. Acetylated microfibrillated cellulose as a toughening agent in poly(lactic acid). *Journal of Applied Polymer Science*. Oct 25 2012;126:E448-E457.
20. Bondeson D, Oksman K. Dispersion and characteristics of surfactant modified cellulose whiskers nanocomposites. *Composite Interfaces*. 2007;14(7-9):617-630.
21. Pei A, Zhou Q, Berglund LA. Functionalized cellulose nanocrystals as biobased nucleation agents in poly(L-lactide) (PLLA) - Crystallization and mechanical property effects. *Composites Science and Technology*. May 2010;70(5):815-821.
22. Fukuzumi H, Saito T, Wata T, Kumamoto Y, Isogai A. Transparent and High Gas Barrier Films of Cellulose Nanofibers Prepared by TEMPO-Mediated Oxidation. *Biomacromolecules*. Jan 2009;10(1):162-165.

23. Kalia S, Dufresne A, Cherian BM, et al. Cellulose-Based Bio- and Nanocomposites: A Review. *International Journal of Polymer Science*. 2011 2011.
24. Habibi Y, Lucia LA, Rojas OJ. Cellulose Nanocrystals: Chemistry, Self-Assembly, and Applications. *Chemical Reviews*. Jun 2010;110(6):3479-3500.
25. Cailloux J, Santana O, Franco-Urquiza E, et al. Sheets of branched poly (lactic acid) obtained by one step reactive extrusion calendering process: Melt rheology analysis. *Express Polym Lett*. 7.
26. Braun B, Dorgan JR. Single-Step Method for the Isolation and Surface Functionalization of Cellulosic Nanowhiskers. *Biomacromolecules*. Feb 2009;10(2):334-341.
27. Rusli R, Shanmuganathan K, Rowan SJ, Weder C, Eichhorn SJ. Stress Transfer in Cellulose Nanowhisker Composites-Influence of Whisker Aspect Ratio and Surface Charge. *Biomacromolecules*. Apr 2011;12(4):1363-1369.
28. Favier V, Canova GR, Shrivastava SC, Cavaille JY. Mechanical percolation in cellulose whisker nanocomposites. *Polymer Engineering and Science*. Oct 1997;37(10):1732-1739.
29. Liu DY, Yuan XW, Bhattacharyya D, Easteal AJ. Characterisation of solution cast cellulose nanofibre - reinforced poly(lactic acid). *Express Polym Lett*. Jan 2010;4(1):26-31.
30. Lu P, Hsieh Y-L. Cellulose nanocrystal-filled poly (acrylic acid) nanocomposite fibrous membranes. *Nanotechnology*. 2009;20(41):415604.
31. Xu XZ, Liu F, Jiang L, Zhu JY, Haagenson D, Wiesenborn DP. Cellulose Nanocrystals vs. Cellulose Nanofibrils: A Comparative Study on Their Microstructures and Effects as Polymer Reinforcing Agents. *ACS Appl Mater Interfaces*. Apr 2013;5(8):2999-3009.

32. Urena-Benavides EE, Kitchens CL. Cellulose Nanocrystal Reinforced Alginate Fibers-Biomimicry Meets Polymer Processing. *Molecular Crystals and Liquid Crystals*. 2012;556:275-287.
33. Barnett J, Bonham VA. Cellulose microfibril angle in the cell wall of wood fibres. *Biological reviews*. 2004;79(2):461-472.
34. Heux L, Chauve G, Bonini C. Nonflocculating and chiral-nematic self-ordering of cellulose microcrystals suspensions in nonpolar solvents. *Langmuir*. Oct 17 2000;16(21):8210-8212.
35. Araki J. Electrostatic or steric? - preparations and characterizations of well-dispersed systems containing rod-like nanowhiskers of crystalline polysaccharides. *Soft Matter*. 2013;9(16):4125-4141.
36. Urena-Benavides EE, Kitchens CL. Wide-Angle X-ray Diffraction of Cellulose Nanocrystal-Alginate Nanocomposite Fibers. *Macromolecules*. May 2011;44(9):3478-3484.
37. Gui Z, Xu Y, Gao Y, Lu C, Cheng S. Novel polyethylene glycol-based polyester-toughened polylactide. *Materials Letters*. Mar 15 2012;71:63-65.
38. Jacobsen S, Fritz HG. Plasticizing polylactide - The effect of different plasticizers on the mechanical properties. *Polymer Engineering and Science*. Jul 1999;39(7):1303-1310.
39. Kulinski Z, Piorkowska E. Crystallization, structure and properties of plasticized poly(L-lactide). *Polymer*. Nov 2005;46(23):10290-10300.
40. Pillin I, Montrelay N, Grohens Y. Thermo-mechanical characterization of plasticized PLA: Is the miscibility the only significant factor? *Polymer*. Jun 2006;47(13):4676-4682.
41. Honary S, Orafai H. The effect of different plasticizer molecular weights and concentrations on mechanical and thermomechanical properties of free films. *Drug Dev Ind Pharm*. 2002;28(6):711-715.

42. Stark TD, Choi H, Diebel PW. Influence of plasticizer molecular weight on plasticizer retention in PVC geomembranes. *Geosynthetics International*. 2005;12(2):99-110.
43. Nijenhuis AJ, Colstee E, Grijpma DW, Pennings AJ. High molecular weight poly(L-lactide) and poly(ethylene oxide) blends: Thermal characterization and physical properties. *Polymer*. Dec 1996;37(26):5849-5857.
44. Saeidlou S, Huneault MA, Li HB, Park CB. Poly(lactic acid) crystallization. *Prog Polym Sci*. Dec 2012;37(12):1657-1677.

CHAPTER FIVE

LIQUID AND SUPERCRITICAL CO₂ EXTRACTION OF FAT FROM RENDERED MATERIALS

Introduction

Rendered materials (RM) are produced from the inedible parts of animals produced for human consumption, which constitutes one third to one half of the total animal mass.¹ In 2009, for example, the U.S produced 33 million cattle, 113 million hogs, 245 million turkeys, and 8.6 billion chickens for human consumption. These animal by-products were processed in the 250 rendering facilities in North America, producing approximately 18 billion pounds of RM.^{2, 3} Of this total production, 52% is a combination of fats and greases, with the remaining 48% representing protein meals composed of meat-and-bone, poultry, and feather meals.³ Fats are non-polar soluble biomolecules consisting of triglycerides and fatty acids that, unlike oils, are solid at room temperature due to the high content of saturated fatty acids.

Approximately 85% of all RMs, including a fraction of the fats, are produced for animal feed ingredients. The rest is used in a diversity of industries with nearly 3,000 applications identified.¹ A large fraction of the fat not used for animal feed is used in the manufacture of soaps and personal care products; however, since 2010 the biofuels industry, which has shown record production, has placed a significant demand on the fat from the rendering industry, more than doubling the amount of rendered fats used for the biodiesel production.⁴ The processing of the inedible raw materials and the use of the by-

products not only make an important economic contribution to this industry but also contribute to environmental and public health since rendering offers a more sustainable solution and a lower carbon footprint than other disposal methods.⁵

The rendering process involves the application of heat, the extraction of moisture, and the separation of fat. First the raw materials are ground to a consistent size and cooked with steam at temperatures ranging from 115°C to 145°C for 40 to 90 min.² Moisture is then boiled off, and the fat associated with the solids is mechanically removed by screw presses while the moisture associated with extracted fat is separated using centrifuges. The two main products of this process are the fats (greases, tallow, lard and poultry fat) and the protein meals, which can contain 8-15% residual fat. Current market trends for inedible fats have resulted in prices of \$0.46 per pound in 2011, representing a 96% increase since 2009 and a 330% increase since 2001.^{3, 4} Thus, it is desirable to find alternative methods that are sustainable and economically viable for a fat selective extraction of rendered materials.

While mechanical extraction offers quite low initial and operational costs and produces uncontaminated oil, it results in relatively low extraction yields, which may or may not be desired depending on the end product. Solvent extraction using organic solvents results in high extraction yields (>99%) but produces a low quality oil that requires refining.⁶ An alternative solvent that has attracted considerable attention for fat extraction is liquid or supercritical carbon dioxide (LCO₂ or SCCO₂). Past research has shown that SCCO₂ extraction of flaxseed oil yields approximately 28% more fat than

screw expression and just 9% less than hexane extraction.⁷ CO₂ offers the advantages of ease of complete separation of the fat with no residual solvent in the matrix or the lipids, and the potential for CO₂ recycling.

CO₂ is a non-toxic, non-flammable, and relatively inexpensive solvent that has been used for a wide variety of applications that include separations, reactions, and material processing.^{8,9} The use of supercritical fluids in the food industry is widely established.⁹⁻¹¹ The first commercial supercritical extraction was performed in 1978 by Hag A.G in Germany for the decaffeination of green coffee beans.¹² Commercial applications at present include decaffeination of coffee and tea, extraction of natural colors, natural flavorings, antioxidants, nutraceuticals, and hops, as well as extraction of lipids and cholesterol from egg yolks, milk fat, beef, and pork.⁹ The supercritical extraction of lipids for the production of biodiesel is also a promising and expanding research area.^{13, 14} Extraction of specialty oils has received a great deal of interest due to the expanding demand for bioactive lipid components and the capability of CO₂ to preserve the flavors and aromas.¹⁵ This is the primary reason LCO₂ is commonly used in the extraction of flowers.¹⁶

SCCO₂ can be advantageous over LCO₂ for extractions from certain matrices when mass transfer limitations exist. This occurs because the density of SCCO₂ is on the order of a liquid while the diffusivity is one to two orders of magnitude higher than the liquid and the viscosity is on the order of a gas. For many supercritical extraction systems a retrograde solubility phenomenon may occur, where decreased solubility of the solute

occurs at elevated temperatures. This phenomena, which occurs below a pressure referred to as the “cross-over” point, is the result of reduced solvent strength as a result of reduced density in the high compressibility region of the fluid (i.e., close to the critical point). The density effect on solubility is not compensated by the increased solute volatility with increased temperature.¹² This effect results in the fat having a higher solubility at the lower temperatures of LCO₂ as compared to SCCO₂ at an equivalent pressure. This phenomenon affords the advantage of using LCO₂ at lower temperatures and pressures for extractions, which are advantageous for capital and operating costs, as well as for the recovery of volatile and thermally labile components.¹⁷

In this work, LCO₂ and SCCO₂ were investigated in a semi-batch configuration for the extraction of the residual fat from rendered poultry meal from the last stage of the rendering plant process. The effect of the temperature (25 °C, 40°C and 50 °C), pressure (69 to 345 bar), flow rate (5 to 25 mL/min), and mass of CO₂ on the extraction yield and the fat solubility were investigated. The composition of fatty acids in the fat was determined by gas chromatography. Solubility data were estimated from the extraction curves and correlated as a function of temperature and density using the Chrastil model. The maximum extraction yields and solubilities of the fat in LCO₂ and SCCO₂ were compared. LCO₂ was found to be more effective for the extraction of fat at the conditions studied in this work.

Materials and Methods

Materials and Chemicals

Pet food grade poultry meal donated by Carolina By-Products and Valley Proteins in Ward, South Carolina, was used as the rendered material as provided with no further sample preparation. The composition of this material was 14.2 ± 0.2 wt. % fat with approximately 7% moisture and 63% crude protein content. The size of agglomerated particles of the poultry meal was 100-300 μm . ACS grade n-hexane was purchased from VWR and industrial grade Carbon Dioxide was purchased from Airgas.

LCO₂ and SCCO₂ Extractions of Rendered Fats

The extraction of fat from rendered materials was accomplished using a laboratory-scale semi-batch unit presented schematically in Figure 5.1. A Teledyne Isco 500HD syringe pump connected to a heating bath was used to continuously deliver CO₂ at a desired temperature and pressure while monitoring the volumetric flow rate. A heating column behind the extraction column was used when the extraction was performed at supercritical conditions in order to maintain the CO₂ at the desired temperatures of extraction. This extraction column accommodated approximately 4 g of RM and consisted of 1/2" stainless steel tubing with 10 micron metal frits at both ends of the column. The CO₂ flow rate was controlled using a heated back pressure regulator (BPR) at the end of the system, and the temperature was monitored using multiple K-type thermocouples and manually controlled with variable transformers connected to heating

tapes. Pressure was monitored with a pressure transducer and indicator connected to the outlet of the extraction tube. A recovery flask was filled with hexane to collect the fat at the end of the system. The extracted RM was sent to the Agricultural Laboratory at Clemson University to determine the remaining fat by a Soxlet hexane extraction.

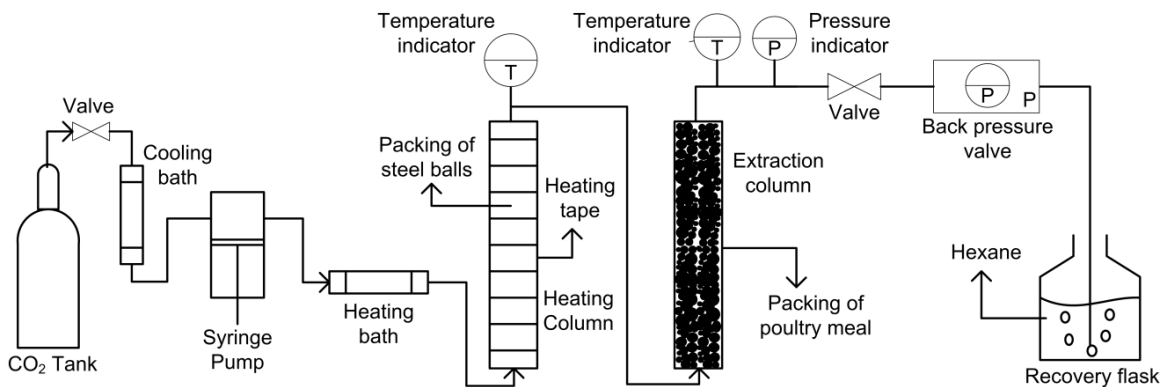


Figure 5.1. Schematic diagram of the semi-batch liquid and supercritical extraction

The extractions were performed at 25°C for LCO₂ and at 40°C and 50°C for SCCO₂ at pressures ranging from 69 to 345 bar. The flow rate utilized in each of these experiments was 5 mL/min (mass flow rates ranged from 3.7 to 4.9 g/min depending of the temperature and pressure). Since for SCCO₂ pressures below 210 bar required an exceedingly large amount of CO₂ to complete the extractions, they were not conducted. Fat solubility for each condition was obtained from a linear regression of the slope of the extraction curves and correlated with the Chrastil model as a function of density and temperature.¹⁸ The effect of the flow rate on the fat extraction was also investigated for LCO₂ at 25°C. The volumetric flow rates were varied between 5 to 25 mL/min, which corresponded to mass flow rates from as low as 3.7 g/min at 69 bar to as high as 23.0 g/min at 207 bar. The solubility was obtained from triplicate runs at a single CO₂/RM

ratio for each pressure and determined at a 50% extraction yield. The density of CO₂ at each temperature and pressure was found in the National Institute of Standards and Technology (NIST) Chemistry WebBook.¹⁹

Gas Chromatography Analysis

The fatty acid composition of the fat before and after the extraction with LCO₂ and SCCO₂ was determined by an Agilent 5975C Series GC/MSD with a Flame Ionization Detector (FID) and using a GLC-90 column. First, the fats were methyl esterified with the following procedure: 20 µl of fat sample was reacted for 90 min at 70°C with 700 µl of KOH 10 N and 6.30 mL of methanol. The same was performed with 60 µl of methylation blank sample of myristic acid. Samples were cooled down and reacted with 700 µl of H₂SO₄ 24N for 60 min at 70°C. After the reaction, the samples were mixed with 4.5 mL of hexane and subsequently centrifuged at 1100 xg for 5 min. The supernatant was 20 times diluted in hexane for the GC injection. The volume of injected sample was 1 µL.

Results and Discussion

The extraction of fat from rendered poultry meal with LCO₂ and SCCO₂ at temperatures of 25°C, 40°C, and 50°C and pressures of 69 to 345 bar gave maximum extraction yields ranging from 87.3% to 96.5% (Table 5.1); where the extraction yield is defined as the fat extracted as a mass percentage of the original fat in the RM. The extraction yields did not show any significant dependence with pressure or temperature.

The minimum amount of CO₂ required for complete extraction among all the conditions tested occurred for LCO₂ at the highest pressure (Figure 5.2a) due to a high solubility of fat at these conditions. For the complete extraction, the lowest fat content remaining after extraction was 1.0±0.3 wt% for all the conditions tested as shown in Figure 5.2a-c.

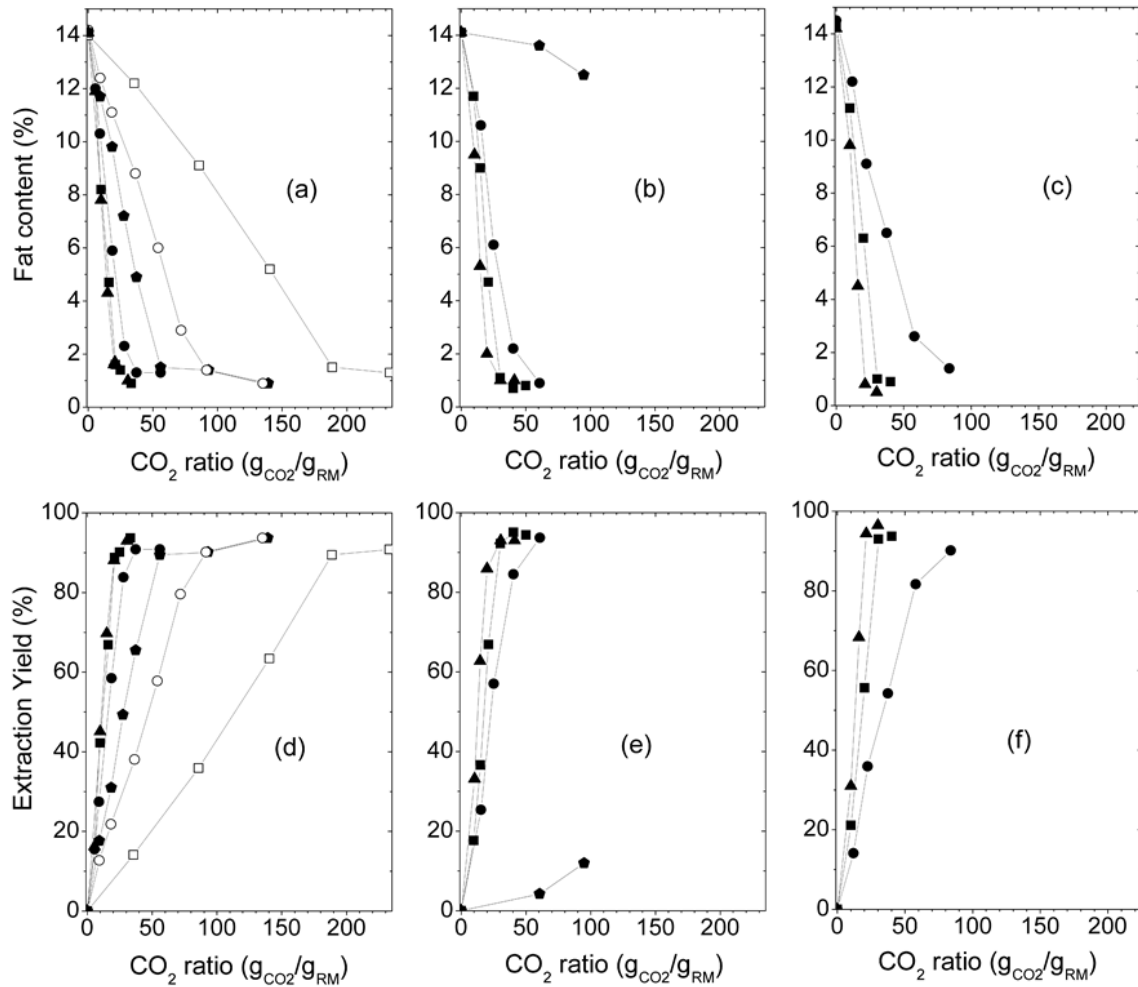


Figure 5.2. Fat extraction curves. (a-c) Fat content in rendered poultry meal after extraction and (d-f) extraction yields as a function of the amount of CO₂. (a and d) Liquid CO₂ at 25°C; (b and e) Supercritical CO₂ at 40°C; and (c and f) Supercritical CO₂ at 50°C. □, 69 bar; ○, 103 bar; ◆, 138 bar; ●, 207 bar; ■, 276 bar; ▲, 345 bar

The Effect of Temperature, Pressure and Flow Rate on Fat Extraction

LCO₂ and SCCO₂ extractions curves in Figure 5.2 present the amount of fat remaining in the rendered poultry meal after extraction (Figure 5.2a-c) and the extraction yield (Figure 5.2d-f) as a function of the CO₂ used at different temperatures and pressures. The extraction curves show the three regions usually found in natural product extractions: constant extraction rate period (first part), which is governed by the equilibrium solubility of the fat in CO₂; the falling rate period (transition); and the diffusion-controlled rate period, which is observed in some of the curves at the end of the run. The slope of the lines observed in the constant extraction period increases with pressure due to an increase of CO₂ solvation power. Although not observed clearly in Figure 5.2, these slopes also increase with decreasing temperature. The solvation power of the CO₂ depends mainly on the CO₂ density and the volatility of the solute (fat), which are directly impacted by pressure and temperature. Due to the high compressibility of CO₂ in the vicinity of the critical pressure, density is more dominant than solute volatility when the conditions are close to this region.

As mentioned above, pressure increases the solvent power of CO₂ due to the increase of density which is more noticeable at pressures near the critical point where the CO₂ is more compressible. As an example, for LCO₂ between 103 and 69 bar (Figure 5.2a), the difference in the CO₂ ratios required for complete extraction is about 80, while for the extractions between 345 and 207 bar this value is only about 35. It can also be observed that as the pressure increases to 345 bar, the slope of the curves become closer to each

other for the 3 temperatures studied. Although it was not studied in this work, it is expected that they will converge at the “cross-over” pressure, which may occur in this system at around 400 bar.

The temperature effect on the solvation power of CO₂ has a competing effect caused by both density and solute volatility. Increasing temperature under constant pressure will decrease density but increase volatility and vice versa. If the conditions are below the aforementioned “crossover” pressure, density will dominate over the solute volatility, thus solubility decreases with increasing temperature. This effect is commonly termed as retrograde solubility phenomenon which occurs in the regions of high compressibility, which is the case for this work. Once the crossover pressure is reached, the change of density with pressure becomes smaller and the volatility becomes dominant.

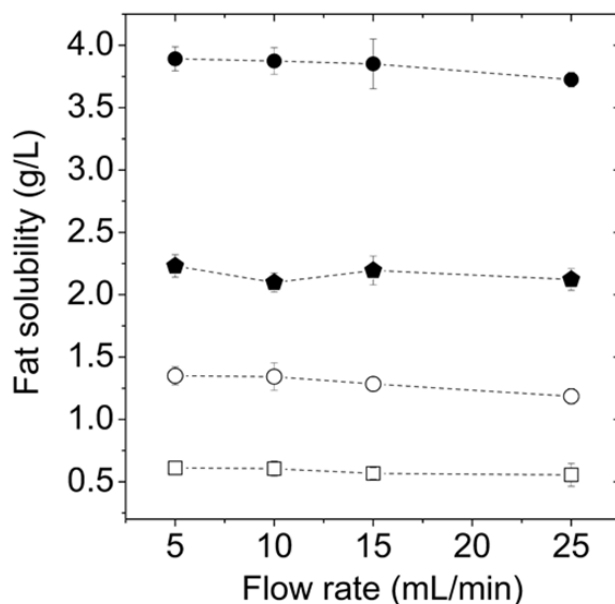


Figure 5.3. Solubility of fat at different liquid CO₂ flow rates with pressures of □, 69 bar; ○, 103 bar; ▲, 138 bar; and ◆, 207 bar; corresponding to CO₂/RM ratios of 80, 60, 40 and 20, respectively.

Variation of CO₂ flow rates between 5 and 25 mL/min had no significant effect on the solubility of fat (total fat extracted per liter of CO₂) as observed in Figure 5.3. These results indicate that the extraction reaches the equilibrium solubility concentration and that the intraparticle diffusion resistance is negligible for the flow rates investigated. If the intraparticle diffusion resistance were more dominant, SCCO₂ may prove to be more effective for the extraction than LCO₂ due to the high diffusivity which would allow easier access through the particle pores. The lack of diffusion resistance is likely due to the particle size of the finely-ground rendered poultry meal and the degraded matrix consistency achieved during cooking in the rendering process.²⁰ The particle size of the rendered material also decreases by an order of magnitude after the extraction from around 200 μm to about 20 μm on average, as observed in Figure 5.4. This can also be another influencing factor on the high extraction yields obtained since the particle size decreases as the extraction is carried out. It should be mentioned that the decreased particle size can lead to material handling issues.

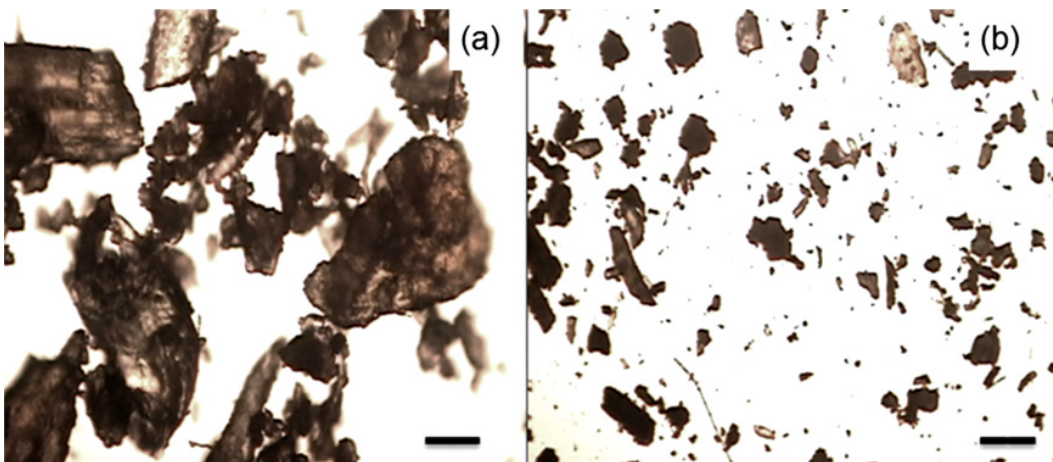


Figure 5.4. Optical Microscope image of RM. Scale bar: 100 μm. (a) Before the CO₂ extraction; and (b) After CO₂ extraction.

Table 5.1. Solubilities and extraction yield of rendered fat in LCO₂ and SCCO₂

	T	P	CO ₂ density	Fat solubility	Solubility Std. Error	Extraction Yield
	°C	bar	g/L	g/L	g/L	(%)
LCO ₂	25	69	738.2	0.491	0.020	90.8
		103	823.0	1.252	0.036	93.6
		138	865.0	1.973	0.074	93.6
		207	918.6	3.957	0.086	90.8
		276	955.6	5.651	0.082	93.6
		345	984.6	6.474	0.442	92.9
SCCO ₂	40	207	846.0	2.563	0.229	93.6
		276	896.0	4.054	0.408	94.3
		345	932.4	5.694	0.622	92.9
	50	207	792.4	1.638	0.078	87.3
		276	854.1	3.717	0.323	93.6
		345	896.5	5.647	0.630	96.5

Solubility Calculation and Correlation with the Chrastil Model

The fat solubility was determined from the linear trend observed in the extraction curves of Figure 5.2a-c. This represents the extraction region that is governed by the solubility equilibrium of the components as proved in the flow rate experiments. The slope of the extraction curve (fat extracted versus amount of CO₂) can be defined as the solubility of the fat in the solvent, c (g/L), and calculated as described by Reverchon.²¹ The equation is modified in this work to be applied to the axis plotted in Figure 5.2 as follows:

$$c = \frac{m_e}{V_s} = \frac{Y}{\left(\frac{V_s}{m_o}\right)} = \frac{-M * d_{CO_2}}{100} \quad \text{Eq.5.1}$$

Where m_e is the mass of fat extracted, V_s is the volume of CO₂ used in the extraction, Y is the extraction yield, m_o is the initial mass of fat in the RM, d is the CO₂ density, and M is the slope of the extraction curve. M was obtained by a linear regression of each extraction curve using the OriginPro7 software, and d from the NIST Chemistry WebBook.¹⁹ The solubility data and the CO₂ densities are presented in Table 5.1. As discussed before, the solubility of fat is higher for LCO₂ than for SCCO₂ due to the retrograde phenomena which makes solubility decrease with temperature, as observed in Figure 5.5a. As the pressure reaches 345 bar, the solubility isotherms get closer to each other and will likely converge to the “cross-over” pressure. Figure 5.5b shows the single effect of the fat volatility on the solubility in CO₂, where at constant density the fat solubility in CO₂ increases with increasing temperature.

The Chrastil model¹⁸ was used to correlate the solubility of the fat as a function of the CO₂ density and temperature. The model is based on the hypothesis that one molecule of solute A (fat component) can be associated with k molecules of solvent B (CO₂). This association forms a complex molecule AB _{k} that is in equilibrium with the solvent. The Chrastil equation is given as follows:

$$\ln c = k \ln d + \frac{a}{T} + b \quad \text{Eq. 5.2}$$

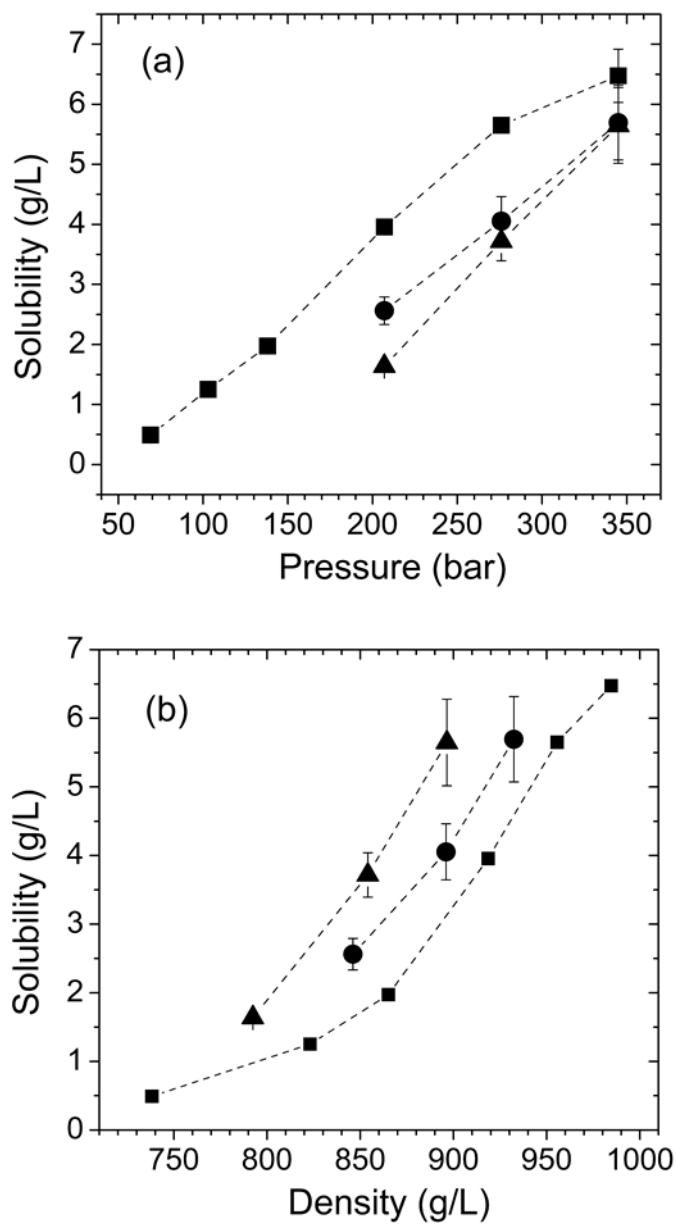


Figure 5.5. Solubility dependence of (a) pressure and (b) density. ■, 25 °C; ●, 40 °C; ▲, 50 °C

Where k , a and b are constants to be determined by fitting the data. The constant k accounts for the solvation, which is the slope of the solubility isotherm and reflects the density dependence of the solubility. The constant, a , represents the heat of solvation and

heat of vaporization of the solute and is also a measure of the temperature dependence of the solubility at constant density. Parameter b is dependent on the solute and solvent molecular weights and the association constant. A nonlinear regression was performed on the fat solubility data using Polymath 5.1 obtaining the following equation:

$$\ln c = 9.272 \ln d - \frac{2417.4}{T} - 53.86 \quad \text{Eq. 5.3}$$

The solubility prediction can be observed in Figure 5.6, which displays the estimated natural logarithms of the solubility versus density. The correlation accuracy was evaluated with the average absolute relative deviation (AARD) obtaining a value of 5.56% under the conditions studied in this investigation.

The modified Chrastil equation proposed by Sun and Li²² was also evaluated to correlate the solubility in order to improve the results over the simple Chrastil model. This modified Chrastil equation is as follows:

$$\ln c = (k + k_1 \cdot d) \ln d + \frac{(a + a_1 \cdot d)}{T} + b \quad \text{Eq. 5.4}$$

This modification includes the additional parameters k_1 and a_1 to account for any nonlinear correlation with CO₂ density. The constants were estimated but the AARD obtained was only 5.58%, which shows no improvement over the simple Chrastil equation shown above.

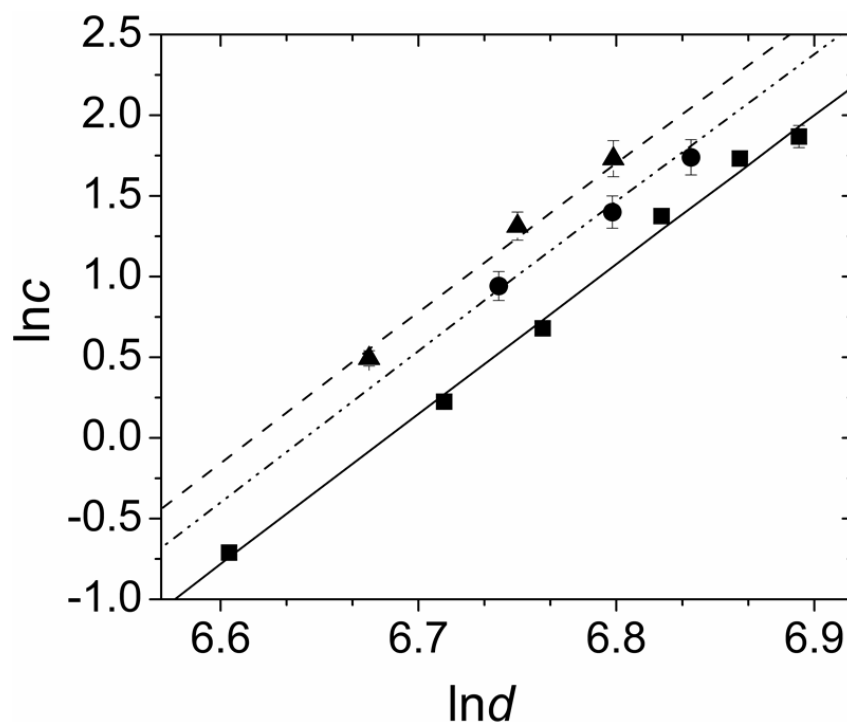


Figure 5.6. Plot of Inc vs Ind using Chrastil model for the experimental data at pressures between 69 and 345 bar and temperatures: ■, 25 °C; ●, 40 °C; ▲, 50 °C. Lines represent the results from the Chrastil model: —, 25 °C; - - - 40 °C; - · - ·, 50 °C.

Fatty Acid Composition

Analysis of the fatty acid fractions of the fat extracted from the rendered poultry meal with hexane and CO_2 was conducted using gas chromatography (GC). A total of 6 fatty acids were identified with a higher proportion of unsaturated fats than saturated as observed in Table 5.2. Most of the fatty acids present in the poultry fat² were identified in the GC analysis except for very small fractions of myristic (C14:0), margaric (C17:0), and α -linoleic (C18:3) acids. The fraction of lauric acid (C12:0) observed in the analysis was significantly higher than the reported literature. The difference observed in the fatty acid fractions between the hexane and the CO_2 extraction was not very significant.

However, the percentages of unsaturated fatty acids are in general higher for the CO₂ extraction as observed in Table 5.2. Literature shows that unsaturated fatty acids are more soluble than saturated ones in pressurized CO₂, up to around three times higher for linoleic (C18:2) than stearic (C18:0) acids.²³ These results also indicate that all the fatty acids extracted with hexane (>99% extraction yield) are also very soluble in CO₂ and that the residual 1% of fat after the CO₂ extraction could be inaccessible fat that may require other conditions to be extracted.

Table 5.2. Fatty acid mass fraction of extracted fats

Compound	Wt.%	
	CO ₂ extraction	Hexane extraction
Lauric (C12:0)	11.44	11.58
Palmitic (C16:0)	22.98	23.69
Palmitoleic (C16:1)	5.24	4.25
Stearic (C18:0)	6.56	9.85
Oleic (C18:1)	34.71	34.34
Linoleic (C18:2)	17.31	14.45
Unknown	1.77	1.84
Saturated	40.97	45.12
Unsaturated	57.26	53.04

Conclusions

LCO₂ and SCCO₂ were used for the extraction of fat from rendered poultry meal at different pressures (69-345 bar) and temperatures (25°C, 40°C and 50°C), obtaining maximum extraction yields between 87% and 97% for all the conditions. The starting material had a fat content of 14.2±0.2% which is residual from the mechanical press and cooking in the rendering plant from which the material was obtained. After the

extractions, the fat content in the samples was reduced to a minimum value of $1.0 \pm 0.1\%$ demonstrating the ability of the CO_2 to efficiently extract the fat from rendering materials. The fat analysis yielded a total of 6 fatty acids, which were identified in agreement with the literature. These fatty acids were present in similar proportions to the fat extracted with hexane and CO_2 , showing an overall higher percentage of unsaturated fatty acids for CO_2 .

Solubilities of the fat in CO_2 were calculated from the slope of the extraction curves at all the conditions tested. This estimation was possible because at the conditions of the extractions, the system reached the equilibrium solubility as proved by the flow rate experiments. These solubilities ranged from 0.491 g/L to 6.474 g/L for LCO_2 at 69 bar and 345 bar, respectively, and the solubility in SCCO_2 were intermittent between these values. It was observed that SCCO_2 at all pressures had lower solubilities than LCO_2 at the same pressures due to the retrograde solubility phenomena. The solubilities were successfully correlated with the Chrastil model obtaining an AARD of 5.56%. It was shown in this investigation that LCO_2 is more efficient than SCCO_2 in the extraction of fat since the maximum extraction yields were the same, but less CO_2 is required for the liquid phase due to the higher solubility.

References

1. Meeker DL. North American Rendering - processing high quality protein and fats for feed. *Revista Brasileira De Zootecnia-Brazilian Journal of Animal Science*. Jul 2009;38:432-U443.

2. Meeker DL. Essential Rendering - All About The Animal By-Products Industry. . In: Association NR, ed. Arlington; 2006.
3. NRS. National Renderers Association. Available at: <http://nationalrenderers.org/>. Accessed March 2012, 2012.
4. Swisher K. Market Report: Industry savors record prices and growing global demand. *Render Magazine*; 2012: 10-18.
5. Gooding CH. Data for the Carbon Footprinting of Rendering Operations. *Journal of Industrial Ecology*. Apr 2012;16(2):223-230.
6. Willems P, Kuipers NJM, de Haan AB. Gas assisted mechanical expression of oilseeds: Influence of process parameters on oil yield. *J Supercrit Fluids*. Jul 2008;45(3):298-305.
7. Pradhan RC, Meda V, Rout PK, Naik S, Dalai AK. Supercritical CO(2) extraction of fatty oil from flaxseed and comparison with screw press expression and solvent extraction processes. *Journal of Food Engineering*. Jun 2010;98(4):393-397.
8. Brunner G. Applications of Supercritical Fluids. In: Prausnitz JMDMFSMA, ed. *Annual Review of Chemical and Biomolecular Engineering, Vol 1*. Vol 1; 2010: 321-342.
9. Sahena F, Zaidul ISM, Jinap S, et al. Application of supercritical CO(2) in lipid extraction - A review. *Journal of Food Engineering*. Nov 2009;95(2):240-253.
10. Catchpole OJ, Tallon SJ, Eltringham WE, et al. The extraction and fractionation of specialty lipids using near critical fluids. *J Supercrit Fluids*. Jan 2009;47(3):591-597.
11. Brunner G. Supercritical fluids: technology and application to food processing. *Journal of Food Engineering*. Mar 2005;67(1-2):21-33.
12. Palmer MV, Ting SST. Applications for supercritical fluid technology in food processing. *Food Chemistry*. 1995;52(4):345-352.

13. Min JA, Li SF, Hao J, Liu NH. Supercritical CO₂ Extraction of Jatropha Oil and Solubility Correlation. *Journal of Chemical and Engineering Data*. Sep 2010;55(9):3755-3758.
14. Halim R, Danquah MK, Webley PA. Extraction of oil from microalgae for biodiesel production: A review. *Biotechnology Advances*. May-Jun 2012;30(3):709-732.
15. Temelli F. Perspectives on supercritical fluid processing of fats and oils. *J Supercrit Fluids*. Jan 2009;47(3):583-590.
16. Rout PK, Naik S, Rao YR. Liquid CO₂ extraction of flowers and fractionation of floral concrete of *Michelia champaca* Linn. *J Supercrit Fluids*. Apr 2011;56(3):249-252.
17. Rout PK, Naik S, Rao YR. Liquid CO₂ extraction of flowers of *pandanus fascicularis* Lam. And fractionation of floral concrete and comparative composition of the extracts. *Journal of Food Biochemistry*. Apr 2011;35(2):500-512.
18. Chrastil J. Solubility of solids and liquids in supercritical gases. *Journal of Physical Chemistry*. 1982;86(15):3016-3021.
19. Technology NIST. NIST Chemistry WebBook -Thermophysical Properties of Fluid Systems. Available at: <http://webbook.nist.gov/chemistry/>. Accessed October 2011.
20. Doker O, Salgin U, Yildiz N, Aydogmus M, Calimli A. Extraction of sesame seed oil using supercritical CO₂ and mathematical modeling. *Journal of Food Engineering*. Apr 2010;97(3):360-366.
21. Reverchon E, Marrone C. Modeling and simulation of the supercritical CO₂ extraction of vegetable oils. *J Supercrit Fluids*. Feb 2001;19(2):161-175.
22. Sun YY, Li SF. Measurement and correlation of the solubility of Ligusticum Chuanxiong oil in supercritical CO₂. *Chinese Journal of Chemical Engineering*. Dec 2005;13(6):796-799.

23. Maheshwari P, Nikolov ZL, White TM, Hartel R. Solubility of fatty-acids in supercritical carbon-dioxide. *J Am Oil Chem Soc.* Nov 1992;69(11):1069-1076.

CHAPTER SIX

CO₂ ASSISTED MECHANICAL EXPRESSION OF FAT FROM RENDERED MATERIALS

Introduction

The rendering industry converts the by-products or inedible parts from the animals produced for human consumption into value-added products, commonly known as rendered materials (RM).¹ There are 250 rendering facilities in North America that annually produce 18 billion pounds of RM per year, representing an important contribution to society and the economy of the food industry.^{2, 3} This industry is also green and environmentally beneficial, reducing the amount of waste while recycling carbon and energy into valuable feed ingredients and biofuels.³ The RMs are constituted of approximately 50% fats, which are commonly used by soap and personal care products manufactures and as a biofuel feedstock.³ This fat is separated from the protein matrix via screw press, which can leave 8 to 15% fat remaining in the protein meals.⁴ Thus, new methods for more efficient fat isolation are desired, especially since the fat is a higher value product.

Screw pressing offers the advantages of producing uncontaminated oil with low initial and operational costs, however, the low separation efficiencies in the current rendering process produces a material with 8-15% residual fat.¹ It is well know that extraction with organic solvents, such as hexane, yield higher efficiencies (>99%), but produces contaminated oil that requires refining.⁵ High pressure CO₂ is a greener

alternative extraction solvent for a clean and selective separation of fats that has been widely used in the extraction of seeds, decaffeination of green coffee beans, and other areas in the food industry.⁶⁻⁹ Past research has shown that extraction of flaxseed oil with supercritical CO₂ yields approximately 28% more fat than screw pressing and just 9% less than hexane extraction.⁴ Liquid and supercritical CO₂ were also recently used for the extraction of fat from rendering materials, reducing the fat content to less than 1%.¹⁰ This process offers the advantages of separating a clean fat and the possibility of facile solvent recycling. However, the amount of CO₂ needed is relatively high due to the low fat solubilities ranging between 0.5 to 6.5 g/L depending on pressure and temperature.¹⁰

GAME (Gas-Assisted Mechanical Expression) is a process that combines mechanical pressures and the presence of CO₂ as a solvent to dissolve into oils and enhance the pressing operation. This enables higher fat recoveries using only a fraction of CO₂ compared to the aforementioned traditional CO₂ extraction. This is possible because the solubility of CO₂ in oils can be 50% higher than the solubility of oil in CO₂.^{11, 12} This process was first introduced by Venter et al. for the separation of cocoa butter.¹³ In GAME, a gas-expanded liquid is formed by saturating CO₂ in the oil or fat, significantly reducing the viscosity of the mixture compared to pure lipids.¹⁴ This reduction of the viscosity allows for an increase in expression yield compared to conventional mechanical expression, since the lipids are drained more easily through the compressed bed.¹⁵ Moreover, this reduction in viscosity is also accompanied by a reduction of energy required for the separation process.¹⁶ Other possible factors affecting the enhanced separation are the freeing of oil due to disruption of the oil cell walls, and a reduction of

interfacial tension of the oil.¹⁶ Additionally, it is possible that the undissolved CO₂, which is in equilibrium with the oil-CO₂ mixture, displaces the oil-CO₂ mixture contained in the filter cake.¹⁷ This behavior can be attributed to a higher density of the oil compared to supercritical CO₂, which actually increases when it is saturated with CO₂.¹⁸

The aim of this work is to increase the fat extraction yield from rendered materials using CO₂ assisted mechanical expression. This method is expected to reduce the amount of CO₂ utilized compared to the liquid and supercritical CO₂ extractions in Chapter 5, and also to reduce the energy requirement compared to conventional mechanical pressing. In this study, mechanical pressures between 300 and 2000 bars and CO₂ pressures between 69 and 241 bars were evaluated and compared to conventional expression. The effect of temperature (25, 40, 60 and 100°C) on the yield was also studied in this work.

Materials and Methods

Materials

Feed grade poultry by-product meal was used as the rendered material (RM) in our testing and was kindly donated by Valley Proteins Inc. The rendered material was used as received without any sample modification. The composition of the material was 12.1 wt.% fat and 7.0 wt.% moisture content. Carbon dioxide used in the experiments was purchased from Airgas and ACS grade n-hexane was purchased from VWR. A 10 ton hydraulic press (Torin™ Big Red jack model #T51003) was purchased from Northern Tools. The extraction cell (piston, upper cylinder, lower cylinder, cylinder stand, and

sieve plate) were designed in Solidworks and manufactured by Clemson Machining and Technical Services. Buna-nitrile O-ring with 2 backup rings was used on the piston assembly to seal the cylinder.

Experimental Set-up

The separation of fat from the rendered material was performed in batch mode using the designed high pressure cell with mechanical pressing capability, equipped with a hydraulic press as seen schematically in Figure 6.1. A Teledyne Isco 500HD syringe-pump connected to a recirculating heating bath was used to deliver the CO₂ at the desired pressure and temperature. A total amount of 5.0 g of RM was used in each experimental run. Heating tapes were wrapped around the top and lower cylinders were connected to an Omega CSC32 temperature controller in conjunction with a Payne Engineering 18TP variable voltage controller. K-type thermocouples provided feedback to the controllers. Before each experimental run, the cylinders were allowed to equilibrate at the specified temperature. The piston was lowered on top of the sample in each run to provide an initial compaction of the material.

High pressure CO₂ was introduced into the extraction cylinder for specific periods of time to reach equilibrium with the RM and fat. After this equilibrium time, the mechanical pressure was raised over the course of one minute to the desired force and held constant for a specific period of time. The expressed lipids passed through a 10 µm frit filter and sieve plate to the collection chamber while the RM remained in the upper cylinder. The cylinder was then depressurized over the course of 1 min and the extracted

fat was collected in a recovery flask filled with n-hexane. The extracted RM was collected and analyzed by the Agricultural Laboratory at Clemson University to determine the remaining fat content by a Soxhlet hexane extraction.

Experimental procedure

The fat separation runs have two time-dependent parameters that can influence the yield of lipid expression. The equilibrium time is required before the mechanical pressure to allow the CO₂ to dissolve and equilibrate with the fat. The correct pressing time will allow a complete drainage of the fat-CO₂ mixture from the RM cake. To evaluate the equilibrium times on the extraction yield, the samples were allowed to equilibrate for 0, 5, 10, 20, and 40 min at 40 °C and CO₂ pressure of 172 bar before applying the mechanical pressure for the extraction for 10 min. In another set of experiments at a fixed equilibrium time, different pressing times in the same range (0 to 40 min) and conditions (40°C and CO₂ pressure of 172) as the previous experiment were evaluated. According to the results obtained, 20 min of equilibrium and 20 min of pressing were sufficient for equilibrium to be reached and used in the remaining experiments.

The effects of the effective mechanical pressure (P_{eff}) (70-1880 bar) and CO₂ pressure (0, 69, 103, 172, and 241 bar) on the extraction yield were studied at 40°C. P_{eff} is defined as the mechanical pressure exerted by hydraulic pump on the RM material minus the pressure of CO₂ inserted in the extraction cell. For these experiments, the CO₂ was introduced at the desired pressures and allowed to equilibrate before exerting specific forces (1, 2, 4.5, 6 US ton) that were converted to the P_{eff} in units of pressure (bars). The

effect of temperature on the rendered fat extraction was studied at a constant mechanical force of 4.5 ton (1410 bar). These experiments were conducted at temperatures ranging between 25 to 100 °C using 103, 172, and 241 bars of CO₂ pressure.

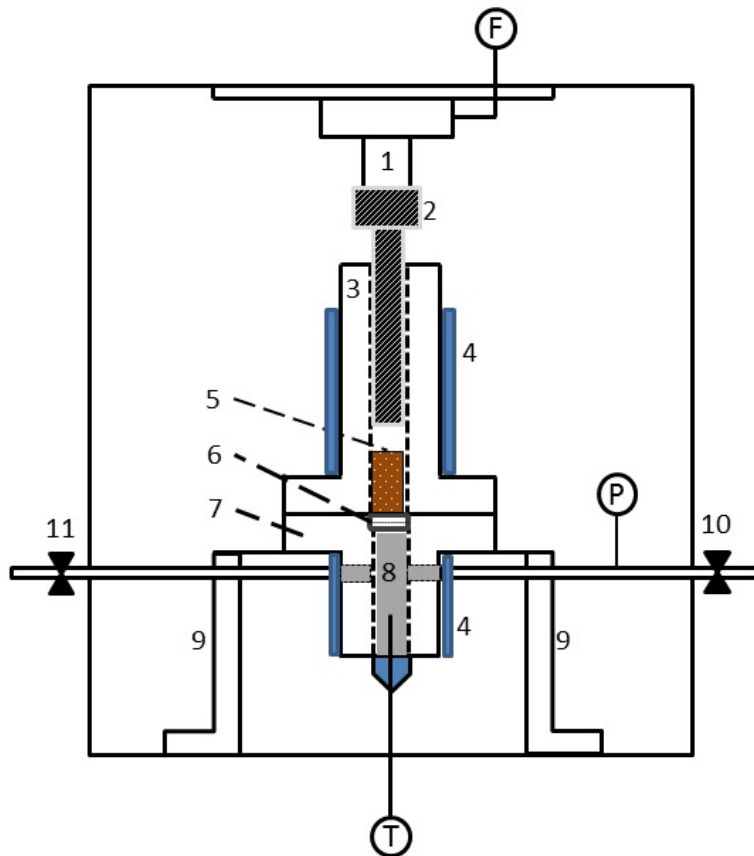


Figure 6.1. Schematic diagram of the CO₂ assisted mechanical expression of rendered materials. (1) Hydraulic Ram; (2) Piston assembly; (3) Upper Cylinder; (4) Heating tape; (5) Rendered Material; (6) Sieve Plate and 10 µm frit filter; (7) Lower Cylinder; (8) Collection Chamber; (9) Cylinder Stand; (10) Inlet CO₂ valve; (11) Outlet CO₂/lipid valve; (F) Mechanical Force gauge; (P) Pressure sensor; (T) Thermocouple.

Results and discussion

Optimum experimental conditions

The necessary time to allow CO₂ to dissolve in the rendered materials was determined by experiments conducted at 40°C and CO₂ pressure of 172 bars. Equilibrium times up to 40 min demonstrated that at least 5 min are needed to reach equilibrium as observed in Figure 6.2. After 5 min, the expression time does not influence the yields, where yield is defined as the fat extracted as a mass percentage of the original fat in the RM. An equilibrium time of 5 min is relatively low compared to other gas-assisted expressions of oilseeds which were reported to be higher than 30 min.⁵ Similar behavior was found in our previous work (Chapter 5), where CO₂ was able to easily penetrate the material and dissolve the fat, because the RM is finely ground with high porosities and particle sizes less than 100 µm after extraction of fat.¹⁰

Figure 6.2 also shows the effect of pressing time on the yield, which is more dependent on the pressing time, requiring a minimum of 20 min of pressing. Previous research report times of around 10 min for the extraction of vegetable oils.^{5, 13} This behavior could be explained by the lower viscosities compared to animal fats, resulting in faster times for the fat to drain from the cake. For the purpose of this work, the extraction at different pressures and temperatures will be conducted for 20 min for both the equilibrium and pressing times.

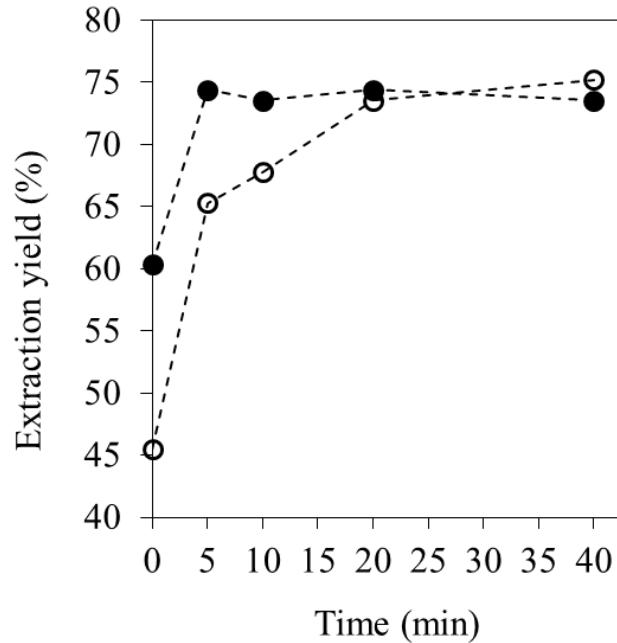


Figure 6.2. Effects of the equilibrium time (●) and pressing time (○) on the extraction yields of rendered fats.

Effect of CO₂ pressure and effective mechanical pressure

The influences of CO₂ pressure and P_{eff} on the expression yield are shown in Figure 6.3. The yields are observed to increase with CO₂ pressures, obtaining a highest value of 81% at CO₂ pressure of 241 bar and P_{eff} of 390 bar. On the other hand, the lowest extraction yields were obtained for the conventional expression which showed at best a 41.3% yield. The separations conducted at the lowest CO₂ pressure, 69 bar, had a 27% higher absolute yield than conventional expression with no CO₂, while increasing the CO₂ pressure from 69 to 241 bar only increased the yields by approximately 12%.

The trend of the extraction yields as a function of P_{eff} in Figure 6.3 exhibit a maximum value at around P_{eff} = 500 bar. This behavior also occurs with the conventional separation without the use of CO₂ and can be explained by understanding the variables

involved in the drainage of the fat through the compressed cake. The superficial velocity of the fat (\hat{v}_F), or fat drainage, is described by the one dimensional version of the Darcy's law¹⁹ as follows

$$\hat{v}_F = -\frac{B}{\eta_F} \frac{dP}{dz} \quad \text{Eq. 6.1}$$

where B is permeability, η_F is the dynamic viscosity of the fluid, and dP/dz is the gradient of fluid pressure. As the mechanical pressure is exerted on the material, the oil pressure (the driving force) increases, while the permeability decreases, leading to a further increase of the oil pressure. However, at some point the permeability becomes so low that it disrupts the fat drainage and reduces the extraction yields.¹⁶ For this system, this point seems to occur at some pressure around 630 bar for the conventional expression, and it may be the reason why some gas assisted expressions of oils reported in the literature are usually conducted at pressures not higher than 550 bar.^{5, 13} This optimum pressure cannot be accurately determined from Figure 6.3, but it is in the range of $P_{\text{eff}} = 600$ bars.

According to Darcy's equation, a reduction of the viscosity increases the drainage of the fat. The dissolution of CO_2 in oils has been shown to reduce the viscosity to 10% of the original oil viscosity at a CO_2 pressure of 150 bar.²⁰ However, other studies have shown that above ~ 150 bar the viscosity of the oil- CO_2 mixture does not vary significantly.^{14, 20} This can explain why in Figure 6.3 the extraction yields between 172 and 241 bar are essentially the same. Hence, it is not advantageous to conduct the RM pressing at CO_2 pressures higher than 150 bar or P_{eff} greater than 600 bar.

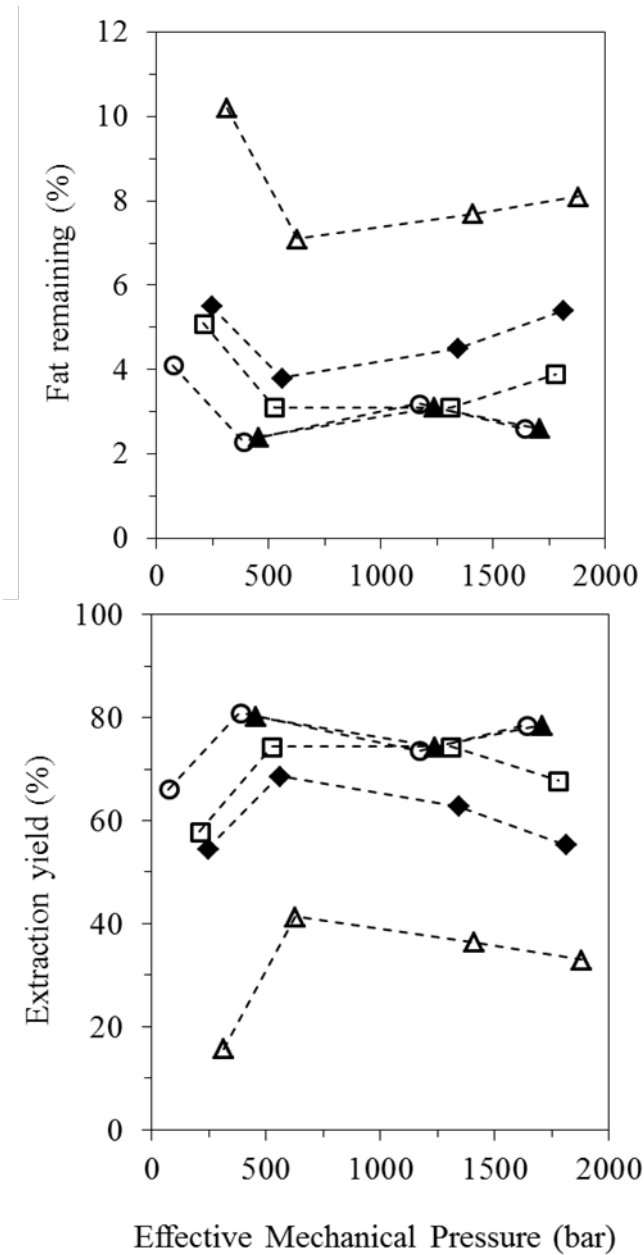


Figure 6.3. Extraction curves at different CO₂ pressures and 40°C as a function of effective mechanical pressure. (a) Extraction yields and (b) fat contents after extraction.

Δ, 0 bar; ◆, 69 bar; □, 103 bar; ▲, 172 bar; ○, 241 bar.

Temperature effect

The effect of temperature on the expression yield was evaluated at pressures of 103, 172, and 241 bar (Figure 6.4). For the lowest pressure, the temperature was observed to have a more pronounced influence, increasing the yield by 20% going from 25°C to 40°C. However, the overall trend suggests that temperature slightly reduces the extraction yield as observed in Figure 6.4. This behavior can be explained by the reduced solubility of supercritical CO₂ in liquids as temperature is increased when the pressure is below a determined critical value.¹⁶

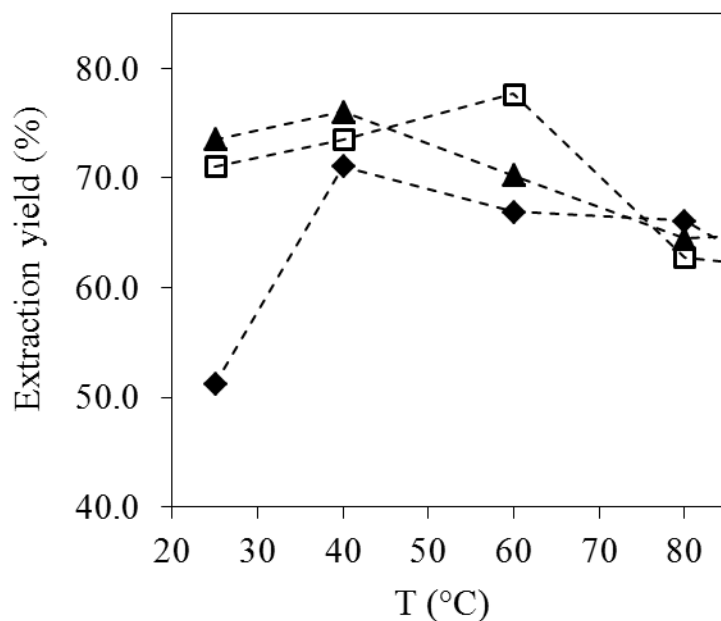


Figure 6.4. Temperature effect on the extraction yield at different pressures. ♦, 103 bar; □, 172 bar; ▲, 241 bar.

Conclusions

CO₂ assisted mechanical expression of fats from rendered material was successfully conducted in this work, obtaining a highest yield of 81% compared to 41% achieved with conventional expression. This yield represents a reduction of the remaining fat content from the initial 12.1% to 2.3%. The minimum equilibrium time before the extraction was found to be 5 min, demonstrating a fast CO₂ dissolution into the fat component of the rendered material. An optimum effective mechanical pressure was observed at around 600 bar, which can be attributed to a reduced permeability of the CO₂-fat mixture through the RM matrix at high mechanical pressures, as described by Darcy's law. The CO₂ pressure increases the extraction yields; however, at pressures higher than 172 bar, the change becomes negligible possibly due to the viscosity of the oil-CO₂ mixture, which has been reported not to decrease significantly beyond such pressure.^{14, 20} Overall, it was demonstrated that high extraction yields can be achieved when conducting a gas assisted extraction on RM, utilizing only a fraction of the amount of CO₂ used for CO₂-only extractions.

References

1. Meeker DL. North American Rendering - processing high quality protein and fats for feed. *Revista Brasileira De Zootecnia-Brazilian Journal of Animal Science*. Jul 2009;38:432-U443.
2. Meeker DL. Essential Rendering - All About The Animal By-Products Industry. . In: Association NR, ed. Arlington; 2006.

3. NRS. National Renderers Association. Available at: <http://nationalrenderers.org/>. Accessed March 2012, 2012.
4. Pradhan RC, Meda V, Rout PK, Naik S, Dalai AK. Supercritical CO₂ extraction of fatty oil from flaxseed and comparison with screw press expression and solvent extraction processes. *Journal of Food Engineering*. Jun 2010;98(4):393-397.
5. Willems P, Kuipers NJM, de Haan AB. Gas assisted mechanical expression of oilseeds: Influence of process parameters on oil yield. *J Supercrit Fluids*. Jul 2008;45(3):298-305.
6. Catchpole OJ, Tallon SJ, Eltringham WE, et al. The extraction and fractionation of specialty lipids using near critical fluids. *J Supercrit Fluids*. Jan 2009;47(3):591-597.
7. Sahena F, Zaidul ISM, Jinap S, et al. Application of supercritical CO₂ in lipid extraction - A review. *Journal of Food Engineering*. Nov 2009;95(2):240-253.
8. Brunner G. Supercritical fluids: technology and application to food processing. *Journal of Food Engineering*. Mar 2005;67(1-2):21-33.
9. Palmer MV, Ting SST. Applications for supercritical fluid technology in food processing. *Food Chemistry*. 1995;52(4):345-352.
10. Orellana JL, Smith TD, Kitchens CL. Liquid and Supercritical CO₂ Extraction of Fat from Rendered Materials. *The Journal of Supercritical Fluids*. 2013.
11. Bharath R, Inomata H, Adschiri T, Arai K. Phase-equilibrium study for the separation and fractionation of fatty oil components using supercritical carbon-dioxide. *Fluid Phase Equilib*. Dec 1992;81(1-2):307-320.
12. Eggers R, Sievers U. Processing of oilseed with supercritical carbon-dioxide. *J Chem Eng Jpn*. Dec 1989;22(6):641-649.

13. Venter MJ, Willems P, Kuipers NJM, de Haan AB. Gas assisted mechanical expression of cocoa butter from cocoa nibs and edible oils from oilseeds. *J Supercrit Fluids*. May 2006;37(3):350-358.
14. Jenab E, Temelli F. Viscosity measurement and modeling of canola oil and its blend with canola stearin in equilibrium with high pressure carbon dioxide. *The Journal of Supercritical Fluids*. 2011;58(1):7-14.
15. Pietscha A, Eggers R. Gas-assisted oilseed pressing - Design of and tests with a novel high-pressure screw press. In: Saravacos G, Taoukis P, Krokida M, et al., eds. *11th International Congress on Engineering and Food*. Vol 1. Amsterdam: Elsevier Science Bv; 2011: 1381-1387.
16. Voges S, Eggers R, Pietsch A. Gas assisted oilseed pressing. *Sep Purif Technol*. Oct 2008;63(1):1-14.
17. Venter MJ, Willems P, Kareth S, Weidner E, Kuipers NJM, de Haan AB. Phase equilibria and physical properties of CO₂-saturated cocoa butter mixtures at elevated pressures. *J Supercrit Fluids*. Jun 2007;41(2):195-203.
18. Tegetmeier A, Dittmar D, Fredenhagen A, Eggers R. Density and volume of water and triglyceride mixtures in contact with carbon dioxide. *Chem Eng Process*. Sep 2000;39(5):399-405.
19. Darcy H. *Les fontaines publiques de la ville de Dijon*: V. Dalmont; 1856.
20. Hobbie M. *Bildung von Tropfen in verdichteten Gasen und stationäre Umströmung fluider Partikel bei Drücken bis zu 50 MPa*. Hamburg, Germany, Hamburg University of Technology; 2006.

CHAPTER SEVEN

FUTURE WORK

Introduction

The purpose of this chapter is to report significant findings, not included in previous sections of this dissertation, in the research areas of cellulose nanocrystals (CNCs) and their properties when added to polylactic acid. These two areas are currently under investigation in my research group and will continue due to their promising applications. The first half of this chapter deals with use of CNCs for the fabrication of microelectromechanical systems (MEMS). Due to the similar properties of CNCs compared to silicon, the goal is to use cellulose as a drop-in replacement for silicon. The second half reports enhanced optical properties of PLA composites upon the addition of CNCs as a result of self-assembly and orientation of the nanocrystals.

Processing and properties of cellulose nanocrystals films for MEMS applications

Introduction

Cellulose nanocrystals (CNCs) have been demonstrated to exhibit great mechanical, optical, and electrical properties that can be applied in different advanced applications.¹ In addition, research has shown that cellulose can be used to fabricate “smart” materials that can react intelligently under environmental stimuli.^{2, 3} In light of this, exploring CNCs for new applications can lead to production of novel materials with innovative properties.

The objective of this work is to investigate the use of CNCs for the fabrication of films that can be applied for the fabrication of microelectromechanical systems (MEMS). This idea is motivated by the need for inexpensive, facile, abundant, renewable, and biodegradable alternatives to silicon.⁴ Silicon is facing increasing supply constraints due to the parallel growth of the microdevice/microelectronic and solar energy industries. In addition, the processing of silicon is often regarded as expensive and environmentally harmful due to high energy requirements and the use of harsh chemicals. These factors make many potential “lab on a chip” applications (i.e., one time use or point of care devices) based on silicon technology cost prohibitive. The surface chemistry of cellulose is similar to hydrophilic silicon oxide, since it has an abundance of hydroxyl groups on its surface, which make CNCs a potential alternative for MEMS devices among other reasons. CNCs have bending strength of 10 GPa⁵ and Young’s Modulus of 143 GPa,⁶ which are comparable to silicon and within an order of magnitude of those of carbon nanotubes.⁷ More recently and in conjunction with our collaborators at Auburn University, we have found that CNC films can be etched using current lithographic techniques used in commercial silicon MEMS. Furthermore, CNC has the added potential to align through liquid crystalline self-assembly and/or upon shearing, opening the possibility to make MEMS with anisotropic properties, which is not achievable with silicon materials.⁸

Our research group has focused on the study of the CNC properties in aqueous and organic solvents. The phase behavior, self-assembly, and the formation of thin films over silicon wafers have been investigated. The thin films will be treated and processed to

fabricate the MEMS devices. CNCs isolated by hydrochloric acid (CNC-HCl) and with acetic acid (CNC-AA) were utilized for this purpose and were isolated as detailed in the Appendix B.1. Sulfuric acid synthesized CNCs (CNC-SA) have also been used in this work for thin film deposition, but the phase behavior has not been studied intensively here since it is widely known in the literature.^{9, 10}

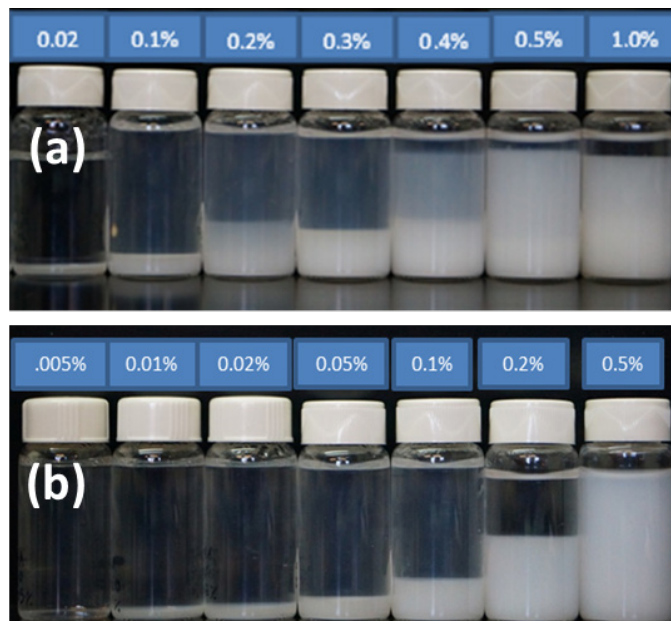


Figure 7.1. Degree of flocculation of CNC suspension at different concentrations. (a) CNC-OH and (b) CNC-AA.

CNC phase behavior in water

CNC suspensions in water are studied for the preparations of MEMS devices since the use of organic solvents can strip the photoresist, which is the mold for the fabrication of the devices. However, CNCs also have to exhibit good compatibility with the substrate, which is also hydrophobic, in order to attach themselves to the photoresist. In this collaborative project, our group is focusing on of the synthesis and properties of

CNCs in water for the successful deposition of films on silicon wafers, while the other groups are working in the fabrication of the MEMS devices.

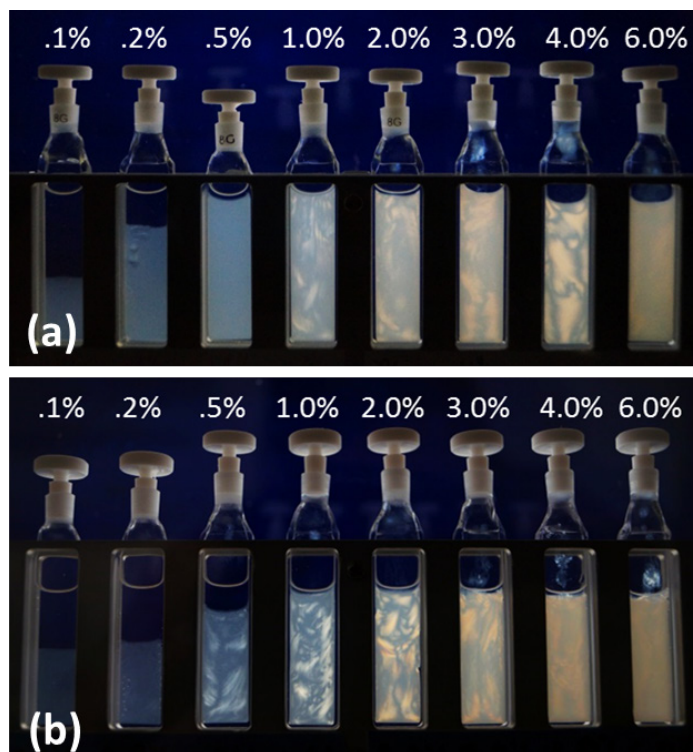


Figure 7.2. Birefringence of CNC-HCl (a) and CNC-AA (b) suspensions in 2mm path length cuvettes between cross polarized films indicating the formation of liquid crystals.

The phase behavior of CNC suspensions was studied by preparing increasing concentrations of CNC-HCl and CNC-AA and they were studied by visual examination of between crossed polarizers. Figure 7.1 shows the phase separation with concentration for both types of suspensions. The behavior for the CNC-AA suspensions seems to display a better trend with concentration. This can be attributed to the reduced hydrogen bonding due to the introduction of the carbonyl groups. For this reason, CNC-HCl, which possesses only hydroxyl groups on the surface, had the tendency to settle faster than for CNC-AA. The concentrations of each of the phases were calculated by means of UV-vis

spectrometry and gravimetric analysis and the detailed results are presented in Appendix D.

CNCs can assemble spontaneously into liquid-crystal phases. This assembly may be important for the development of MEMS devices that require mechanical stiffness in different directions. Figure 7.2 shows the self-assembly of both CNC types in water at concentrations between 0.1% and 6.0%. Birefringence patterns can be clearly observed indicating the formation of liquid crystals, probably a nematic phase. For CNC-AA the birefringence begins at a lower concentration than for CNC-HCl and also display higher intensities, which is also believed to be as a result of a better dispersion.

For the MEMS fabrication, well-dispersed aqueous suspensions of CNC are needed for a smooth and strong film. However, observation under polarized microscope of CNC suspensions in water showed agglomeration at various CNC concentrations after the isolation process (Figure 7.3). The process of removing the agglomerations effectively is a current work in the research group, and results suggest that a combination of 10-15 min of sonication and 5 min of centrifugation can reduce these agglomerates significantly. Although agglomeration can be clearly observed, an appearance of bright phase at high concentrations is indicative of liquid crystal formation as shown in Figure 7.3. There is not a significant amount research in the study of liquid crystals formed by these types of CNCs, which is reason why this is a current research area in our research group.

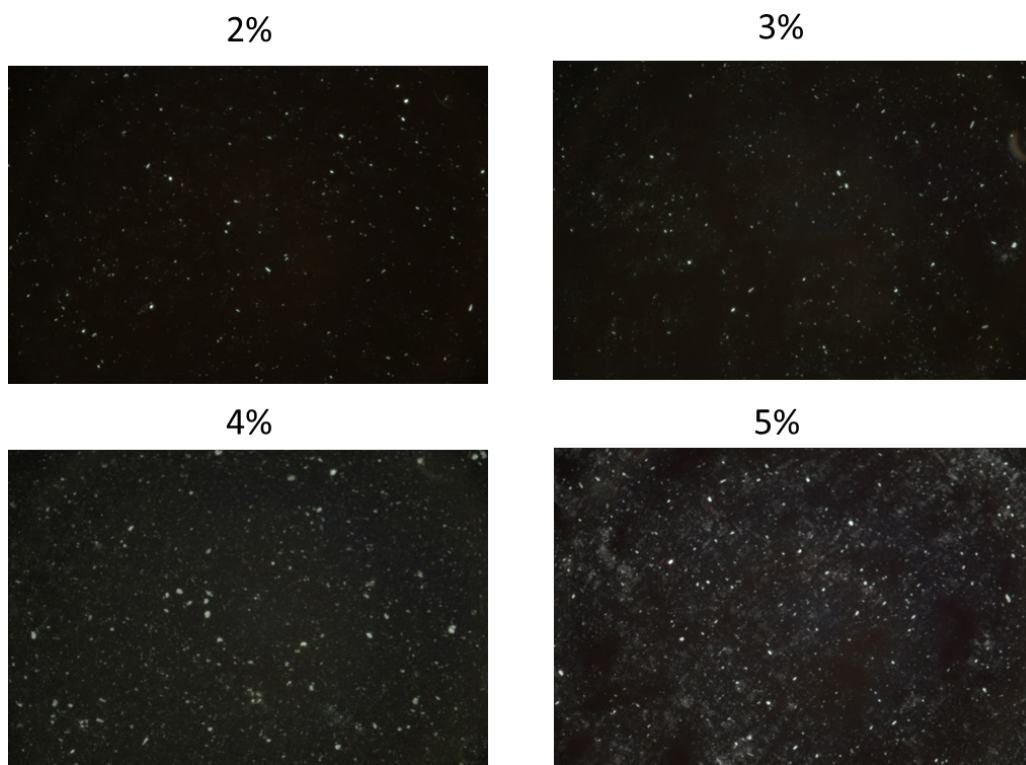


Figure 7.3 Polarized microscopy of CNC-HCl suspensions, displaying bright phases and agglomerates (white dots). Length of the longest side of each image: 1.5mm

CNCs films were deposited on round silicon wafers using spin-coating (Appendix B.4). The wafers were treated with N-(6-aminohexyl) aminopropyl-trimethoxysilan in order to change the surface chemistry for better compatibility with future steps in the fabrication of MEMS. The film quality was studied by visual examination and by atomic force microscopy (AFM). In addition to CNC-HCl and CNC-AA, sulfuric acid synthesized CNC (CNC-SA) was also evaluated. As observed in Figure 7.4, the most uniform films were form when using CNC-AA, which is the least hydrophilic of the nanocrystals used. This was also demonstrated by measuring the height through AFM, which indicated that CNC-AA films had a thickness of approximately 1.5 μm . CNC-HCl

and CNC-SA on the other hand, showed a thickness in the order of 0.2 μm . The ideal thickness for the fabrication of MEMS is around 3 μm , while smooth surfaces are also required. The CNC-SA films showed the smoothest surfaces compared to the other nanocrystals, probably due to the high dispersibility of CNC-SA as a result of the surface charge. CNC-AA and CNC-HCl have the tendency to agglomerate as discussed above, but with the appropriate removal of agglomeration, CNC-AAs are a promising material for the fabrication of MEMS.

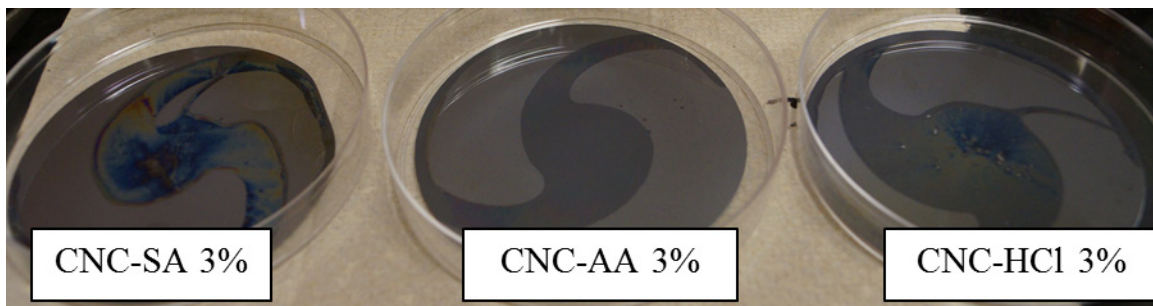


Figure 7.4. Picture of the CNC films deposited over silicon wafers.

Nanocomposites with optical properties

PLA-CNC nanocomposites were prepared to test the mechanical properties and to study the optical properties provided by the self-assembly of CNCs. In Chapter 3, polarized microscopy of the films demonstrated the increase of nanocrystal self-assembly with concentration. The nanocomposites with 10% CNC, which is the highest concentration prepared, showed a colorful arrangement between crossed polars especially when their thickness was varied by overlapping the films as shown in Figure 7.5. In this figure, the composites with surfactant decylamine (DA) are presented, and in Figure 7.6 the images at the different rotation angles are presented.

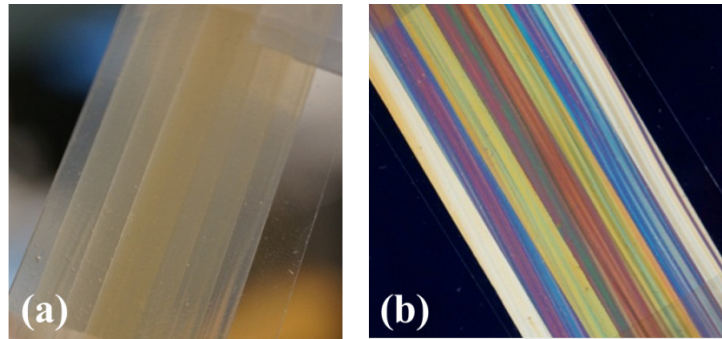


Figure 7.5. Overlapping layers of nanocomposites of PLA and 10% DA-modified CNC showing optical properties (a) normal light, and (b) between crossed polars

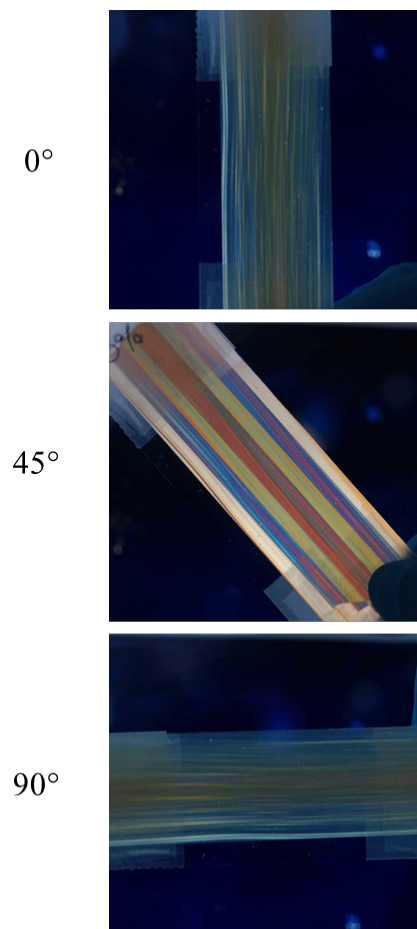


Figure 7.6. PLA with 10% CNCs modified with DA rotated between crossed polars at 0° , 45° , and 90° .

The orientational alignment observed in the films at lower concentrations in Chapter 3 appears to be predominantly in the direction of the extrusion as observed in Figure 7.6.

At 0° and 90° , CNC alignment in the composite will not create retardation because they will be either parallel or perpendicular to the polarized filter. However, at 45° , the composite creates retardation that is dependent on the thickness of the sample, displaying the different colors. Figure 7.7 shows an image of the sample obtained from the polarized microscope for a closer observation of the birefringent colors.

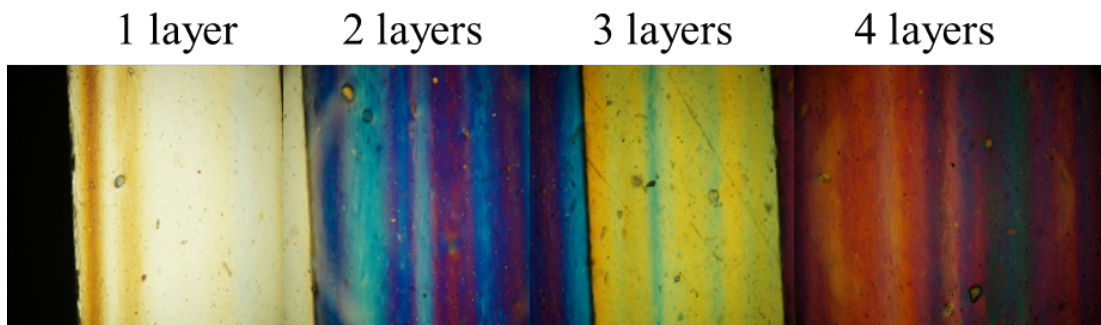


Figure 7.7. Low magnification polarized-light microscopy of the nanocomposites of PLA with 10% CNCs showing colored optical properties

The samples were prepared with the modified CNCs (DA and CTAB) and also with unmodified CNCs. These colors began to be noticeable for the 5% CNC films, and the colors varied depending on the CNC functionality as observed in Figure 7.8. The films with more color intensity were the unmodified and DA-modified films, which also demonstrated less agglomeration as reported in Chapter 3. CTAB-modified CNC composites were less transparent and although they showed some color, they were not as bright as the other modifications. This self-assembly may also be in accord with results presented in Chapter 2, where CNC-DA showed a better organization within organic solvents in a stationary state and upon shearing. In addition, the CNC-DA films also

exhibit the best mechanical properties, increasing toughness by 61% compared to neat PLA.

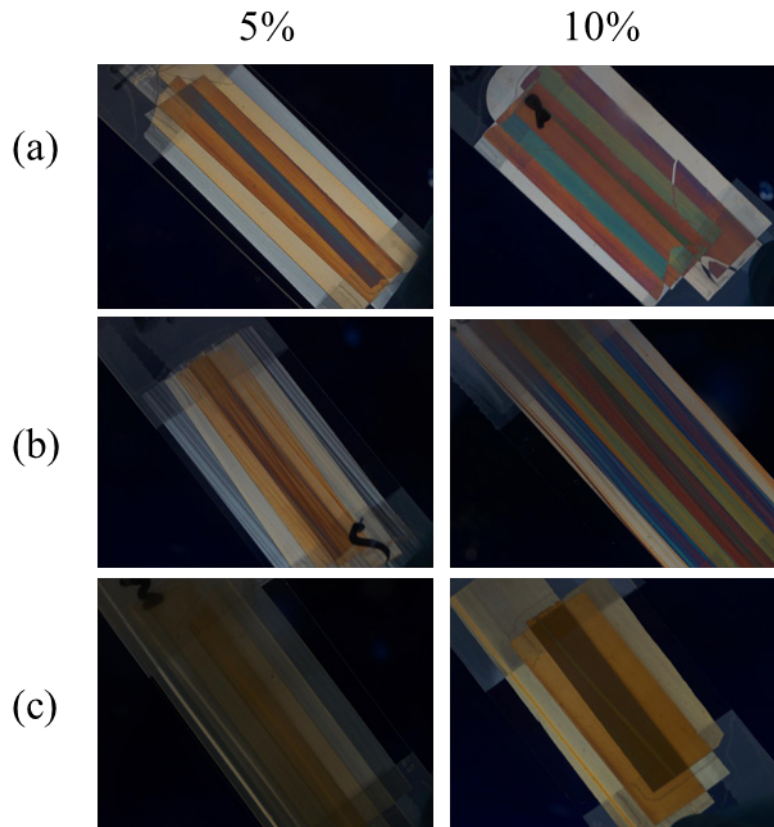


Figure 7.8 PLA composite films with unmodified CNCs (a); DA-modified CNCs (b); and CTAB-modified CNCs (c).

Although, the 10% CNC films demonstrated poor mechanical properties, their intricate optical properties make them potential materials for applications such as decorative coatings, security papers, displays, specialty textiles and defense applications among others. Current and future research of these films in our research group will explore the specific origin of the structural color in terms of nanoscale structure, as well as the conditions that result in the formation of the liquid crystal structures including processing method, CNC functionality and concentration within the composite, and also

the nature of the matrix. The formations may be analyzed by polarized microscopy, AFM, TEM and X-ray scattering in order to determine the specific orientation of the nanocrystals that arises in these unique properties.

References

1. Eichhorn SJ. Cellulose nanowhiskers: promising materials for advanced applications. *Soft Matter*. 2011 2011;7(2):303-315.
2. Qiu XY, Hu SW. "Smart" Materials Based on Cellulose: A Review of the Preparations, Properties, and Applications. *Materials*. Mar 2013;6(3):738-781.
3. Kim J, Bae S-H, Lim H-G. Micro transfer printing on cellulose electro-active paper. *Smart materials and structures*. 2006;15(3):889.
4. de Mello A. Focus: Plastic fantastic? *Lab on a Chip*. 2002;2(2):31N-36N.
5. Azizi Samir MAS, Alloin F, Dufresne A. Review of Recent Research into Cellulosic Whiskers, Their Properties and Their Application in Nanocomposite Field. *Biomacromolecules*. 2005/03/01 2005;6(2):612-626.
6. Sturcova A, Davies GR, Eichhorn SJ. Elastic modulus and stress-transfer properties of tunicate cellulose whiskers. *Biomacromolecules*. Mar-Apr 2005;6(2):1055-1061.
7. Podsiadlo P, Choi SY, Shim B, Lee J, Cuddihy M, Kotov NA. Molecularly Engineered Nanocomposites: Layer-by-Layer Assembly of Cellulose Nanocrystals. *Biomacromolecules*. 2005;6(6):2914-2918.
8. Habibi Y, Lucia LA, Rojas OJ. Cellulose Nanocrystals: Chemistry, Self-Assembly, and Applications. *Chemical Reviews*. Jun 2010;110(6):3479-3500.

9. Urena-Benavides EE, Ao GY, Davis VA, Kitchens CL. Rheology and Phase Behavior of Lyotropic Cellulose Nanocrystal Suspensions. *Macromolecules*. Nov 2011;44(22):8990-8998.
10. Revol J-F, Bradford H, Giasson J, Marchessault R, Gray D. Helicoidal self-ordering of cellulose microfibrils in aqueous suspension. *International journal of biological macromolecules*. 1992;14(3):170-172.

CHAPTER EIGHT

CONCLUSIONS AND RECOMMENDATIONS

Conclusions

This dissertation explores two research areas, cellulose nanocomposites and CO₂ extraction of rendered fat, with the ultimate goal of developing new bio-based materials for advanced and commercial applications. In the first half, a comprehensive study of the properties of surface-modified CNCs for the reinforcement of biodegradable polymers is provided, while in the second, more efficient and greener fat extractions using CO₂ are conducted on rendered materials to broaden their applications.

Surface modification of CNCs is required to obtain good dispersions in non-polar organic solvents and polymeric matrices. Although surfactants are an easy and effective way to increase this dispersibility, high concentrations are frequently required for the stabilization, causing a potential reduction of composite performance.^{1, 2} In the investigation reported here, the functionalization of CNCs was successfully achieved by the addition of surfactants at only 1 wt% with respect to the CNC weight, increasing the stability in organic solvents and the toughness of PLA composites. The reason for the effectiveness of the addition of surfactants is believed to be due to the prior acetylation of CNCs, a process which reduces hydrogen bonding and, therefore, also the agglomerations.

Decylamine-modified CNCs in THF were the most stable suspensions observed, remaining without significant phase separation for at least a month. This modification of

CNCs was also responsible for the highest increase in toughness (61% higher than neat PLA) observed in the PLA composites using a 1% CNC loading. In addition, these CNC systems, dispersions and composites demonstrated self-assembly when observed under polarized light. Birefringence patterns were observed in the stationary state and under the influence of shear, indicating a possible nematic phase formation as it was also confirmed by the lack of fingerprint textures, characteristic of cholesteric assemblies, when observed through polarized microscopy. The ability of decylamine modified-CNCs to assemble suggests the presence of well-dispersed crystals due to enhanced interactions with the solvent and with the polymer. This low degree of agglomeration was observed by studying the samples under a polarized microscope.

Higher degrees of agglomeration in the composites, obtained at higher CNC concentrations or incompatible functionalities, produced a significant reduction in toughness. The formation of agglomerates, even for the most compatible modification in this work, caused the nanocomposites to exhibit an optimum reinforcement at a low CNC loading, as is frequently reported in the literature. The addition of low concentrations of CNCs not only increased the toughness of PLA but also maintained the already good tensile strength and modulus. These improvements are promising from an economic perspective because of the low amounts of CNCs and surfactant required for these enhancements. Additionally, PLA was further enhanced by grafting polyacrylic acid (PAA), which provided a stiffer and more hydrophilic surface for the addition of the CNCs and polyethylene glycol. The nanocrystals decreased the toughness of PLA-PAA

copolymer but increased the modulus in this case, an effect that was attributed to an increase in the crystallinity of the polymer upon addition of CNC.

The nanoscale structure of nanocomposites has been shown to play an important role in the determination of their mechanical properties. The orientation of these structures studied through polarized microscopy demonstrated the self-assembly of CNCs in the composites, which was observed to be more prominent for the least agglomerated CNCs and for high concentrations. Similar to the behavior observed in cellulose fibers in nature, the alignment of CNCs was observed to be more randomly distributed in different angles along the extrusion line of the toughened composite.³ This finding is important for understanding the toughening mechanisms of CNC composites. This analysis of films through polarized microscopy, a less intensive method compared to others such as x-ray diffraction, has not been widely used in studying the orientation of CNC composites.

In the second half of this dissertation, liquid and supercritical CO₂ (LCO₂ and SCCO₂) were used for the extraction of fat from rendered poultry meal with the goal of producing a low fat content material. These extractions reduced the fat content to as low as 1.0±0.1% with extraction yields as high as 97%. The extraction curves revealed significantly higher fat solubilities in LCO₂ than in SCCO₂ due to a retrograde phenomenon. The high diffusivities of SCCO₂ had almost no effect on the yields, perhaps because of the small particle size and porosity of the grounded rendered material. These findings are advantageous for the separation of rendered fats at low temperatures and relatively low pressures resulting in higher yields than the screw pressing currently used

in the industry. However, this extraction requires high amounts of CO₂ due to low fat solubilities. This issue was addressed here using the CO₂-assisted mechanical expression, resulting in yields up to 81%, compared to 41% obtained through conventional mechanical separation, and significantly reducing the amount of CO₂ used compared to the LCO₂ extraction.

Recommendations

Recommendations for Future Research

CNC nanocomposites

One of the limiting factors in this research is the tendency of CNCs to form agglomerates even after the addition of surfactants. In recent experiments not included in this work, the research group has shown that these agglomerates in water can be broken by a combination of ultra-sonication, which breaks most of the agglomerates, and precipitation by means of centrifugation, which separates the biggest, unbroken agglomerations. One of the first recommendations for this work is to find the best way to easily break up the agglomerates from the organic suspensions either by sonication and centrifugation. This was one of the limitations of this work since mixing by means of a vortexer for extended periods of time, usually around an hour, were needed to visually reduce the agglomerates. Also, the effect of the agglomerations on the phase behavior in suspension and in nanocomposites of CNCs can be evaluated and compared to this work if better dispersions can be achieved. A better dispersion may provide significantly higher enhancements of the composite toughness and a better assembly of CNCs.

It is important to evaluate the damage that can be caused to the CNCs by sonication in the breaking of agglomerates. This strong process may contribute to the delamination of CNCs, removing the surface-modified layers and exposing more hydroxyl groups. FTIR after sonication and centrifugation can be a good analysis to determine any reduction of the functionality of the carbonyl group on the CNCs, and thus evaluating the CNC susceptibility to sonication.

After mixing CNCs and PLA in a solvent, in this case chloroform, some limitations were encountered in this investigation. First, it was found that excess solvent (~5%) was remaining after drying at ambient pressure for 8-10 h in a vacuum oven at 70 °C. In an effort to reduce the remaining solvent, the films were additionally heated to 120 °C for a 90 min. This produced stiffer films not only due to the lack of solvent but also from a higher crystallization induced by the temperature, resulting in difficulties in the compounding of the composite in the extruder. This high-temperature drying is not frequently found in literature, suggesting that this residual chloroform may not affect significantly the properties of some films. Therefore, it is recommended to dry the films at a slightly higher temperature than the T_g of the polymer and the boiling point of the solvent. Furthermore, sufficient mass of composite has to be prepared (~20 g) since extrusion can have a startup/finishing period that will produce non-uniform films at the beginning and the end of the process. At least 10 films (90 mm x 10 mm) have to be obtained from extrusion since tensile testing of films may exhibit high variability.

For the purpose of further improving the toughness of PLA without reducing tensile strength and modulus, it is recommended to continue the investigation on the PLA-PAA copolymer using various proportions of both PEG and CNCs. Acetylated CNCs may provide the stiffness needed due to enhanced crystallization, while toughness can be significantly increased by the addition of PEG.

Wide-angle X-ray diffraction (WAXD) has been used previously in our research group for the analysis of the nanoscale structure of CNCs in polymers.⁴ It would be interesting to determine the nanocrystal orientation within the films using WAXD and to compare these results to the analysis with polarized microscopy. Similar results may confirm the practical use of microscopy for the determination of the oriented material as it was done in this dissertation. In addition, the further study of the nanoscale structures and their relationship with the increase in toughness (especially after removing agglomerations) seems an important and promising explanation for the toughening mechanism of composites filled with rigid nano-rods.

Another potential enhancement after the addition of CNCs is the reduction of the permeability of PLA as it has been reported in the literature.⁵ Permeability experiments can be performed on nanocomposites to determine if the surface-modified CNCs can improve the gas barrier properties of the films, since the high permeability is one of the disadvantages that need to be addressed in PLA.

Fat separation from rendered materials

On the fat extraction of rendered material using CO₂, it would be interesting to study the effect of supercritical CO₂ on the fat solubility above the crossover point, where no retrograde phenomenon occurs and where CO₂ may be more effective than liquid CO₂ for the fat extractions. The proper design has to be taken in to account to securely reach pressures above 400 bar and temperatures up to 100°C.

It was found in Chapter 5 that a maximum in the fat extraction was reached at all experimental conditions, leaving a minimum fat content of approximately 1%. This fat is likely to be inaccessible by the CO₂ at the conditions studied in this work. The fat could be extracted perhaps with higher diffusivities resulting from the high temperatures and pressures of SCCO₂, such as in the experiment suggested above. This may not be economically viable since it is only 1% of fat but it is interesting from a scientific perspective. Furthermore, it is recommended to do a better analysis on the fat and to determine the free fatty acid concentrations, since they would be expected to have a significantly lower solubility than the fat and could also be the un-extracted material obtained after the CO₂ extractions.

Recommendations for Additional research

An interesting study proposed here as further research involves the preparation of different CNC functionalities and the evaluation of their reinforcement in PLA. For instance, composites with surface-charged CNCs and steric-stabilized CNCs, such as the surfactant modifications used here, can be prepared at increasing concentrations of CNCs

between 1 and 25%. However, the issue becomes that for most surface-charged nanocrystals, the thermal degradation is too low for a melt extrusion of the polymer. There are two options for addressing this concern: solvent casting or solvent spinning of fibers. The solvent-casting method may favor the formation of the percolation network, while the forces involved in the wet spinning may reduce it. These two options and different types of surface-modified CNCs can significantly contribute to the understanding of the reinforcement effect of CNCs in PLA. Furthermore, PLA fibers can be prepared, and the CNC structure and orientation can be studied. It would be interesting to compare fibers and films involving various proportions of the surface-modified nanocrystals. A spiral structure could be formed more easily in fibers than in films, allowing for a greater increase in toughness and further orientation-dependent properties that can be controlled by the fiber-processing parameters.

References

1. Elazzouzi-Hafraoui S, Putaux JL, Heux L. Self-assembling and Chiral Nematic Properties of Organophilic Cellulose Nanocrystals. *Journal of Physical Chemistry B*. Aug 2009;113(32):11069-11075.
2. Kim J, Montero G, Habibi Y, et al. Dispersion of Cellulose Crystallites by Nonionic Surfactants in a Hydrophobic Polymer Matrix. *Polymer Engineering and Science*. Oct 2009;49(10):2054-2061.
3. Barnett J, Bonham VA. Cellulose microfibril angle in the cell wall of wood fibres. *Biological reviews*. 2004;79(2):461-472.
4. Urena-Benavides EE, Kitchens CL. Wide-Angle X-ray Diffraction of Cellulose Nanocrystal-Alginate Nanocomposite Fibers. *Macromolecules*. May 2011;44(9):3478-3484.

5. Fukuzumi H, Saito T, Wata T, Kumamoto Y, Isogai A. Transparent and High Gas Barrier Films of Cellulose Nanofibers Prepared by TEMPO-Mediated Oxidation. *Biomacromolecules*. Jan 2009;10(1):162-165.

APPENDICES

Appendix A

Additional Polarized Microscopy Images

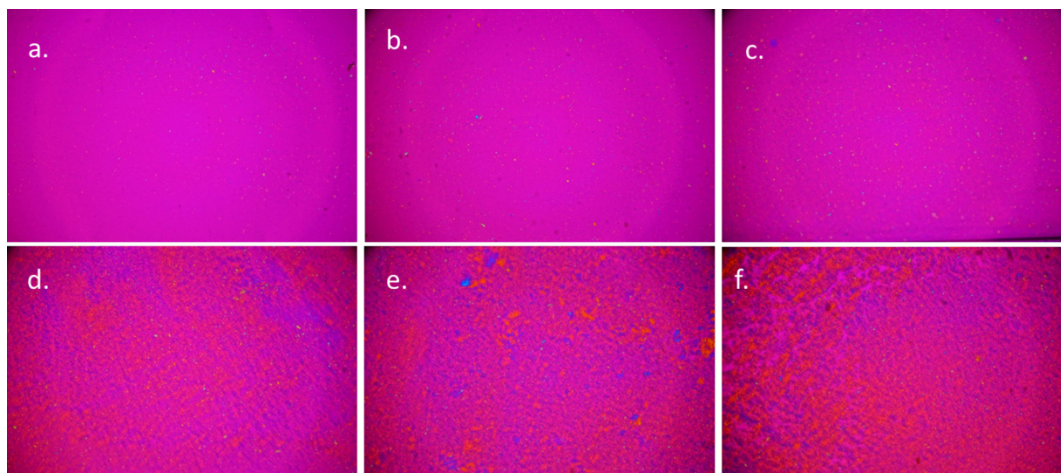


Figure A.1. Polarized Microscopy of CNC-AA-DA suspensions in THF at different concentrations: a) 0.5%, b) 1%, c) 2%, d) 3%, e) 4%, f) 5%.

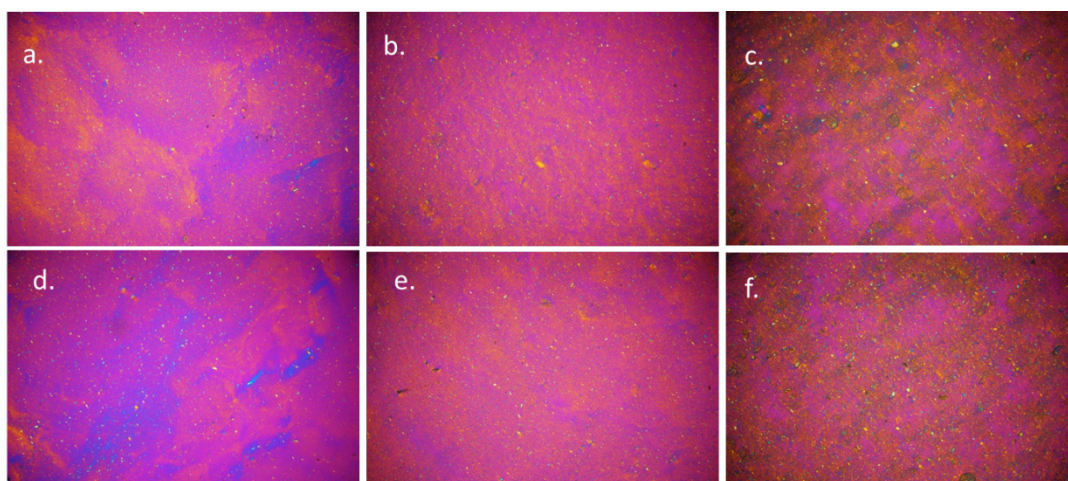


Figure A.2. Polarized Microscopy of dried CNC films over glass slides. Top micrographs: Plain CNC-AA; bottom micrographs: CNC-AA using surfactant. Solvents: (a and d) THF; (b and e) Ethyl acetate; (c and f) chloroform.

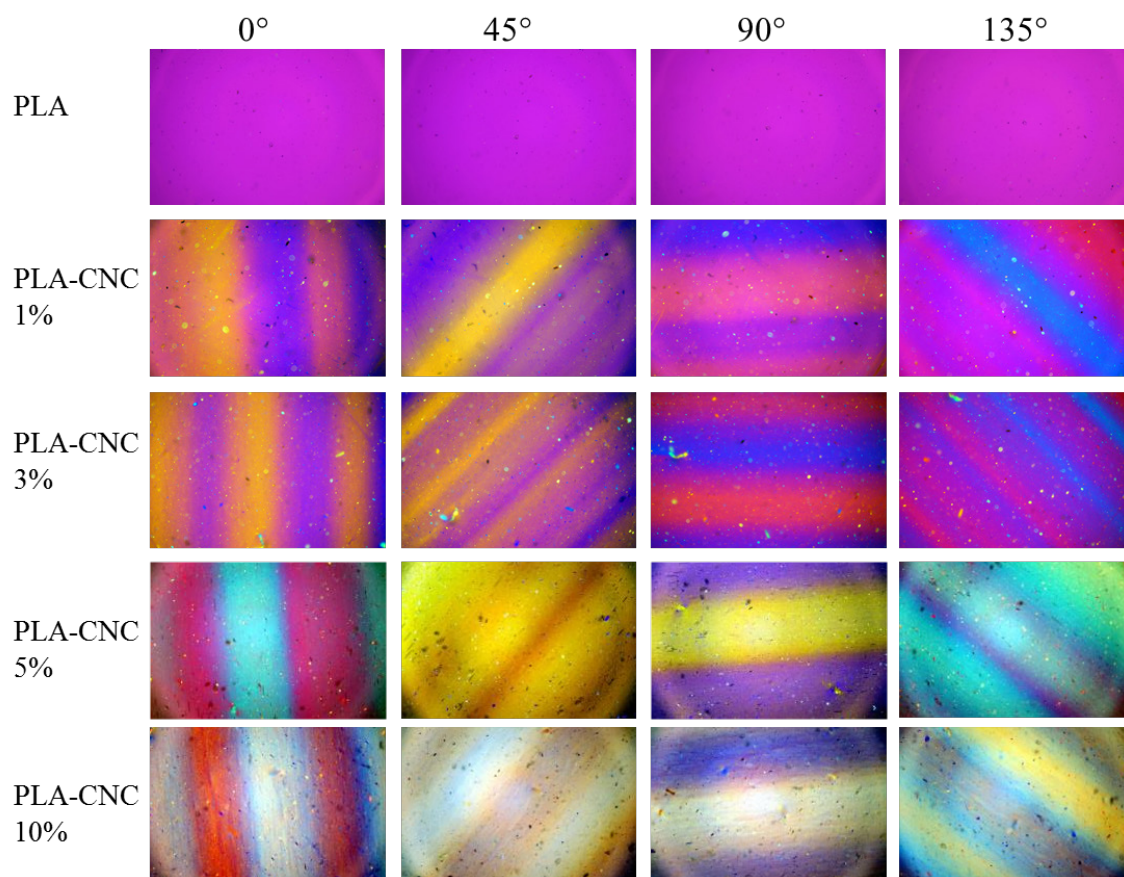


Figure A.3. Polarized microscopy of PLA-CNC-DA films at different CNC loads using a first order red plate (5% and 10% were not presented in Chapter 3)

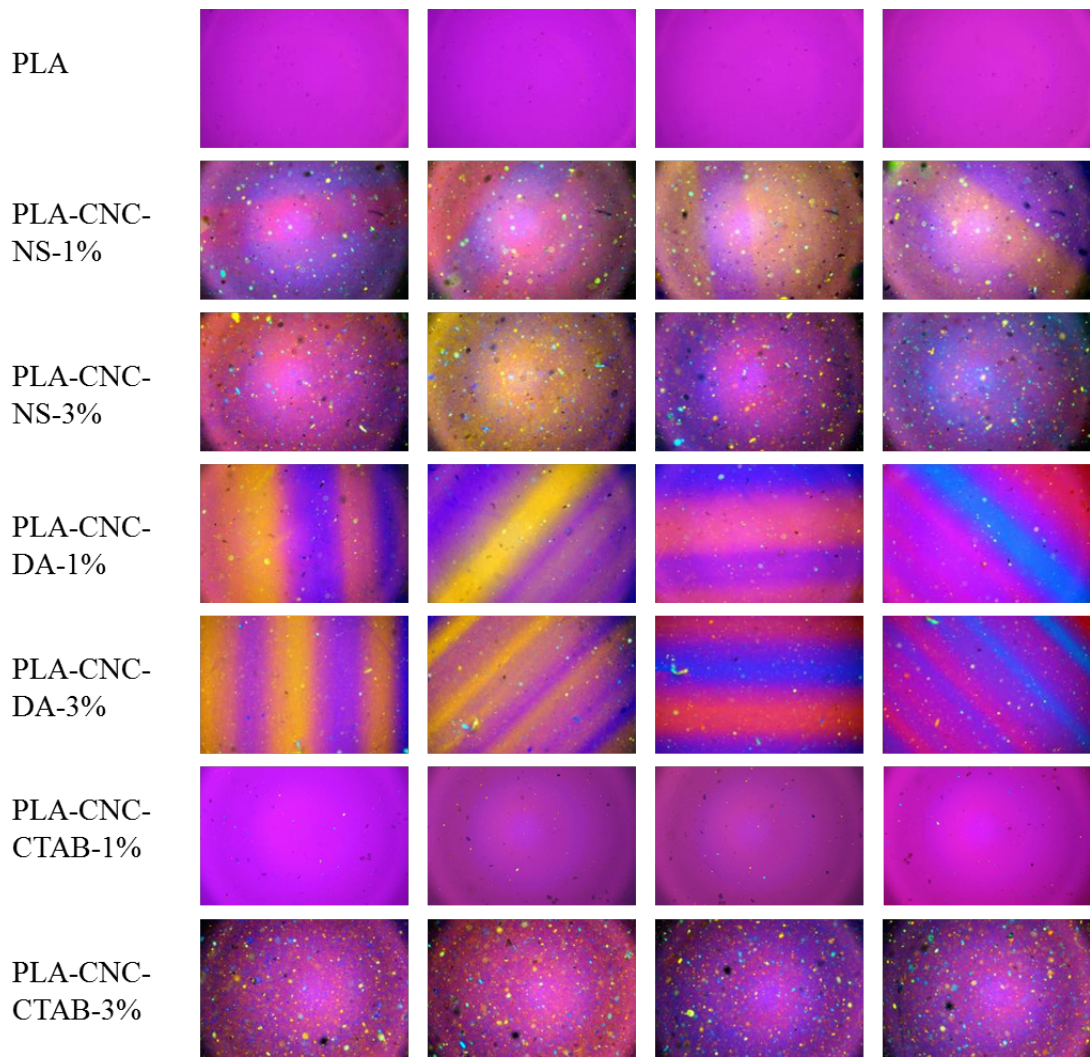


Figure A.4. Polarized microscopy of PLA-CNC films with and without surfactant at 1 and 3% CNC loads using a first order red plate

Appendix B

Experimental Methods

B.1 Detailed synthesis procedure for CNC-AA and CNC-HCl

Preconditioning of Cellulose

- Soak 15 grams of cotton ashless powder/filter clippings in a round-bottom flask overnight in either 337.5 milliliters (mL) of acetic acid to form CNC-AA or in 200 milliliters (mL) of deionized (DI) water to prepare CNC-HCl
- Prepare the set-up as observed in Figure B.1. Attach a reflux column to the round-bottom flask with the soaked cellulose with a previously placed stir bar. Connect a temperature controller to a heating mantle to keep a constant temperature (ensure heating mantle is not yet plugged in until reaction begins). Position a stirring plate (≥ 750 rpm) under the heating mantle.

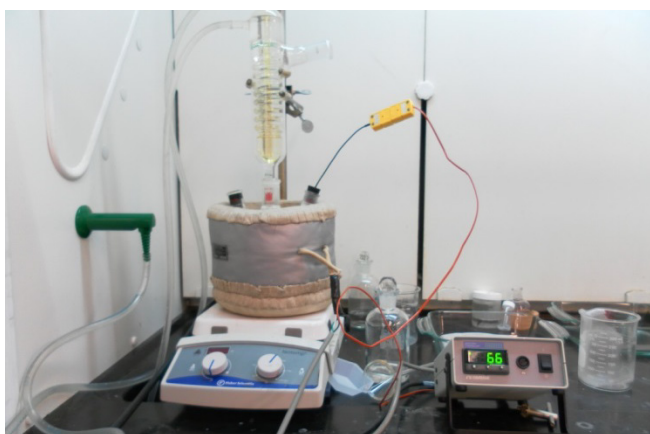


Figure B.1. Set-up for the synthesis of CNC-HCl and CNC-AA

Reaction of CNC-AA

- Add 36.75 mL of DI water and 1.2 mL of 36-38% HCl
- Heat the mixture in the heating mantel at 105 °C for 10 hours

Reaction of CNC-OH

- Add 53 mL of 36% HCl to the cellulose (previously soaked in DI water) to obtain an HCl concentration of 2.5 M
- Heat the mixture at 103 °C for 60 minutes

Both Reactions

- Cool the mixture after reaction in an ice bath for 15 minutes
- Pour the mixture into centrifuge tubes (~30 mL per tube)
- Centrifuge at 8,600 rpm for 3 minutes and after collecting the precipitate pour remaining acid liquid into a container for posterior treatment
- Pour DI water (~30 mL) into tubes and mix thoroughly in vortex to wash
- Centrifuge and wash two more times, adding only 10 mL of water for last wash
- Combine the suspensions in a plastic beaker
- Sonicate for 35 minutes at a power of ~7.5-8.0 (7 minute pulse, 2 minute rest, 5 cycles)
- Add water in order to approximately double the volume and do two more washes; in the third wash (possibly the second wash if supernatant is observed) recover the supernatant after centrifugation (8,600 rpm for 3 minutes)

- Add more water and repeat the process until no supernatant can be recovered (3 or 4 times)
- Combine supernatant and evaporate water if desired to increase the CNC concentration
- Measure the concentration of the CNC water suspension using weighting plates
 - a. Place 3-5 mL of sample onto weighing boats/vessels
 - b. Weigh empty vessels and vessels with sample and record results
 - c. Vacuum dry and then weigh vessel with dry cellulose sample
 - d. Calculate CNC concentration and record results

B.2 Procedure for Polarized Optical Microscopy Olympus Light Microscope BX60

1. Turn on the microscope light using the switch on the machine behind the microscope, ensuring that the switch is flipped so light source is below platform and light is at full (12) power.

4. Take lens cap off the microscope and fully rotate the ring (A) counter-clockwise. Adjust the focus using the rotating handles (B) until a hexagon is clearly outlined when looking through the eye pieces (C).

5. Center the hexagon that is observed through the eye piece (C) using the metallic screws D and E.

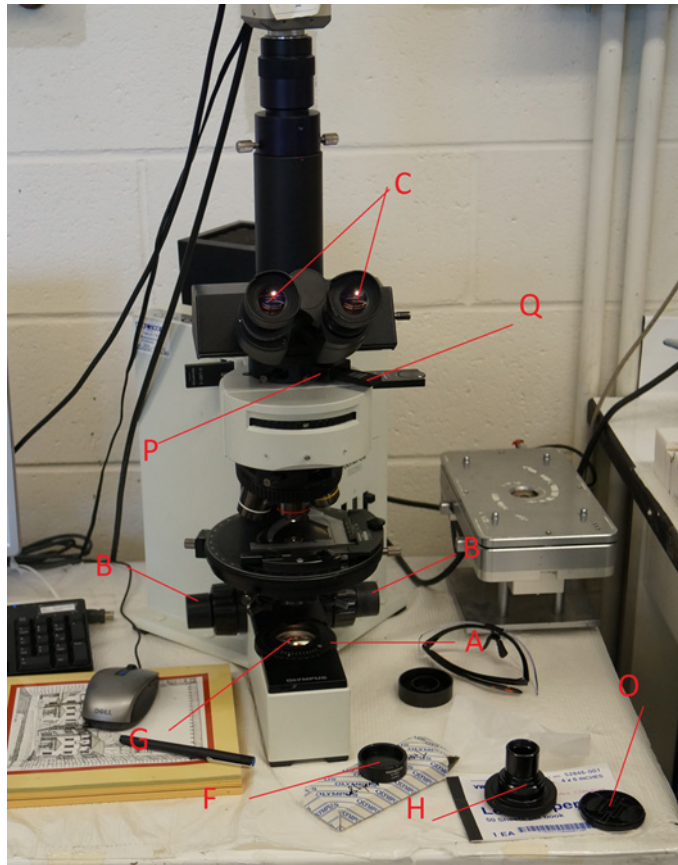


Figure B.2. Polarized microscope parts

6. Open the ring A clockwise so that the entire field of view is filled with light – the hexagon encompasses the entire view through the eyepiece (C)

7. Place the polarizer (Olympus U-POT) (F) on the lens of the light source (G) and the analyzer (U-ANT) (P) in the position indicated in Figure B.2. Rotate the polarizer until the field of view becomes dark (extinction position). For the study of the specific liquid crystal orientations insert the first order red plate (530 nm U-TP530) within the analyzer holder.

8. If using an external camera (DSLR) to obtain the polarized images follow this procedure. Remove the lens from the DSLR camera and connect the adaptor (H) for the Sony alpha 55 camera. Remove eye pieces from the microscope and place the camera on the left eyepiece socket. Usually, a single microscope slide does not provide enough distance for focusing in the sample. To address this, place two blank, clean slides on platform with the mechanism (I) in Figure 3, and then place sample slide on top of them.

10. Focus on the sample carefully without letting the lens touch the glass slide. Adjust shutter speed, magnification and ISO of camera to acquire picture of sample. Automatic mode may not adjust the right light level for the polarized images.

11. Move the sample using the screws J and K. The stage can be rotated every 45° to observed the liquid crystals at different angles. Make sure the stage is centered before this step by adjusting the metallic screws L and M and rotating the sample so that the center of rotation is on the center of the field of view.

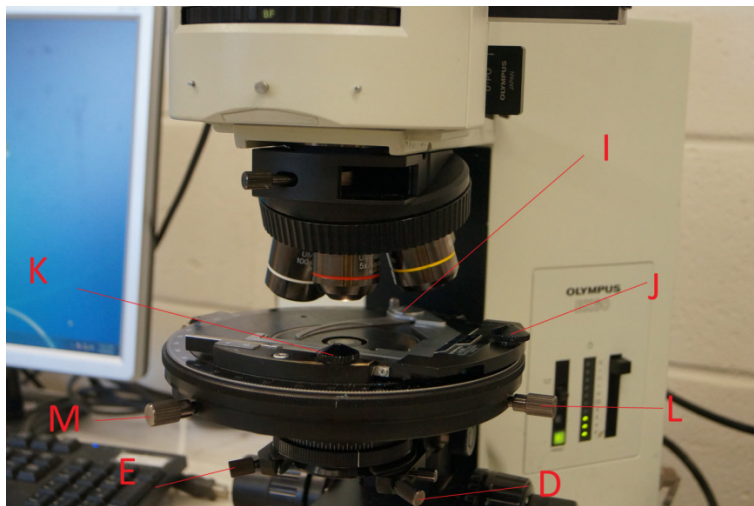


Figure B.3. Rotating stage of polarized microscope

12. At the end of the observations, remove slides from platform and lower stage using the focusing knobs (B). Place polarizer (F) and lens adapter (H) back into drawer (N). Make sure that the analyzer is out of the slot. Turn off microscope, place cover back on entire instrument, and sign out with the proper exit time


Notes

- Remember to record all results using the number of picture taken with the camera
- Use lens paper (VHR Scientific Products, Cat. No. 52846-001, Size: 4 x 6 inches) (O) to clean any dusty slides or lenses
- Use proper petri dishes (R) to hold micro-slides to avoid dust accumulation.

B.3 Image analysis of liquid crystal structures

Image analysis was used to quantify the colors in the PLA-CNC composite films when observed through the polarized-light microscope. The analysis used in this dissertation and described in this appendix is based on the software Photoshop; however, other software can such as GIMP (free and open source) and ImagePro Plus can also be used. The procedure consists in two main steps, an image correction and the quantification of colors, and this is described below.

1. Image levels adjustment. This manipulation corrects the tonal range and color balance of an image by adjusting intensity levels of image shadows, midtones, and highlights. Open Photoshop and open the picture that is to be analyzed.

2. Select the region of interest with the marquee tool  from the tool bar as shown in Figure B.2.

3. Click on Image→Adjustments → Levels or Ctrl+L. A dialogue box as in Figure B.2 will appear and click on “Auto” and then “OK”. The levels of the selected area should now be adjusted (Figure 3)

4. Quantifying color. First, the total number of pixels on the selected area has to be counted. Click on Window → Histogram. A window with information including the total number of pixels of the area will appear. Record the pixels.

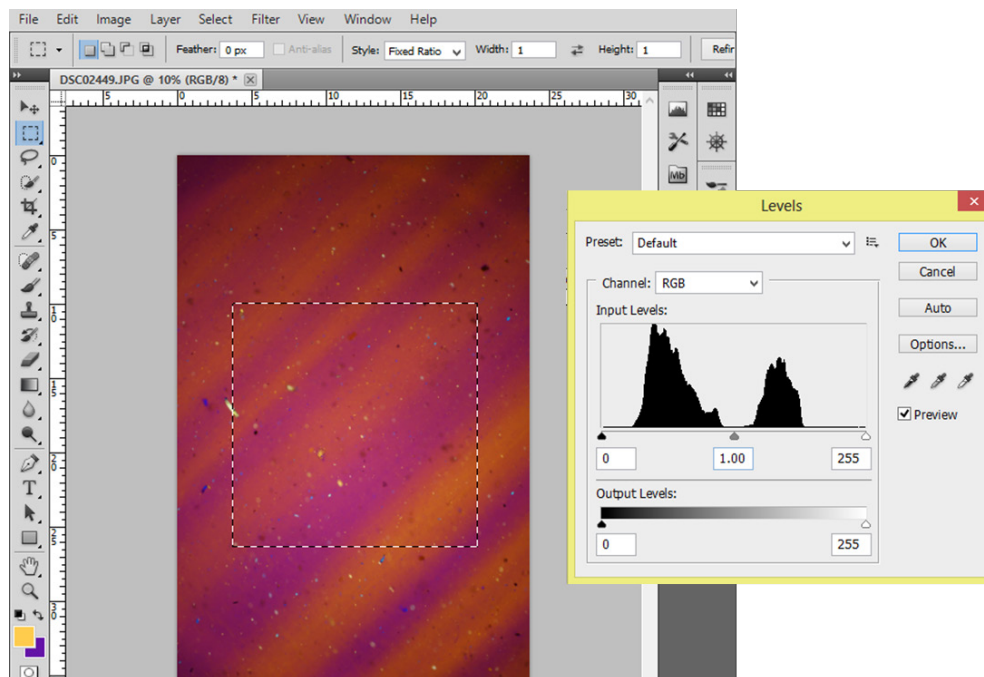


Figure B.4. Screenshot of selected area for image analysis of films and window to adjust the color levels.

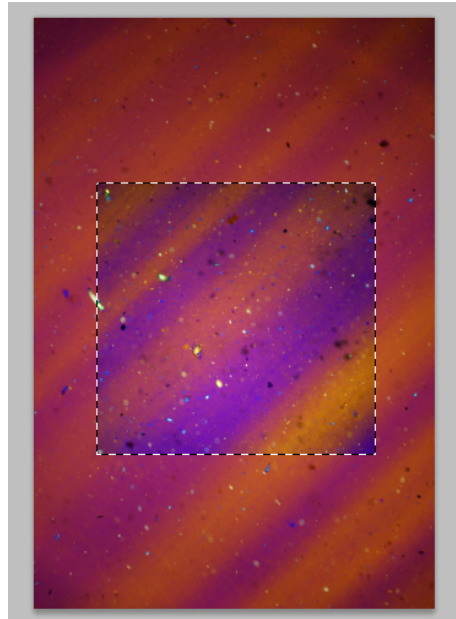



Figure B.5. Selected area with the level adjusted automatically.

5. To count the colored pixels click on Select→Color Range. On the dialogue box (Figure 4) select the specific color to be quantified (e.g. Magentas) and then click “OK”.

6. Open the Histogram window again and refresh the information with the icon: . Record the count of pixels of that specific color and divide this value by the total pixels recorded earlier to determine to the percentage of the area.

7. For easier manipulation, click on Edit → Undo color range. Repeat step 5 and 6 for another color and determine the percentage.

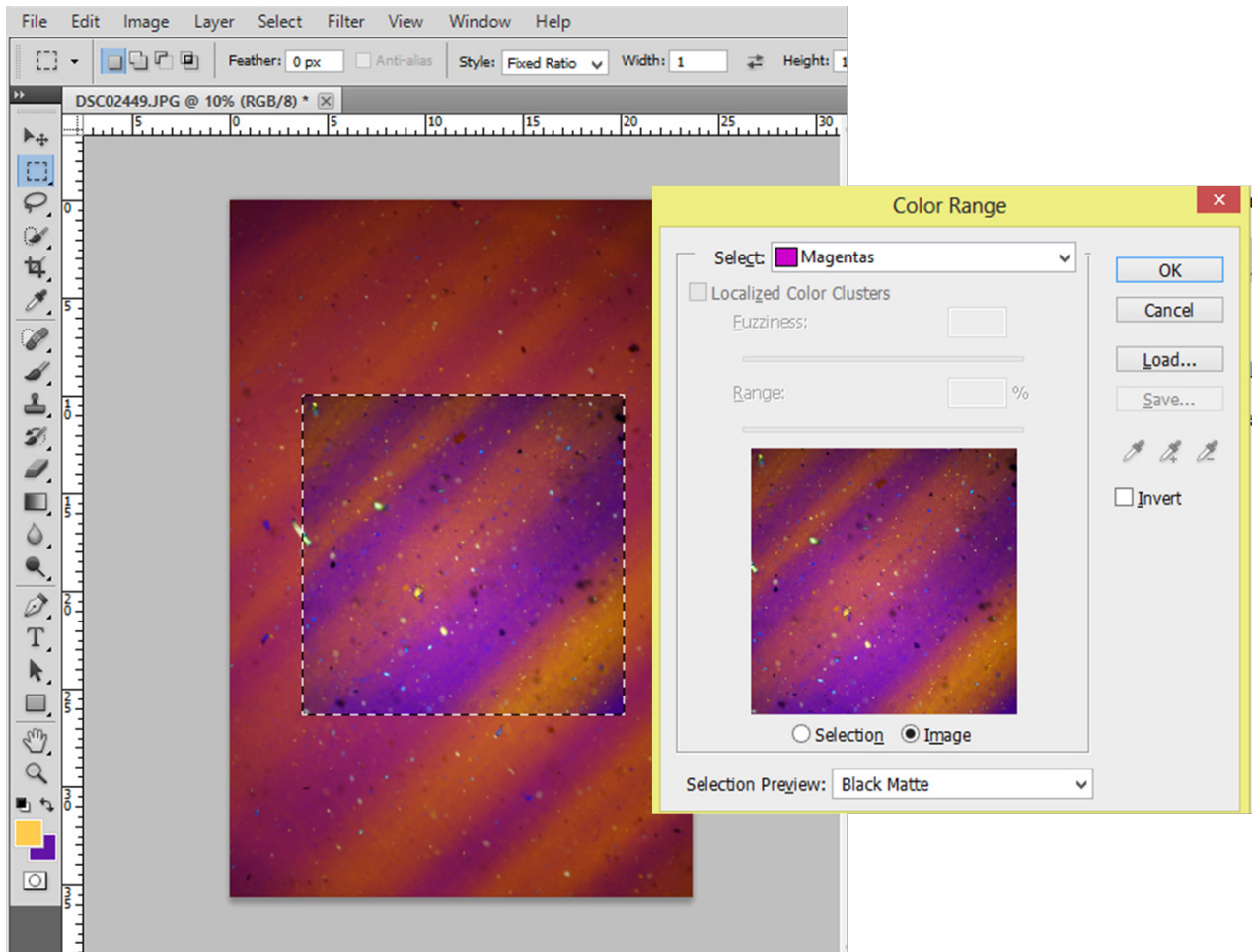


Figure B.6. Screenshot of the color range selection window.

8. Alternatively for step 5, the colors to be analyzed can be picked from the image with the “sampled colors” option from the drop-down list. After this, go to step 6 to obtain the pixels.

B.4 Spin Coating with Round Silicon Wafers

Piranha pretreating: Be sure to wear heavy gloves, safety glasses, lab coat, and perform all steps under a working hood. Piranha solution is extremely corrosive and releases fumes.

1. Make a piranha solution of 7:3 of sulfuric acid and hydrogen peroxide, respectively. Place this in a glass container that can accommodate the wafer to be coated.

2. Place the wafer in the piranha solution. Sonicate for 30 min at about 70 °C in water. Remove the wafers from the piranha with metal tweezers. If modifying the wafer with an amine, go to step 3. Rinse liberally with deionized water and then dry with nitrogen. Place in clean, dry disposable petri dish.

3. If coating with an amine, rinse with deionized water followed by drying with nitrogen. Soak in 2% amine solution in ethanol (reagent alcohol used in our case) for about 10-20 minutes. Rinse further with ethanol to remove excess amine. Dry with nitrogen and place in plastic petri dish.

On the Computer:

4. Open the software on the computer program Spin3000. Check to make sure the computer and the spin coater are connected. Refresh the program to view all programs. To make a new one, fill in proper velocity, time, and acceleration into the spreadsheet and save new program. Then refresh the program to move from the computer to the spin

coater. Note that the acceleration should be equal to the difference between initial speed and final speed. Usually start with 10 s at 300 rpm followed by 30 seconds at 600 rpm.

On the Spin Coater:

5. Press the “Process/Select” button. Then highlight the program desired and press “run mode”.

6. Check the highlighted status bar. (“CDA” = clean dry air) Turn on the vacuum switch behind the machine but do not run the vacuum in the spin coater yet. Turn on the nitrogen supply.

7. Place the wafer so that it is as close to the center as possible. Close the lid making sure it is latched.

8. Activate the “Vacuum” button on the machine.

9. Using a clean pipette, place the amount of CNC suspension desired for spin coating.

10. Push the green “Start” button and the spin coater will start. Once finished, remove wafer.

Drying Procedure:

11. Place wafers on a paper towel in the vacuum oven and heat at 100-120 °C with and 25 inHg. Leave for 30 minutes to 1 hour depending on prior moisture of the wafers. Remove and let cool before placing in a disposable, clean plastic petri dish.

Appendix C

Extraction of other rendered materials and characterization

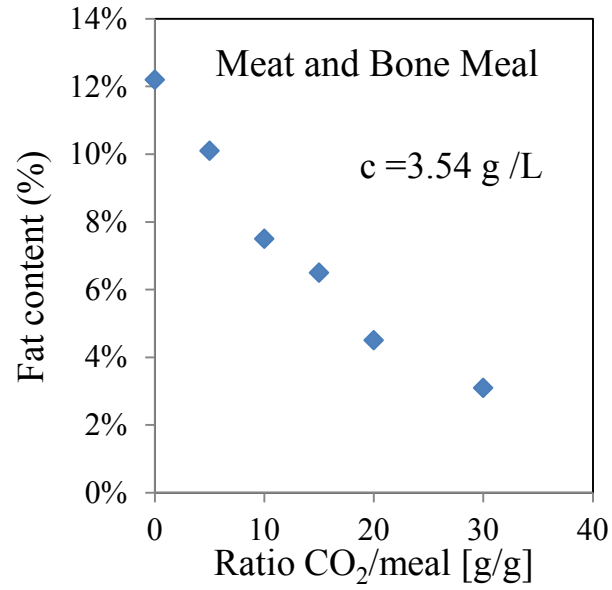


Figure C.1. Fat content in meat and bone meal after CO₂ extractions (c=solubility)

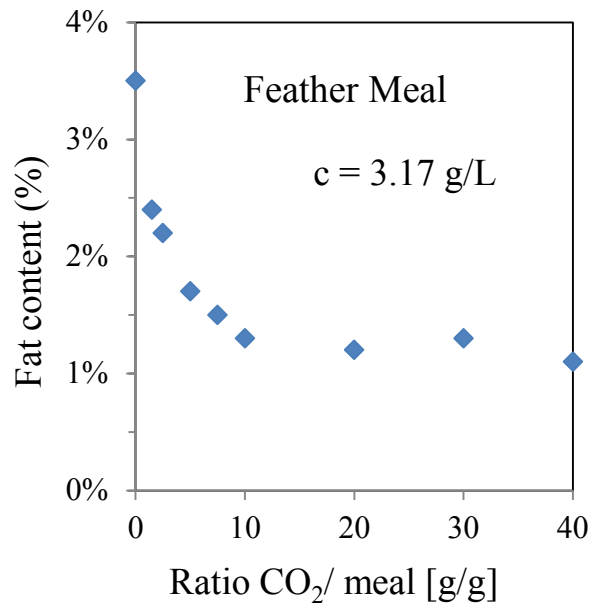


Figure C.2. Fat content in feather meal after CO₂ extractions (c=solubility)

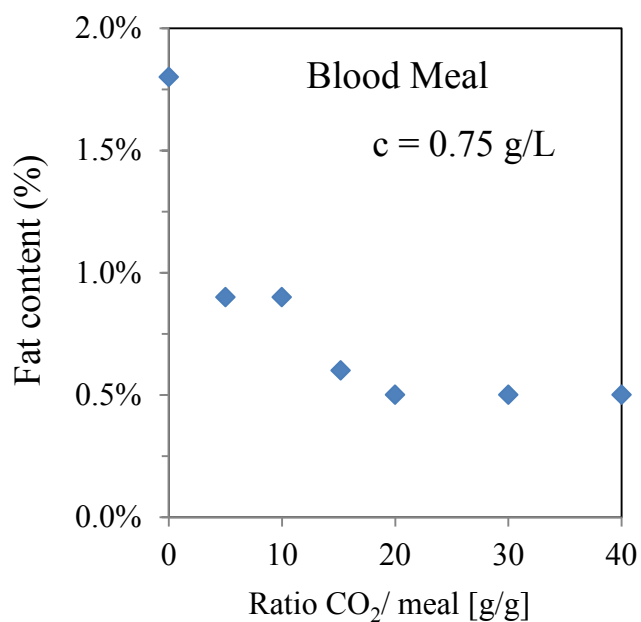


Figure C.3. Fat content in blood meal after CO₂ extractions (c=solubility)

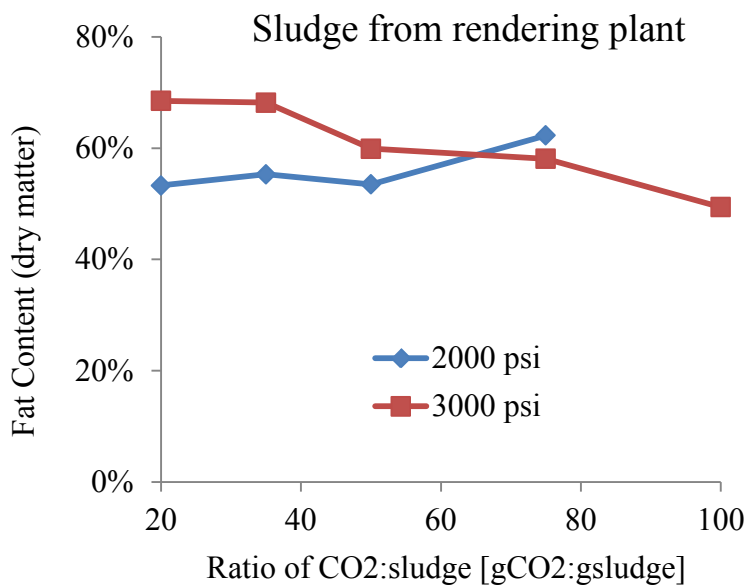


Figure C.4. Fat content in sludge after CO₂ extractions at different pressures

Characterization of Rendered Materials

Table C.1. Rendered Materials Composition

As-sampled	Fat	Protein	Ash	Moisture	Total
Poultry Meal	13.6	65.9	11	7.4	97.9
Plain Prime Poultry	11.9	66.6	10.7	6.4	95.6
Plain Poultry Meal low ash	13.2	69.1	8.2	6.9	97.4
Meat and bone meal	8.4	52.3	28.8	6.6	96.1

Table C.2. Sludge Composition

Sludge sample	Fat	Protein	Ash	Moisture	Total
Sample 1	36.6	3.6	0.8	58.7	99.7
Sample 2	39.9	6.4	0.4	52.2	98.9
Sample 3	29.2	6.4	2	61.8	99.4

Table C.3. Extracted Rendered Materials Composition

Extracted RM	Fat	Protein	Ash	Moisture	Total
CO₂ poultry meal	0.9	77.3	13.5	-	91.7
Hexane poultry meal	0.1	75.8	12.7	-	88.6

Appendix D

Phase behavior of CNC-HCl and CNC-AA in water

Determination of phase concentrations by UV-Vis Spectrometer

Ultraviolet-Visible Spectrophotometer (UV-Vis) was used to determine the concentrations of the top phases of suspensions of CNC-AA and CNC-HCl since they presented too low concentrations to be determined by gravimetric methods. First, a calibration curve was prepared with known low concentrations of both types of CNC in water. The range of wavelength examined was between 650 nm to 350 nm and the absorbance of each sample was taken at a wavelength of 500nm. The concentrations were obtained by using the regressed equation obtained from the calibration curve.

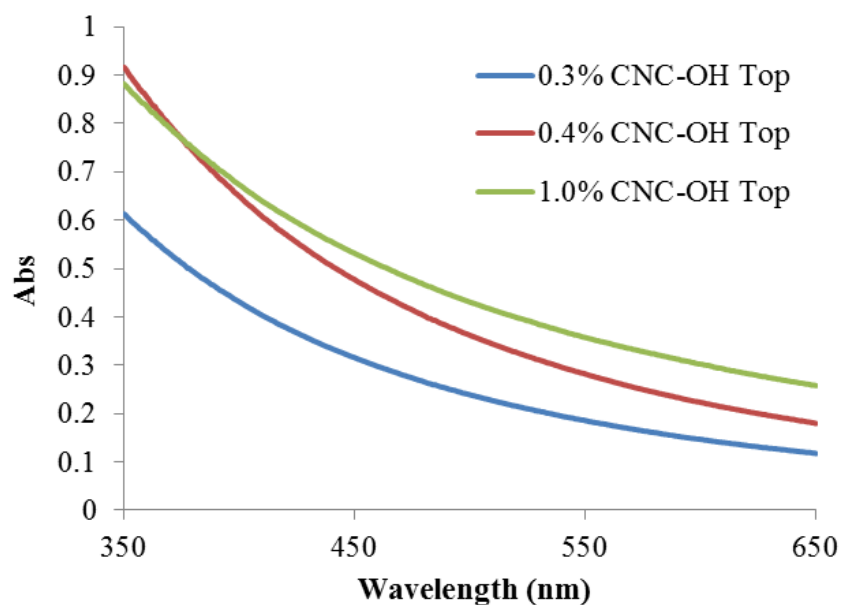


Figure D.1. Example of the absorbance of CNC-OH suspensions

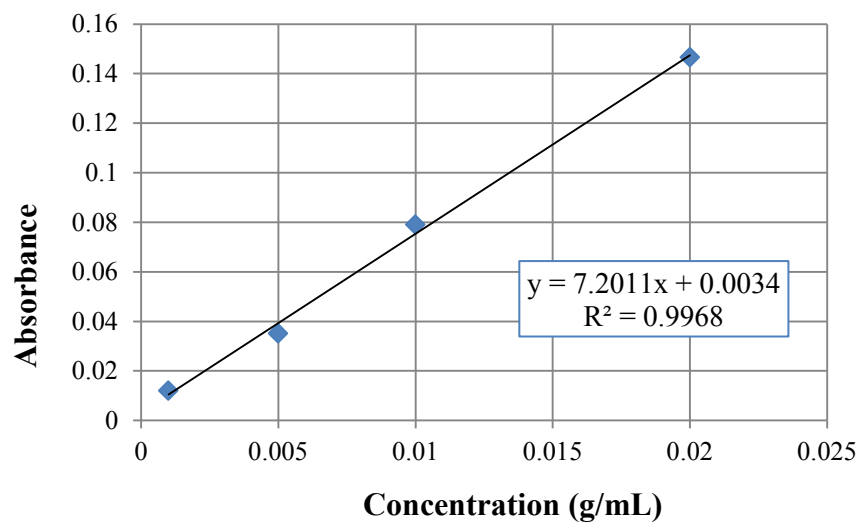


Figure D.2. Calibration curve for CNC-OH suspensions at low concentrations.

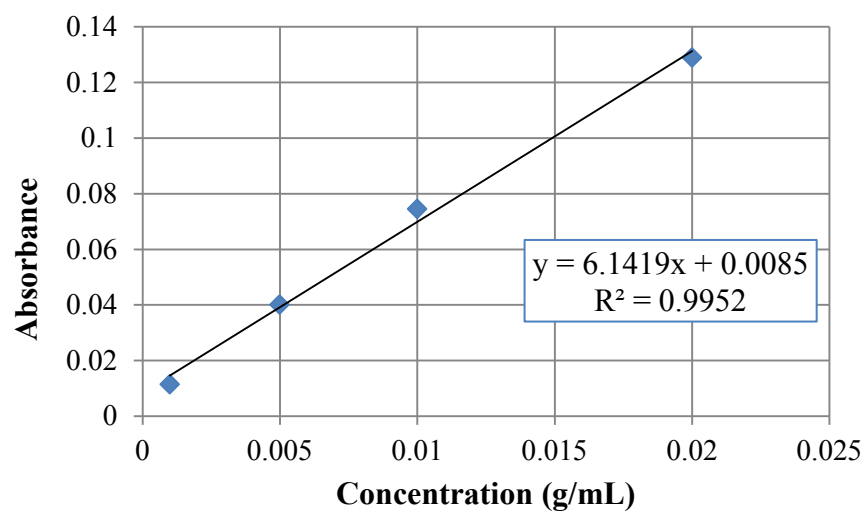


Figure D.3. Calibration curve for CNC-AA suspensions at low concentrations.

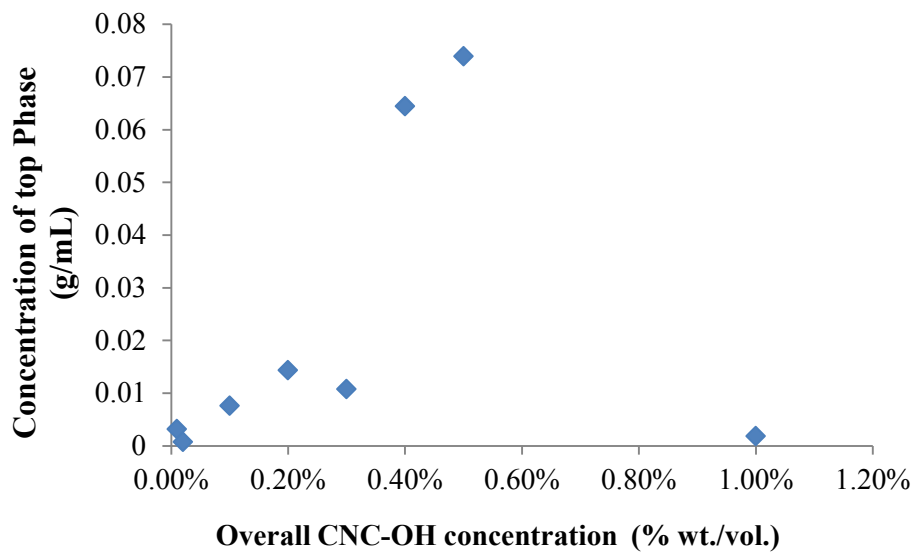


Figure D.4. Concentration of the top phase of phase separated CNC-OH suspensions.

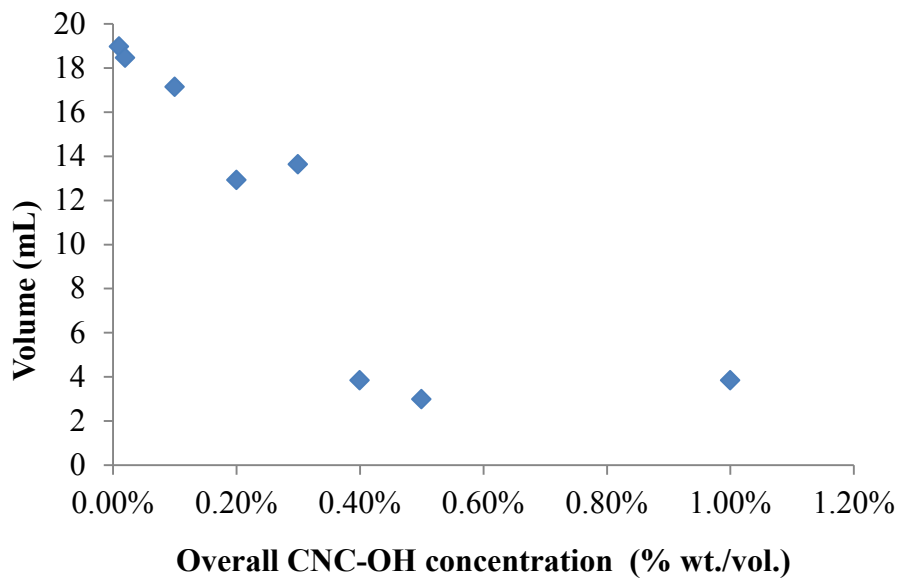


Figure D.8. Top phase volume of various CNC-OH suspensions.

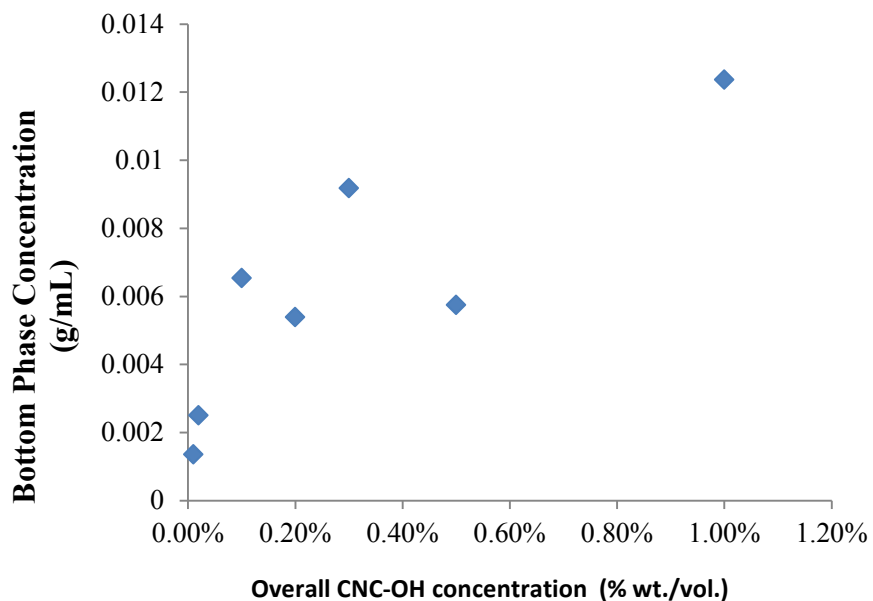


Figure D.5. Concentration of the bottom phase of various CNC-OH suspensions obtained based on the top concentration and the separated bottom phase volume at each concentration.

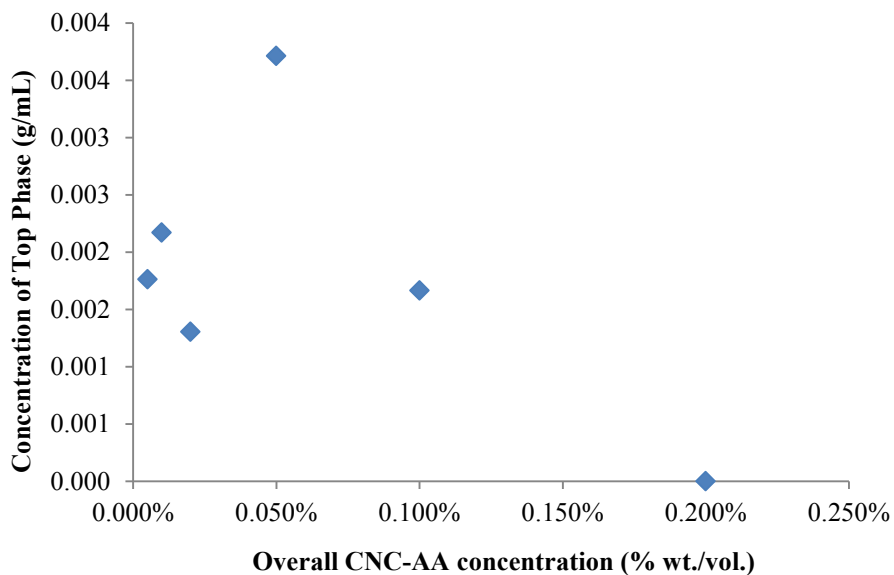


Figure D.6. Concentration of the top phase of phase separated CNC-AA suspensions.

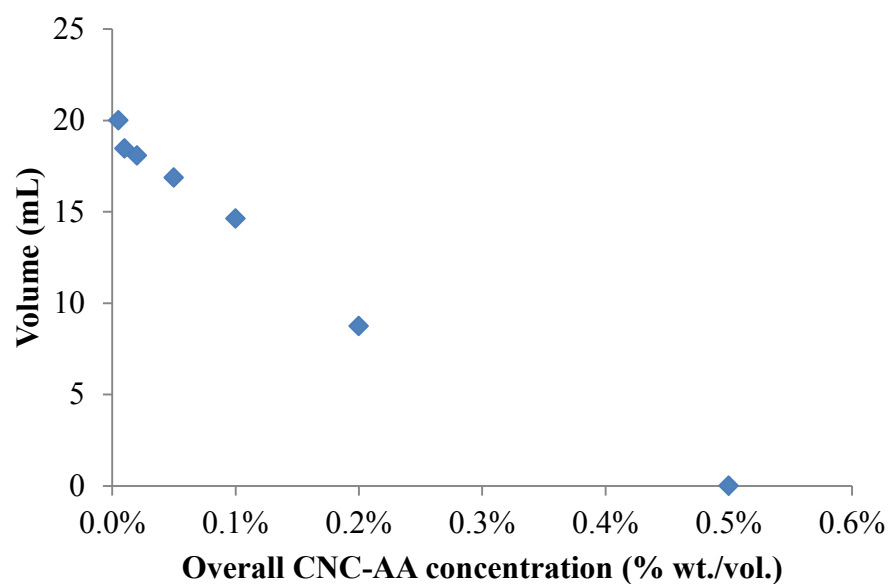


Figure D.9. Top phase volume of various CNC-AA suspensions.

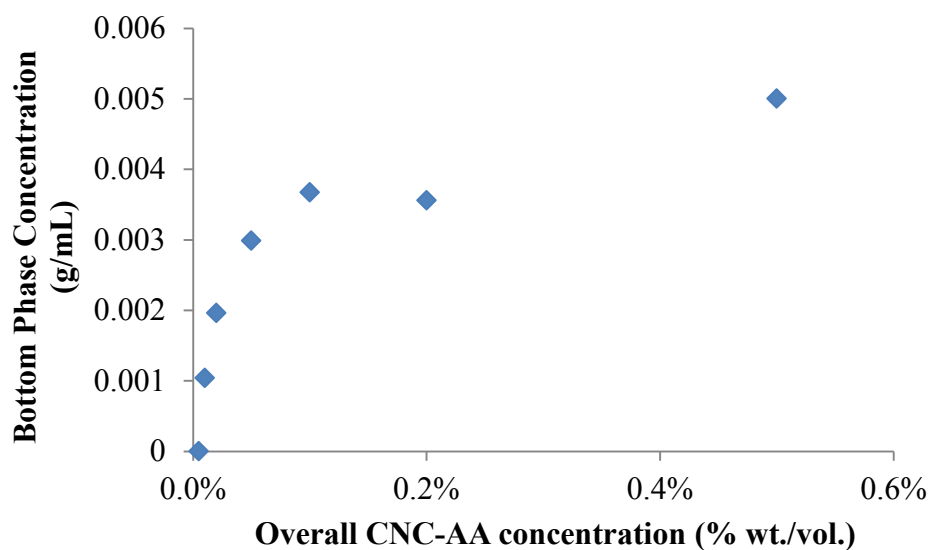


Figure D.7. Concentration of the bottom phase of various CNC-AA suspensions obtained based on the top concentration and the separated bottom phase volume at each concentration.

CNC films preparation over silicon wafers

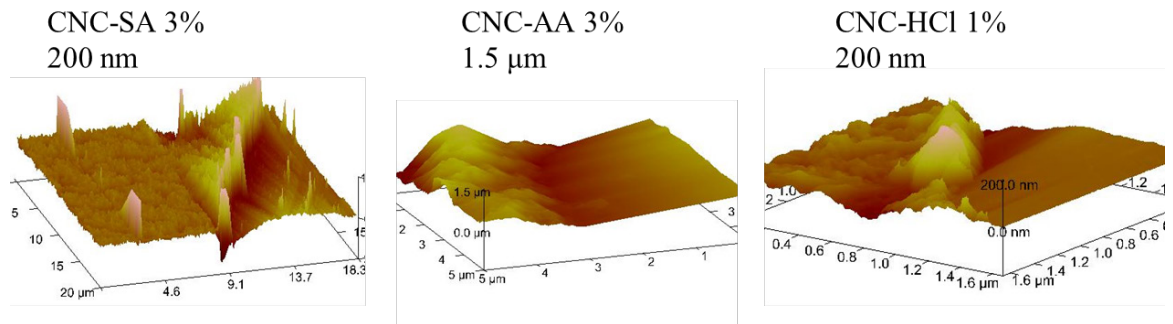


Figure D.10. Atomic force microscopy of CNC-SA, CNC-AA and CNC-OH films over silicon wafers.

Appendix E

Permissions

ELSEVIER LICENSE
TERMS AND CONDITIONS

Jun 06, 2013

This is a License Agreement between Jose L Orellana ("You") and Elsevier ("Elsevier") provided by Copyright Clearance Center ("CCC"). The license consists of your order details, the terms and conditions provided by Elsevier, and the payment terms and conditions.

All payments must be made in full to CCC. For payment instructions, please see information listed at the bottom of this form.

Supplier	Elsevier Limited The Boulevard, Langford Lane Kidlington, Oxford, OX5 1GB, UK
Registered Company Number	1982084
Customer name	Jose L Orellana
License number	3163250867266
License date	Jun 06, 2013
Licensed content publisher	Elsevier
Licensed content Publication	Carbohydrate Polymers
Licensed content Title	Microfibrillated cellulose – Its barrier properties and applications in cellulosic materials: A review
Licensed content author	Nathalie Lavoine, Isabelle Desloges, Alain Dufresne, Julien Bras
Licensed content Date	1 October 2012

Licensed content
Volume 90 number

Licensed content
Issue 2 number

Number of pages 30

Start Page 735

End Page 764

Type of Use reuse in a thesis/dissertation

Portion figures/tables/illustrations

Number of
figures/tables/illustrations 1

Format both print and electronic

Are you the author of this Elsevier article? No

Will you be translating? No

Order reference number

Title of your thesis/dissertation

BIO-BASED ADVANCED MATERIALS FROM RENEW ABLE RESOURCES: AN INVESTIGATION ON CELLULOSE NANOCRYSTAL COMPOSITES AND CO2 EXTRACTION OF RENDERED MATERIALS

Expected completion date Aug 2013

Estimated size (number of pages) 160

Elsevier VAT number GB 494 6272 12

Permissions price 0.00 USD
VAT/Local Sales Tax 0.0 USD / 0.0 GBP

Total 0.00 USD

**SPRINGER LICENSE
TERMS AND CONDITIONS**

Jul 25, 2013

This is a License Agreement between Jose L Orellana ("You") and Springer ("Springer") provided by Copyright Clearance Center ("CCC"). The license consists of your order details, the terms and conditions provided by Springer, and the payment terms and conditions.

All payments must be made in full to CCC. For payment instructions, please see information listed at the bottom of this form.

License Number	3196070032583
License date	Jul 25, 2013
Licensed content publisher	Springer
Licensed content publication	Cellulose
Licensed content title	Grafting onto microfibrils of native cellulose
Licensed content author	Elsa Lasseguette
Licensed content date	Jan 1, 2008
Volume number	15
Issue number	4
Type of Use	Thesis/Dissertation
Portion	Figures
Author of this Springer article	No
Order reference number	
Title of your thesis / dissertation	BIO-BASED ADVANCED MATERIALS FROM RENEWABLE RESOURCES: AN INVESTIGATION ON CELLULOSE NANOCRYSTAL COMPOSITES AND CO2 EXTRACTION OF RENDERED MATERIALS
Expected completion date	Aug 2013
Estimated size(pages)	160
Total	0.00 USD
Terms and Conditions	

Introduction

The publisher for this copyrighted material is Springer Science + Business Media. By clicking "accept" in connection with completing this licensing transaction, you agree that the following terms and conditions apply to this transaction (along with the Billing and Payment terms and conditions established by Copyright Clearance Center, Inc. ("CCC"), at the time that you opened your Rightslink account and that are available at <http://myaccount.copyright.com>).

Limited License

With reference to your request to reprint in your thesis material on which Springer Science and Business Media control the copyright, permission is granted, free of charge, for the use indicated in your enquiry.

Licenses are for one-time use only with a maximum distribution equal to the number that you identified in the licensing process.

This License includes use in an electronic form, provided its password protected or on the university's intranet or repository, including UMI (according to the definition at the Sherpa website: <http://www.sherpa.ac.uk/romeo/>). For any other electronic use, please contact Springer at (permissions.dordrecht@springer.com or permissions.heidelberg@springer.com).

The material can only be used for the purpose of defending your thesis, and with a maximum of 100 extra copies in paper.

Although Springer holds copyright to the material and is entitled to negotiate on rights, this license is only valid, subject to a courtesy information to the author (address is given with the article/chapter) and provided it concerns original material which does not carry references to other sources (if material in question appears with credit to another source, authorization from that source is required as well).

Permission free of charge on this occasion does not prejudice any rights we might have to charge for reproduction of our copyrighted material in the future.

Altering/Modifying Material: Not Permitted

You may not alter or modify the material in any manner. Abbreviations, additions, deletions and/or any other alterations shall be made only with prior written authorization of the author(s) and/or Springer Science + Business Media. (Please contact Springer at (permissions.dordrecht@springer.com or permissions.heidelberg@springer.com))

Reservation of Rights

Springer Science + Business Media reserves all rights not specifically granted in the combination of (i) the license details provided by you and accepted in the course of this licensing transaction, (ii) these terms and conditions and (iii) CCC's Billing and Payment terms and conditions.

Copyright Notice:Disclaimer

You must include the following copyright and permission notice in connection with any reproduction of the licensed material: "Springer and the original publisher /journal title, volume, year of publication, page, chapter/article title, name(s) of author(s), figure number(s), original copyright notice) is given to the publication in which the material was originally published, by adding: with kind permission from Springer Science and Business Media"

Warranties: None

Example 1: Springer Science + Business Media makes no representations or warranties with respect to the licensed material.



Title: Phase Behavior and Rheology of SW NTs in Superacids

Author: Virginia A. Davis et al.

Publication: Macromolecules

Publisher: American Chemical Society

Date: Jan 1, 2004

Copyright © 2004, American Chemical Society

Logged in as: Jose Orellana

Account #: 3000664641

PERMISSION/LICENSE IS GRANTED FOR YOUR ORDER AT NO CHARGE

- This type of permission/license, instead of the standard Terms & Conditions, is sent to you because no fee is being charged for your order. Please note the following:
- Permission is granted for your request in both print and electronic formats, and translations. If figures and/or tables were requested, they may be adapted or used in part.
- Please print this page for your records and send a copy of it to your publisher/graduate school. Appropriate credit for the requested material should be given as follows: "Reprinted (adapted) with permission from (COMPLETE REFERENCE CITATION). Copyright (YEAR) American Chemical Society." Insert appropriate information in place of the capitalized words.
- One-time permission is granted only for the use specified in your request. No additional uses are granted (such as derivative works or other editions). For any other uses, please submit a new request.



RightsLink®

Home

Account Info

Help



**Molecular Crystals and
Liquid Crystals**

Title: Cellulose Nanocrystal Reinforced Alginate Fibers—Biomimicry Meets Polymer Processing
Author: Esteban E. Ureña-Benavides, Christopher L. Kitchens
Publication: Molecular Crystals and Liquid Crystals
Publisher: Taylor & Francis
Date: May 3, 2012
Copyright © 2012 Taylor & Francis

Logged in as:

Jose Orellana

Account #:
3000664641

LOGOUT

Thesis/Dissertation Reuse Request

Taylor & Francis is pleased to offer reuses of its content for a thesis or dissertation free of charge contingent on resubmission of permission request if work is published.

BACK

CLOSE WINDOW

Copyright © 2013 [Copyright Clearance Center, Inc.](#) All Rights Reserved. [Privacy statement.](#) Comments? We would like to hear from you. E-mail us at customer@copyright.com

ELSEVIER LICENSE TERMS AND CONDITIONS

Jul 13, 2013

This is a License Agreement between Jose L Orellana ("You") and Elsevier ("Elsevier") provided by Copyright Clearance Center ("CCC"). The license consists of your order details, the terms and conditions provided by Elsevier, and the payment terms and conditions.

All payments must be made in full to CCC. For payment instructions, please see information listed at the bottom of this form.

Supplier	Elsevier Limited The Boulevard, Langford Lane Kidlington, Oxford, OX5 1GB, UK
Registered Company Number	1982084
Customer name	Jose L Orellana
Customer address	818 College Ave apt 18 CLEMSON, SC 29631
License number	3186851021262
License date	Jul 12, 2013
Licensed content publisher	Elsevier
Licensed content publication	The Journal of Supercritical Fluids
Licensed content title	Liquid and supercritical CO ₂ extraction of fat from rendered materials
Licensed content author	Jose Luis Orellana, Tyler D. Smith, Christopher L. Kitchens
Licensed content date	24 February 2013
Licensed content volume number	79
Licensed content issue number	None
Number of pages	7
Start Page	55
End Page	61
Type of Use	reuse in a thesis/dissertation
Intended publisher of new work	other
Portion	full article
Format	both print and electronic
Are you the author of this Elsevier article?	Yes
Will you be translating?	No
Order reference number	None
Title of your thesis/dissertation	BIO-BASED ADVANCED MATERIALS FROM RENEWABLE RESOURCES: AN INVESTIGATION ON CELLULOSE NANOCRYSTAL COMPOSITES AND CO ₂ EXTRACTION OF RENDERED MATERIALS
Expected completion	Aug 2013

date	
Estimated size (number of pages)	160
Elsevier VAT number	GB 494 6272 12
Permissions price	0.00 USD
VAT/Local Sales Tax	0.00 USD
Total	0.00 USD
Terms and Conditions	

INTRODUCTION

1. The publisher for this copyrighted material is Elsevier. By clicking "accept" in connection with completing this licensing transaction, you agree that the following terms and conditions apply to this transaction (along with the Billing and Payment terms and conditions established by Copyright Clearance Center, Inc. ("CCC"), at the time that you opened your Rightslink account and that are available at any time at <http://myaccount.copyright.com>).

GENERAL TERMS

- Elsevier hereby grants you permission to reproduce the aforementioned material subject to the terms and conditions indicated.
- Acknowledgement: If any part of the material to be used (for example, figures) has appeared in our publication with credit or acknowledgement to another source, permission must also be sought from that source. If such permission is not obtained then that material may not be included in your publication/copies. Suitable acknowledgement to the source must be made, either as a footnote or in a reference list at the end of your publication, as follows:
"Reprinted from Publication title, Vol /edition number, Author(s), Title of article /title of chapter, Pages No., Copyright (Year), with permission from Elsevier [OR APPLICABLE SOCIETY COPYRIGHT OWNER]." Also Lancet special credit - "Reprinted from The Lancet, Vol. number, Author(s), Title of article, Pages No., Copyright (Year), with permission from Elsevier."
- Reproduction of this material is confined to the purpose and/or media for which permission is hereby given.
- Altering/Modifying Material: Not Permitted. However figures and illustrations may be altered/adapted minimally to serve your work. Any other abbreviations, additions, deletions and/or any other alterations shall be made only with prior written authorization of Elsevier Ltd. (Please contact Elsevier at permissions@elsevier.com)
- If the permission fee for the requested use of our material is waived in this instance, please be advised that your future requests for Elsevier materials may attract a fee.
- Reservation of Rights: Publisher reserves all rights not specifically granted in the combination of (i) the license details provided by you and accepted in the course of this licensing transaction, (ii) these terms and conditions and (iii) CCC's Billing and Payment terms and conditions.
- License Contingent Upon Payment: While you may exercise the rights licensed immediately upon issuance of the license at the end of the licensing process for the transaction, provided that you have disclosed complete and accurate details of your proposed use, no license is finally effective unless and until full payment is received from you (either by publisher or by CCC) as provided in CCC's Billing and Payment terms and conditions. If full payment is not received on a timely basis, then any license preliminarily granted shall be deemed automatically revoked and shall be void as if never granted. Further, in the event that you breach any of these terms and conditions or any of CCC's Billing and Payment terms and conditions, the license is automatically revoked and shall be void as if never granted. Use of materials as described in a revoked license, as well as any use of the materials beyond the scope of an unrevoked license, may constitute copyright infringement and publisher reserves the right to take any and all action to protect its copyright in the materials.
- Warranties: Publisher makes no representations or warranties with respect to the licensed material.
- Indemnity: You hereby indemnify and agree to hold harmless publisher and CCC, and their respective officers, directors, employees and agents, from and against any and all claims arising out of your use of the licensed material other than as specifically authorized pursuant to this license.
- No Transfer of License: This license is personal to you and may not be sublicensed, assigned, or transferred by you to any other person without publisher's written permission.
- No Amendment Except in Writing: This license may not be amended except in a writing signed by both parties (or, in the case of publisher, by CCC on publisher's behalf).
- Objection to Contrary Terms: Publisher hereby objects to any terms contained in any purchase order, acknowledgment, check endorsement or other writing prepared by you, which terms are inconsistent with these terms and conditions or CCC's Billing and Payment terms and conditions. These terms and conditions, together with CCC's Billing and Payment terms and conditions (which are incorporated herein), comprise the entire agreement between you